RECONSTRUCTION OF THE PALEO AND NEO STAGES OF POÁS AND TURRIALBA VOLCANOES, COSTA RICA: COMPETING PROCESSES OF GROWTH AND DESTRUCTION

By

PAULO RUIZ CUBILLO

A Dissertation submitted to the

Graduate School-New Brunswick

Rutgers, The State University of New Jersey

in partial fulfillment of requirements

for the degree of

Doctor of Philosophy

Graduate Program in Geological Sciences

Written under the direction of

Dr. Michael J. Carr

And approved by

_____

_____

_____

_____

New Brunswick, New Jersey,

October, 2012

ABSTRACT OF THE DISSERTATION

Reconstruction of the Paleo and Neo stages of Poás and Turrialba volcanoes, Costa Rica: Competing processes of growth and destruction

By

PAULO RUIZ CUBILLO

Dissertation Director:

Dr. Michael J Carr

This study is about two problems a) growth and b) erosion of the Poás and Turrialba volcanoes during the last ~ 600 ka. For the growth problem, we studied both volcanoes, meanwhile for the erosion problem we focused only in the erosion generated by the recurrent phenomenon of coseismic landslides on Poás. The detailed study done here for Poás, showed how its actual edifice has grown in the last ~600 Ky and how it is comprised by at least 14 volcanic units (4 from the Paleo-temporal phase and 10 from the Neo-phase). The geochemistry data showed the variation of these volcanic units between two main magmatic components (Sabana Redonda and the Von Frantzius Geochemical Components). We presented a landslide inventory for the 2009 (M_w 6.2) Cinchona earthquake based on LiDAR images. Mass wasting calculations then were extrapolated and used to calculate erosion rates based on this phenomenon for Poás (~ 300 ± 150 km^3/km/Myr, a rate comparable to estimates of magma flux at arc volcanic systems). Furthermore, the catalog was used to create a landslide susceptibily model, that maps

landslide risk for any shallow earthquake on the volcano and determine which areas could be affected by landslides. For Turrialba, this study includes mostly the geochronology and stratigraphy of eight lava flow units that yield ages that range from 251 to 3 ka (one unit from the Paleo-temporal phase and 7 from the Neo). Three of these units, gave remarkably young $^{40}Ar/^{39}Ar$ ages (25 ka or less), among the youngest lavas dated in Central America (CA) by this method. The Neo-Turrialba flows consist of a low silica and a high silica group. The data and methodology followed here for the reconstruction of the Poás and Turrialba volcanoes can be used to obtain a new net extrusive volcanic flux, which may be used as a parameter for the rest of volcanoes of CA. The effective use of the information generated for the coseismic landslide susceptibility model for Poás by planners could reduce the impact of future landslides on the population and on the important civil infrastructure located in the study area.

ACKNOWLEDGMENTS

I would like to thank Mike, for trust in me to be part of the Ph.D program at Rutgers where I had the opportunity to continue working on my favorite volcano since I was a kid (Poás). During the execution of this project Mike always treated me like a colleague and not as his student, for this reason, I am sure that every person that ever worked with him will be thankful, because this is the best way to learn from him. Also I would like to thank him for finally giving me the secret of how to win running races, at least in the corresponding age category "to win you have to suffer". Thanks to my committee members: Brent Turrin for all the help in dating samples, Mark Feigenson for all the ideas and corrections, Guillermo Alvarado for being the link between ICE and Rutgers. Special thanks to Gerardo Soto for all the help and the volcanological support, also to Andrea Borgia, Sergio Mora, Scott Burns, Claude Herzberg, Carl Swisher, Flavia Salani and Esteban Gazel from whom I have learned a lot. Writing this dissertation would not have been possible without the support of my family, Erayda C. Alexander R., Quillo, Mario, Mau, Eduardo, J. Maio, M. Calderon, F. Meza, Ofo, Ale, Celeste and Andres who were always there for me during this period. Thanks to my friend Sara for running next to me all this 4 years. To all the graduate students who I met in these years, I enjoyed your company. To Jovani R. and Johanny Z. who always made the paperwork easier. Speciall thanks to Pedro A. who was with me in the field at Poás when the Cinchona earthquake stroke, I am glad that he was with me that day, and that we scaped from increasing the

stadistical number of geologist dying on an active volcano. To everyone that ever worked with me and I did not mention here, thank you all.

PREFACE

Volcanoes in Central America, as in the rest of the world, experience two main processes during their evolution, a) construction and b) destruction. The former is determined by the different episodes of volcanic activity and can experience different growth rates depending on the volcano's setting. The later is mostly associated with erosion processes and commonly occurs primarily after the volcano ceases activity. However, in tropical areas (e.g. Central America) the destruction of the volcanic edifices is accelerated by climatic conditions and chemical weathering, so that volcanoes in this part of the world experience these two main processes contemporaneously.

My dissertation work involves a comprehensive study of volcanic growth and destruction for two volcanoes of the Costa Rican Central Volcanic Range (CVR). The construction phase was conducted for the Poás and Turrialba volcanoes. This part of the project includes systematically mapping of all the volcanic units that form these volcanic edifices and the determination of key characteristics like: petrography, thicknesses, age, straigraphic position, and geochemistry. The erosion problem was only considered for the Poás volcano and it was based on the measurements of material removed by coseismic landslides. Furthermore, due to the location of important civil infrastructure around the area of Poás, and because coseismic landslides have been a recurrent phenomenon in this volcano's evolution, the erosion study also included a coseismic landslide susceptibility analysis. This dissertation is divided into three main chapter described below. Each chapter provides an introduction, a geologic and tectonic background, previous work, data and analytical methods, results, conclusions and references.

Chapter 1

This chapter is mostly based on the paper Geochemical and petrographical characterization of the geological units of Poás volcano massif, Costa Rica by Ruiz et al., (2010), which was published in the special volume for the Poás volcano in the Revista Geológica de América Central. This special volume came out as a response to the scientific interest and attention obtained by Poás volcano after the 6.2 M_w Cinchona earthquake of January 8, 2009. In the last two years, some changes and improvements to the original Ruiz et al., (2010) geologic map and stratigraphic section of Poás volcano have been made and are presented here as well. Finally, this first chapter includes also part of my contribution to the detailed study of the three Poás maar craters (Hule, Pata de Gallo and Río Cuarto) published by Alvarado et al. (2011).

I have been part of field campaigns on Poás volcano flanks since 2004, my contribution to the mapping of this volcano was mainly in the southern flank and then I checked and re-mapped most of the volcanic edifice through the years following previous works and aerial photo interpretation from the LiDAR images. The results presented in this chapter are consequence of a collaborative work with G. Alvarado, M. Carr, G. Soto, E. Gazel and others that had work on Poás volcano before. I used the data that I collected through the years and previous mapping information from different authors and, in 2010 I was able to create the first complete geologic map for the Poás volcano. Also, based on the field and geochronologic control, I was able to define the first chrono-stratigraphic section for this volcano. I compiled a geochemistry database from published and unpublished sources that includes more than 136 major and trace elements, several

$^{40}Ar/^{39}Ar$ and ^{14}C ages and petrographic descriptions for the Poás volcano. The geochemical database was used to characterize all the volcanic units that form this composite volcano and together with the geochronology data I studied the chemical evolution of this volcano. Furthermore, each volcanic unit was associated with one of the two magmatic components of Poás (the Sabana Redonda Geochemical Component or the Von Frantzius Geochemical Component). My contribution on the maars paper (Alvarado et al 2011) includes the geographic and geomorphological parameters (i.e. length, maximum and minimum height of volcanic rims, area, perimeter and volumes) of the different volcanic features of the Hule, Pata de Gallo and Río Cuarto maars. These features were obtained using for the first time in a Central American volcano a set of high resolution LiDAR images. The geochemically characterization of the Bosque Alegre Unit products was also part of my contribution to this study.

The geochronologic control obtained for the Poás volcano units and the complete geologic map produced for these papers served as the basis for understanding the occurrence and distribution of coseismic landslides from the Cinchona Earthquake (Chapter 2).

This work produced two published papers:

Alvarado, G., Soto G., Salani F., **Ruiz, P**., Hurtado L., 2011. The formation and evolution of the Hule and Río Cuarto maars, Costa Rica. **Journal of volcanology and Geothermal Research** 201. 342-356.

Ruiz, P., Gazel, E., Alvarado, G.E., Carr, M.J., & Soto, G.J., 2010. Geochemical and petrographical characterization of the geological units of Poás volcano massif, Costa Rica. **Rev. Geol. Amer. Central**, 43: 37-66.

Chapter 2

On January 2009, I was on the Poás volcano conducting research for this thesis project, when the Cinchona earthquake (6.2 M_w) struck. About 1 km from the epicenter Pedro Acosta and I escaped from getting buried in falling debris. After witnessing one of the trigger events that produced high peaks of erosion rates on the Poás volcano, I started working together with G. Alvarado, M. Carr, G. Soto and others on a project to measure the area affected by the landslides, estimate the volume removed by this event and extrapolate the results to past and future events in order to study how this volcano is being destroyed as it grows.

With the acquisition of LiDAR images of the affected area by the Costa Rican Institute of Electricity (ICE), I had the opportunity to study in detail one of the most recent coseismic landslide events in Central America. From this study I created a coseismic landslide catalog for the Cinchona earthquake and was I able to measure the area and volume removed by one of these events. Furthermore, with the coseismic landslide catalog and following the Mora - Vahrson approach (Mora et al., 1993) with some modifications I created the first coseismic landslide susceptibility model the Poás volcano. The most important difference of the model presented here and the Mora-Vahrson method is the

ability of my model to use different locations magnitudes and depths for the earthquake trigger event also its ability to rapidly obtain different susceptibility maps for the area. This flexibility allowed us to model historical events and projected or forecast the expected results of future earthquakes.

This chapter resulted in one submitted paper:

Ruiz, P., Carr M.J., Alvarado G.E., Soto G.J., Mana S, Feigenson M.D.& Sáenz L.F. Coseismic landslide susceptibility analyses using LiDAR images and SIGs: The case of Poás volcano (Costa Rica), as the first approach in Central America. (Geomorphology), in revision.

Chapter 3

Chapter 3 is focused on Turrialba volcano, which is a currently erupting volcano located close to a highly populated area. It has not been thoroughly studied even though it presents significant risk. This chapter adds new knowledge to the geochronology, geochemistry and stratigraphy of the volcano. In this study I worked with B. Turrin, G. Soto, M. Carr, R. del Potro and others. This chapter is a contribution to a wider project in the study of the reconstruction and evolution of Turrialba volcano. My contribution was in the preparation, analysis, correlation and interpretation of the $^{40}Ar/^{39}Ar$ ages and the geochemistry. The $^{40}Ar/^{39}Ar$ ages obtained are in agreement with the stratigraphy and three of the lavas sampled gave remarkably young $^{40}Ar/^{39}Ar$ ages (25 ka or less), among the youngest lavas dated in Central America by this method. Moreover $^{40}Ar/^{39}Ar$ ages are in agreement with prior ^{14}C age determinations. The success in measuring these young

samples by $^{40}Ar/^{39}Ar$ is attributed to a relatively high concentration of K in the samples and a careful analytical protocol that closely monitors the mass spectrometer mass discrimination during the measurements.

I generated a geologic map for Turrialba volcano based on unpublished data from G. Soto and, with the new ages, generated cross sections that show the stratigraphic positions of the Turrialba units. The flanks of the volcano were mapped and most of the youngest volcanic units sampled. Geochronological and geochemical data show that the lavas of Turrialba in the last 100 kyr consist of a low silica group and a high silica group. In this range of time at least four episodes of effusive activity: 99 - 90, 61 - 60, 25 and 10 - 3 ka occurred. Three of these episodes include lavas from both the high silica group and the low silica group, consistent with the presence of a zoned magma chamber with a silicic top and mafic base.

This chapter resulted in one submitted paper:

Ruiz P., Turrin B., del Potro R., Gagnevin D., Gazel E., Soto G. J., Carr M.J., Mora M. & Swisher III C. $^{40}Ar/^{39}Ar$ ages of Late Pleistocene-Holocene lavas from Turrialba volcano Costa Rica, some of the youngest lavas reported in Central America by this method. (G3), in revision.

Table of Contents

ABSTRACT OF THE DISSERTATION ii
ACKNOWLEDGMENTS iv
PREFACE vi
Table of Contents xii
Chapter 1 1
The formation and evolution of Poás Volcano 1
1. Introduction 2
2. Study area 3
3. Regional Setting 4
4. Field and analytical methods 5
5. Results 8
5.1.1 Colima Formation 8
5.1.2 Tiribí Formation 9
5.1.3 Río Sarapiquí Unit 10
5.1.3 La Paz Andesites Unit 11
5.1.4 Achiote Unit 12
5.1.5 Río Cuarto Lavas Unit 12
5.1.6 Von Frantzius Unit 13
5.1.7 Cerro Congo Unit 13
5.1.8 Poás Summit Unit 14
5.1.9 Bosque Alegre Unit 15
5.1.10 Laguna Kopper Unit 15
5.1.11 Poasito Unit 15
5.1.12 Poas Lapilli Tuff 16
5.1.13 Fluvial and unconsolidated epiclastics Unit 17

5.2. Detail geology and morphometric parameters of the Hule and Río Cuarto maars 17
5.2.1 The Hule maar 17
5.2.2 The Río Cuarto maar 18
5.3. Poás volcano geochemistry 19
5.3.1 Río Sarapiquí Unit 20
5.3.2 La Paz Andesites Unit 20
5.3.2 Tiribí Formation 20
5.3.3 Río Cuarto Lavas Unit 21
5.3.4 Achiote Unit 21
5.3.5 Poasito Unit 21
5.3.6 Sabana Redonda 22
5.3.7 Cerro Congo Unit 22
5.3.8 Von Frantzius Unit 22
5.3.9 Poás Summit Unit 23
5.3. 9.1 Poás Summit Botos Sub-unit 23
5.3. 9.2 Poás Summit Main Crater Sub-unit 23
5.3.10 Bosque Alegre Unit 24
5.3.11 Poas Lapilli Tuff 25
6. Geologic history of Poás volcano 25
7. Geochemistry evolution of Poás volcano 26
8. Discussion and conclusions 28
9. References 29
Figure captions 35
Figure 1 37
Figure 2 38
Figure 3 39
Figure 4 40
Figure 5 41
Figure 6 42
Figure 7 43
Figure 8 44
Figure 9 45

Table 1 46
Table 2 47
Table 3 48
Table 4 49
Chapter 2 50
Destruction of Poás volcano 50
Abstract 50
1. Introduction 51
1.1 Study area 53
1.2 Tectonic setting of Costa Rica and around Poás volcano 54
1.3 Historical coseismic landslides in Costa Rica and around Poás volcano 55
1.4 The Cinchona earthquake and its impact 55
1.5 Geology and geomorphology setting of the affected region 56
1.5.1 Platanar volcano 57
1.5.2 Barva volcano 57
1.5.3 Poás volcano 58
1.6 Orographic regions and climatic conditions around Poás volcano 58
1.7 Land cover and soil type 59
2. Methodology 62
2.1 Coseismic landslide catalog for the Cinchona earthquake 62
2.2 Coseismic landslide susceptibility model 66
2.3 Evaluation of the methodology 70
3. Data and results 70
3.1 Post-Cinchona earthquake landslide inventory 71
3.1 .1 Landslide distribution by orographic regions (Caribbean-Pacific) 71
3.1.2 Landslide distribution by type of land cover 73
3.1.3 Landslide distribution by volcanic edifice 73
3.1.4 Landslide distribution by volcanic unit 74
3.1.4 Landslide distribution by volcanic temporal phase units (Paleo-Neo) 75
3.1.5 Landslide distribution by slope angle 76
3.1.6 Types of landslides and types of material that they involved 76
3.1.7 Distance to the epicenter 77

3.1.8 Area and volume removed from the coseismic landslides 77
3.1.9 Comparison of the Cinchona event with other coseismic worldwide events 79
3.2 Coseismic landslides susceptibility model for the Poás volcano 81
3.2.1 Lithological susceptibility (S_l) 81
3.2.2 Slope angle susceptibility (S_s) 81
3.2.3 Ground moisture susceptibility (S_h) 82
3.2.4 Earthquake trigger (Earthq Trig) 82
3.2.5 Slope susceptibility to slide (H) 84
3.3 Methodology evaluation 85
3.5 Use of the coseismic landslide susceptibility model in other events near Poás volcano 87
3.5.1 The Sarchí earthquake (June 12-1912, 5.5M_w, depth 18 km) 87
3.5.2 Hypothetical earthquake case: extension of Ángel fault (6.0 M_w, depth 10 km) 88
3.5.3 Hypothetical earthquake case: San Miguel fault (7.0 M_w, depth 10 km) 89
4. Discussion 89
5. Conclusions 93
6. References 95
Figure Captions 102
Figure 1 105
Figure 2 106
Figure 3 107
Figure 4 108
Figure 5 109
Figure 6 110
Figure 7 111
Figure 8 112
Figure 9 113
Figure 10 114
Table 1. Summary of the main features of tectonic faults and their historical activity around the Poás volcano. 115
Table 2 116
Table 3 117
Table 4 119

Table 5 120
Table 6 120
Table 7 121
Table 8 122
Table 9 123
Table 10 123
Table 11 124
Chapter 3 125
Reconstruction of Turrialba volcano 125
Abstract 125
1.Introduction 126
2. Geology of Turrialba volcano 128
3. 40Ar/39Ar methods and data handling 130
4. Data and Results 133
5. Discussion 138
5.1. Stratigraphic constraints 138
5.2 Parallel evolution of high and low silica magmas at Turrialba volcano 141
6. Summary and conclusions 143
7. References 146
Figures Captions 150
Figure 1 153
Figure 2 154
Figure 3 155
Figure 4 156
Figure 5 160
Figure 6 161
Figure 7 162
Figure 8 163
Figure 9 164
Curriculum Vita 173

Chapter 1

The formation and evolution of Poás Volcano

This chapter resulted in two published papers:

Alvarado, G., Soto G., Salani F., **Ruiz, P**., Hurtado L., 2011. The formation and evolution of the Hule and Río Cuarto maars, Costa Rica. **Journal of volcanology and Geothermal Research** 201. 342-356.

Ruiz, P., Gazel, E., Alvarado, G.E., Carr, M.J., & Soto, G.J., 2010. Geochemical and petrographical characterization of the geological units of Poás volcano massif, Costa Rica. **Rev. Geol. Amer. Central**, 43: 37-66.

Abstract

The present study defines the stratigraphy of Poás volcano by using geologic, petrographic, geochronologic and geochemical analyses made on the Poás units. The northern flank of the volcano is comprised of the following units: Río Sarapiquí, La Paz Andesites, Tiribí Formation (from Barva volcano, but interdigitated with Poás stratigraphy), Río Cuarto Lavas, Von Frantzius, Cerro Congo, Bosque Alegre and Laguna Kopper. The units on the southern flank are Colima Formation, La Paz Andesites, Tiribí, Achiote, Poasito, Sabana Redonda and Poás Lapilli Tuff. The central part of the volcano is made by the Poás Summit Unit, which includes the Main and Botos craters. The composition of the rocks spans the range from basalts to dacites. These units were

geochemically correlated with two magmatic components: 1. The Sabana Redonda Geochemical Component (TiO_2 > 1%) enriched in HSFE and other trace elements, present in La Paz Andesites, Lavas Río Cuarto, Poasito, Sabana Redonda, Poás Lapilli Tuff and some from Botos crater lavas. 2. The Von Frantzius Geochemical Component (TiO_2 < 0.8 %) is present in lavas of the Main crater, Von Frantzius, Achiote, Bosque Alegre, Cerro Congo and some Botos crater lavas. During the last 600 ka the content of K_2O and other oxides (TiO_2 and P_2O_5) and traces (Zr, Ba) have varied significantly through time, suggesting the presence of these two geochemical end-members since the beginning of the magmatic activity of Poás. Within similar ranges of time, units with high and low values of these elements have coexisted; the latter is true for Botos lavas and the Main crater. For units that possibly shared a common vent, such as La Paz Andesites, Achiote and Main crater, the percentages of K_2O and TiO_2 have decreased through time.

1. Introduction

The Poás volcano is one of the five active volcanoes of Costa Rica, it is part of the Costa Rican Central Volcanic Range (CVR) and its active vent is located at Lat $10^o11'$N and Lon $84^o13'$W (Fig. 1). The scientific importance that Poás represents, being close to major cities and, its accessibility to the main active crater helped to conduct in the past three decades several studies on it. These studies focused mainly in the geology, geophysics and geochemistry of the main crater. Much progress has been made toward understanding its historical eruptive cycle and its present activity (e.g., Thorpe et al., 1981, Casertano et al., 1983, Prosser & Carr, 1987, Cigolini et al., 1991, Rymer et al., 2009). In addition, few studies on the flanks of the volcano have been conducted too (e.g.,Tournon 1984, Borgia et al., 1990, Soto 1999, Alvarado & Salani 2004, Gazel &

Ruiz 2005, Carr et al., 2007). The paper from Ruiz et al., (2010) was the first attempt to complete the first geological map that studied the volcano as a whole edifice, from its northern and southern flanks at about 400 m a.s.l. to its summit at 2708 m a.s.l.

Here we followed the study from Ruiz et al., (2010), to present the results from new mapping and present a more complete version of the geological map for the entire Poás volcano. The main goals of this study are to characterize petrologically and geochemically all the volcanic units that compose this massif. Placing them in time and space, to understand the changes that the volcano had experience in its last two stages of activity, during the past 600 ka. The level of detail in this study for the geologic mapping of the volcano, together with the relatively complete geochemical and geochronology databases, provided one of the few opportunities to study the evolution of a complex composite volcano in Central America. The results from this study will guide us toward better understanding of how volcanoes growth in a volcanic front.

2. Study area

The Poás volcano units that were studied here enclosed a total area of about 415 km^2. This area is limited by Lavas Río Cuarto Unit in the northern flank of the volcano and the Alajuela reverse fault scarp in the southern flank (Fig. 2). The limits to the east and west are respectively the rivers Tambor and Sarchí in the southern part of the volcano, and the Toro and Sarapiquí rivers in the northern part (Fig 2). The geologic units described and interpreted here are divided in three sectors: north, south and central (actual vent). The northern flank of the volcano is comprised of the following units; Río Sarapiquí, La Paz Andesites, Tiribí Formation (from Barva volcano, but interdigitated), Río Cuarto lavas,

Von Frantzius, Cerro Congo, Bosque Alegre and Laguna Kopper. The units on the southern flank are: the Colima Formation, La Paz Andesites, Tiribí, Achiote, Poasito, Sabana Redonda and Poás lapilli tuff. The central part of the volcano is the Poás Summit Unit, which includes the Main and Botos craters.

3. Regional Setting

The CVR of Costa Rica is located on the Central American volcanic front, which extends parallel to the Middle American Trench from Guatemala to Costa Rica (Fig 1). Its volcanic activity is the product of the subduction of the Cocos Plate under the Caribbean Plate, which has a convergence rate that increases to the southeast from ~83 mm yr^{-1} off southern Nicaragua to ~89 mm yr^{-1} off southern Costa Rica (DeMets, 2010). The lavas from Poás volcano as the rest of volcanoes from central Costa Rica present an anomalous OIB signature different from the rest of lavas of the Central America volcanic arc. Several models have been postulated to explain this (e.g. Herrstrom et al., 1995, Russo and Silver 1994, Feigenson et al., 2004, Goss and Kay 2006, Hoernle et al., 2008) the latest model presented by (Gazel et al., 2009) considers that this signature is derived from the Galapagos hot spot tracks subduction beneath Costa Rica and Panamá.

The Poás currently active eruptive vent lies within a volcano-tectonic fracture that runs north-south. Other structures inside this fracture are; the pyroclastic cones of Sabana Redonda, the Botos Crater, Von Frantzius cone, the Congo volcano and the explosive craters (maars) of Hule and Río Cuarto (Prosser, 1983; Soto & Alvarado, 1989). The north and south flanks of the volcanic edifice are limited by the scarps of the Alajuela and San Miguel reverse faults. There are other tectonic structures (especially strike-slip

faults) on the east and west flanks of the volcano with historical and destructive seismic activity. Some of the most important earthquakes are; 1772 (M_w 6.0), 1851 (M_s 6.0), 1888 (M_w 6.0), 1911 (M_w 6.0), 1912 (M_w 5.5), 1955 (M_w 6.1) and 2009 (M_w 6.2) all of them located in the area of the towns of Bajos del Toro-Fraijanes-Vara Blanca-Poás (Peraldo & Montero 1999; Montero et al. 2010).

The main crater of Poás has been frequently active during the last 200 years, with eruptions characterized by periodic phreatic explosions (Alvarado, 2009). Because the active vent is located only 20 km from the second largest city of Costa Rica, Alajuela, and just 30 km from the capital, San José, the volcano is a significant hazard. Most of the slopes of the volcano are used for agriculture and dairy cattle. During the last two decades, tourism has become a major activity in the volcano and its surroundings, being the Poás Volcano National Park, the most visit National Park in Costa Rica. Since 1980, the Costa Rican Institute for Electricity (ICE) and private companies developed hydroelectric projects in the north side of Poás, taking advantage of the high mean annual precipitation of the zone (3000 - 6000 mm), and the steep slopes (between 25 to 30^o) of this volcano flnak. Several of the geologic studies made in the zone by ICE, were executed to provide the geologic characterization necessary for the construction of these projects.

4. Field and analytical methods

The geologic map from the Poás volcano that we introduced in this study (Fig 2) is an upgrade of the one presented by Ruiz et al., (2010). Herein we completed the geological mapping and presented more details areas that were not included in previous works.

These areas are especially located in the northwest sector of the Congo volcano, the area of Bajos del Toro, and the east flank of the volcano where the road of Vara Blanca-San Miguel (Road 126) is located. Fieldwork was carried out during 2009, six months after the Cinchona earthquake, taking advance of the new exposed outcrops after the landslides produced by the earthquake.

The complete geological map of the Poás volcano (Fig. 2) has as background a digital elevation model (DEM) made with the topographic maps scale 1.50 000 of Poás, Barva, Rio Cuarto, Quesada and Naranjo from the National Geographic Institute of Costa Rica (IGN).

Borehole profiles from ICE hydroelectrically projects were used to obtain some of the volcanic units thickness. We included several $^{40}Ar/^{39}Ar$ (matrix) and calibrated ^{14}C ages in a geochronology database. The results of the $^{40}Ar/^{39}Ar$ (matrix) dating were obtained in the Nobel Gas Laboratory of Rutgers University and were done following the same methods published in Carr et al., (2007) and described in chapter 3. We also presented thin section descriptions for the geologic units of Poás volcano. The geochemical database compiled for this study includes 136 analyses that were taken from two previous compilations made by Kussmaul et al. (1982), Kussmaul (1988) and different authors: McBirney and Willians (1965), Krushensky (1982), Prosser (1983), Tournon (1984), Alvarado (1985), Paniagua (1985), Prosser and Carr (1987), Cigolini et al. (1991), Malavassi (1991), Soto (1999), Patino et al. (2000), Carr (2002), Gazel and Ruiz (2005) and Carr et al. (2007).

The present study makes a geochemical and petrographic characterization for the different geologic units from the Poás volcano. The Peccerillo and Taylor (1976) diagram (SiO_2 vs. K_2O) which is commonly used in volcanic rocks saturated in silica from island arcs, was used to make a rock type classification. This and other major and trace elements diagrams were made using IGPET 2009. The different databases (geochemistry-geochronology- petrography) compiled for this paper are available upon request from the authors.

For the detail study of the Río Cuarto and Hule maars, as a novelty in Central America, the geographic and geomorphological parameters (i.e. length, maximum and minimum height of volcanic rims, area, perimeter and volumes) of the different volcanic features were obtained using a set of high resolution LiDAR images. These images were obtained during the course of an airplane flight in April 2009 by the Spanish company STEREOCARTO with an ALS50-II LEICA system. The resolution of these LiDAR images is three points per m^2, which is enough to created DEM with a resolution of 50 cm in the x and in the y axis, and 15 cm in the z. The differences in altitude from the images and the benchmarks of the topographic maps are less than 11 cm. The high resolution of these data has allowed unprecedented resolution to identify volcanic features that were previously not recognized using standard photo-grammetric techniques. These images were prossed using the following commercial software packages: Quick Terrain Modeler SURFER 9.0 and GLOBAL MAPPER 10.0. The maars study also included a compilation of previous chemical analyses of rocks from Hule area. The data have been plotted in a geochemical diagram for interpretations based on the stratigraphy.

5. Results

5.1 Geology and stratigraphy of Poás volcano

The Poás is located between the Platanar and Barva volcanic centers (Fig 1c). It was formed by the stacking of volcanic rocks during at least three principal stages (Proto-Paleo-Neo) occurring over almost one million years (Soto 1994, Soto 1999 and Ruiz et al. 2010). Here we present a description of the geologic units that build up the Poás volcano and because no outcrops of the Proto Poás stage have been found we are focusing on the lithologies of the two last construction stages of the volcano. The geologic map (Fig 2.) does not include the pyroclastic units that cover the volcano in order to facilitate the understanding of the underlying units and show in as clear way as possible the geographic distribution of the units. A stratigraphic sketch (Fig. 3) shows where the volcanic units are located according to their geographic position relative to the main crater.

5.1.1 Colima Formation

Williams (1952) named this unit first as Intracanyon. However Fernández (1969) uses the name of Colima Formation that remains until today. It corresponds to the local basement of the south part of the study area (Fig 2). It is overlain by the ignimbrite of the Tiribí Formation. It is composed by three members: a) Lower Colima, b) Puente Mulas and c) Upper Colima (Fig. 3). Based on data calculated from water wells in the area by (Campos et al., 2004), the average thickness of this formation is ~ 100 m (50 m for the lower member, 20 m for Puente Mulas and 30 m for Upper Colima). The Lower Colima

member is mainly composed by porphyritic lavas with phenocrysts of plagioclase, augite, hypersthene, magnetite and some olivine in a matrix with intersertal texture. The intermediate member, Puente Mulas, is a package of ignimbrites, however in the rivers Tacares and Prendas it is a sequence of tuffs and lake sediments (Borgia et al., 1990). The Upper Colima lavas present an aphyric texture with only 4 % of phenocrysts inside a flow matrix with elongated vesicles. Radiometric $^{40}Ar/^{39}Ar$ ages from Marshall & Idleman (1999), Marshall et al. (2003) and Gans et al., (2003) establish an age for this formation between 758 ka (Lower Colima) and 330 ka (Upper Colima; Table 1).

Kussmaul (1988) highlights that the chemical compositions from the Colima Formation lavas are different from the stratovolcanoes of the CVC and is very similar to the Tiribí Formation. For this reason, geomorphology aspects and its lateral extension the same author suggest that these lavas are probably the result of effusions along volcanic fissures with a northeast-southwest trend.

5.1.2 Tiribí Formation

Named originally as Avalancha Ardiente by Williams (1952), this unit begins with a pumice layer (a fall deposit) with a maximum thickness of 3 m, followed by an ignimbrite deposit with different welding facies. The outcrops of this formation are mainly in the south part of the study area, however outcrops in the northern side have been found and lithological and geochemically correlated with the well characterized and well exposed Tiribí in the Valle Central on the south side of Poás (Soto 1999 and Soto et al., 2008). The outcrops on the northern side are restricted to the intersection of the María Aguilar and Sarapiquí rivers, about 1 km away from the San Miguel scarp fault (Fig. 2).

In the southern sector of the Poás volcano, this formation appears on river valleys like Rosales, Poás, Puente de Piedra and several places close to the Alajueja fault scarp, especially quarries (Echandi, 1981; Borgia et al., 1991; Campos et al., 2004).

On the northern side the ignimbrite overlies the Rio Sarapiquí unit and La Paz Andesites units, whereas on the south sector it overlies the Colima Formation (Fig. 3). On both sides of the study area it appears to be under the La Paz Andesites Unit. It is possible that the reverse faults of Alajuela and San Miguel cause a repetition in the sequence causing Tiribí to appear to be under La Paz Andesites. Other possibility is that because it is flow deposit, it preferentially traveled through river canyons, and was deposited between two units of greater age in lateral contacts. The other possibility is that, what has been interpreted as Tiribí on the north side, it is actually an older unit, like the Puente Mulas Member. More geochronologic data are needed to solve this question.

The thickness of this formation is limited to a few meters on the north side, whereas in the south; the thickness reaches 40 m (Campos et al., 2004). The most recent radiometric ages (Perez et al., 2006) are 322 ± 2 ka (table 1.). Perez (2000) interprets the ignimbrites as deposits originating at the top of Barva volcano in a powerful explosion that created the major caldera of Barva.

5.1.3 Río Sarapiquí Unit

The outcrops of this unit only appear in the Sarapiquí river canyon and its tributaries. It forms the local basement on the northeast side of the volcano. It is underlying the La Paz Andesite Unit and its base is not cropping out. It consists mostly of breccias and ash-flow

tuffs, with epiclastic lenses and subordinate lavas interdigitated between them. The minimum thickness of this unit is estimated to be 50 m, but may be hundreds of meters. Geochemically, the lavas from this unit range from basalts to andesites. Based on stratigraphic correlations Ruiz et al. 2010 speculate an age of 0.6-0.7 Ma for this unit, but could be older (Fig. 3).

5.1.3 La Paz Andesites Unit

It appears mainly in the northeast flank of Poás volcano. Some patches of this unit that are located in the northwestern side of the Poás volcano as well and the river canyon of Poás river in the southern flank of the volcano (Fig. 3). It overlies unconformably the Río Sarapiquí Unit and is overlaid by the products emitted by Cerro Congo and Von Frantzius cones, in the northern slope of the Poás edifice.

It consists mainly of several (at least seven) andesitic lava flows with a characteristic porphyritic texture with megaphenocrysts of plagioclase (2-3cm) (Ruiz et al., 2010). These phenocrysts and the glassy matrix are easily weathered, which turns difficult to find fresh outcrops of these lava flows. The texture of these lavas together with its oldness (0.6 and 0.5 Ma, Gans et al., 2003 and Ruiz et al., 2010) could be responsible for facilitating the high the development of residual soils and reducing considerably their geotechnical conditions, making the slopes more susceptible to slide. This unit also includes breccias and tuffs interdigitated. A maximum thickness of ~260 m was measured for this unit (Ruiz et al., 2010). Geochemically, the composition of this unit ranges from basalts to dacites, although most are basaltic andesites. Morphologically, this unit is similar to the Paleo-Barva Unit, presenting uneven slopes with angles between 30^{o}

to 60°. These slopes are covered by tuffs and weathered lapilli tuffs with thickness between 5 to 40 m. It has deeply eroded river valleys which are truncated mainly by right lateral faults.

5.1.4 Achiote Unit

This unit crops only in the southern part of the Poás edifice. It is contemporaneous with the La Paz Andesites unit and could overlie it in some sectors (south of the study area). The Poasito and Sabana Redonda units overlie it in some areas. The Achiote Unit consists of several lava flows. These flows present different textures and all of them can reach a thickness of about 110 m. In some areas they are covered by material from the Lapilli Tuff Unit (see below) and/or residual soils (Campos et al., 2005 and Montes 2006). Geochemically, these lavas are basalts and andesites which Ruiz et al. (2010) dated at 540-200 ka. The geomorphology of this unit is similar to the La Paz Andesites Unit with uneven slopes that have angles between 30°to 60°, although its river valleys are less truncated and arranged in a sub-parallel to parallel drainage system.

5.1.5 Río Cuarto Lavas Unit

The main outcrops of this unit are in the vicinity of the Río Cuarto town located in the northern sector of the study area. This unit consists of a lava field that extends beyond the north face of the San Miguel fault scarp with a slight downward slope (3°-5°) to the north and with a parallel drainage system. (Fig. 3). Stratigraphically, this unit overlies the La Paz Andesites Unit and underlies the Cerro Congo and Laguna Kopper units. This lava field has a thickness of ~15m. Geochemically, this lava field corresponds to basaltic-

andesitic lavas with characteristic aphyric and fluidal textures. Carr et al. (2007) dated this unit in 201 ± 30 ka with $^{40}Ar/^{39}Ar$.

5.1.6 Von Frantzius Unit

This unit is located north of the active crater of Poás volcano (Fig. 3). Its stratigraphic position is above the La Paz Andesites Unit, contemporaneous with part of the Cerro Congo Unit and below the deposits from Bosque Alegre Unit. It is mainly composed of lava flows with breccias, epiclasts and pyroclasts on the top for a total maximum thickness of 70 m, Residual soils rarely surpass 5 m of thickness. The lavas from this unit range from basaltic andesites to dacites, and have an age range from 41 ka to 10 ka (Gans et al., 2003 and Ruiz et al. 2010). The geomorphology of this unit is similar to the Cerro Congo Unit, presenting a semi-radial drainage system with smooth slopes of angles between 30^{o} to 60^{o}.

5.1.7 Cerro Congo Unit

The Cerro Congo volcano is a composite cone located in the northern side of the study area, between the Von Frantzius cone and the San Miguel fault (Fig. 3). Stratigraphically, this unit underlies the Von Frantzius unit although the uppermost Cerro Congo lavas could be contemporaneous with the Von Frantzius unit. It consists of lavas, epiclasts and pyroclastic flows. It has a minimum thickness of ~60m and in some is only covered by ~5 m of residual soils. Geochemically, the products of this unit range from basalts to andesites and, according to Ruiz et al. (2010), the age of this unit ranges between 10 ka to 40 ka. The Cerro Congo cone does not have a well defined crater; instead it is open in

two main landslide scarps to the NNW and NNE (Fig. 3). After witnessing the erosive consequences that this cone suffered from the Cinchoma Earthquake, it appears likely that these gullies formed by an erosive process that has repeated many times during similar seismic events over the last few thousand years. This unit shows a radial drainage system with smooth slopes that present angles mainly between 30^{o} to 60^{o}.

5.1.8 Poás Summit Unit

This unit is located in the central zone of the study area, and consists of the products that have been emitted by the Botos and Main craters (Fig. 3). This is the unit that belongs to the Neo-Poás temporal stage. The products from the main crater sub-unit are exposed in the crater walls and outcrops that extend westward. The lava flows from the Botos sub-unit extend eastward and overlie a thick set (~10 m) of pyroclasts in the Pulga stream valley on the eastern flank of the volcano. This area was also severely affected by landslides.

The Botos lavas vary from basalts to dacites while the Main Crater lavas range from basaltic andesites to dacites. Based on ^{14}C age and $^{40}Ar/^{39}Ar$ ages Ruiz et al. (2010) gave an age range from 56 ka to 8 ka to the Botos lavas and proposed that the lavas from the main crater could be contemporaneous or younger than the lavas from Botos. The slopes on this unit have a big range with angles $>15^{o}$ in some areas (south of Botos cone) and close to 60^{o} in river valleys.

5.1.9 Bosque Alegre Unit

It is located north of the Cerro Congo unit, in the northern side of the study area (Fig. 3). It comprises the eruptive products of the Hule and Pata de Gallo maars. The explosion crater from Hule has steep slopes (~60^{o}) on its walls. The two small cones within the crater and the Pata de Gallo maar have less steep slopes (~40^{o}). Stratigraphically, Bosque Alegre Unit overlies the Cerro Congo and Von Frantzius units. The tephra products of this unit are mainly pyroclastic surges, flow and fall deposits outside the maar (Alvarado et al., 2011). Within the maar the two cones produced at least three basaltic lava fields. Hule was formed 6.2 ka ago and Pata de Gallo probably 2.8 ka ago, while the intra-maar products could have ages of 1.7 or 0.7 ka (Alvarado et al., 2011).

5.1.10 Laguna Kopper Unit

This unit is located in the extreme north of the study area (Fig. 3). It comes from another maar also known as Laguna Río Cuarto, which presents walls with steep slopes (~60^{o}). The fall products of this unit appear in a narrow axis with direction east-west from the maar over two kilometers with a variable thickness (no more than 15 m) that quickly disappears. Locally, they unconformably overlie the Río Cuarto Lavas Unit (Fig. 3). The deposits are collations of lithics, pumice and pyroclasts. Alvarado et al. 2011, estimated the age of this maar in 3-4 ka.

5.1.11 Poasito Unit

This unit is only presented in the southern side of Poás volcano, with the main outcrops in the rivers canyons near Poasito town (Fig 2). It consists of massive lava flows with

aphyric and fluidal textures. It rests unconformably on the Achiote Unit, congruent with or in some sectors overlies the Sabana Redonda Unit. The lavas of this unit have a composition that ranges from basaltic andesitic to andesitic. It has a minimum thickness of 80 m. Based on stratigraphic correlations, Ruiz et al. 2010 estimated an age between 40 ka and 25 ka for this unit. Since it is mostly covered by the Poás Lapilli Tuff Unit and/or residual soils (7 m in some areas), it presents a smooth topography with a parallel to sub-parallel drainage system and slope angles between 10^{o} to 30^{o}.

5.1.12 Poas Lapilli Tuff

This pyroclastic unit was defined by Prosser & Carr (1983) and later analyzed and studied by Campos et al 2004, Gazel and Ruiz (2005) and Montes 2006. It extends from the summit of Poás volcano to the area of Grecia, 15 km to the southwest. It consists of a juvenile lapilli tuff with a maximum thickness of 7 m. In the sector of Sabana Redonda the Poas Lapilli Tuff appears in road cuts, which after the Cinchona Earthquake of January 2009 were better exposed and presented thickness greater than 7 m. The tuff and lapilli are light grey when they are fresh; the colors orange, brown and purple are common when they are weathered. Based on geochemistry and its distribution, Gazel and Ruiz (2005) associated this unit with the Botos crater. To show more clearly the distribution of the lava units (Achiote and Poasito units) on the south sector of the study area, this unit was not included in the geologic map (Fig. 2).

5.1.13 Fluvial and unconsolidated epiclastics Unit

This unit occurs in several sectors of the study area, but mainly on the north side, where it represents the distal facies of Congo and the "pie de monte" from the San Miguel fault scarp. It also occurs in the zone of Bajos del Toro, bordering the Poás massif to the west. Its lithology is fluvial deposits with lahars and colluvial material, reaching tens of meters in thickness.

5.2. Detail geology and morphometric parameters of the Hule and Río Cuarto maars

5.2.1 The Hule maar

Hule is a subcircular volcanic depression (Fig. 4), with the major axis of 2.3 km and the minor axis of 1.8 km, for a total area of ~ 3.5 km^2. The walls range from 230 m high in the northern rim (978 m a.s.l.) to only 20 m high (777 m a.s.l.) in the southern rim, with variable slopes (27-45^o). Two intra-maar pyroclastic cones are present, called Bosque Alegre, since thought to be only one cone. The detailed features have been recognized with the new LiDAR images, and are clearly younger than the maar itself, because they are growing into it. The older cone shows part of the crater preserved, into which the younger cone, which shows a relatively well preserved crater (ca. 138 m high, 878 m a.s.l.) grew and one lava flow from it breached the eastern rim of the first cone. At least one lava field appears to be the first cone (Lava 1 in Fig. 4) and two lava fields to the second cone (Lava 2 and 3 in Fig. 4).

Another maar (25-50 m deep), called Pata de Gallo or Los Angeles, is 400 m in diameter and is located less than one kilometer of the southeastern rim of Hule maar (Fig. 4).

The Hule basin is presently occupied by three lakes (740 m a.s.l.)., (Fig. 4): Hule (54.7 ha, 26.5 m deep), Congo (14.9 ha, 14.6 m deep) and an unnamed one (0.6 ha, 4 m deep) (Horn and Haberyan, 1993). Hule lake overflows at its northeastern end, through the Hule river. Despite similarities in size and depth, Hule is stratified with elevated CO_2 in the lower part, whileCongo is freely mixing from top to bottom and contained very little CO_2 when sampled in 1993 (Haberyan and Horn, 1999). In repeated measurements at Hule Lake, Umaña (1993) found surface water temperatures to vary between 22.2 and 26.5^o C, while temperatures at 25 m depth varied between 20.9 and 21.4^o C, indicating a thermal stratification. He estimated a water volume of 6.9 x 10^6 m^3.

5.2.2 The Río Cuarto maar

The Río Cuarto lake (361 m a.s.l.), also known as the *Laguna de los Misterios* ("Lake of the Mystery", probably due to seclusion as well as fish kills), Laguna Kopper (after the landowner's family name of the owner), Laguna Yurro Hondo or Río Hondo (*Deep Ravine*, due its great depth). It is a crater with a rim that reaches some 52 m above the water level (412 m a.s.l. Fig 5). The crater rim has an E-W axis of 847 m, a mean width of 707 m, and the lake (361 m a.s.l.) has an E-W axis of 758 m, a mean width of 581m, and a surface of 0.33 km^2 (Fig. 5)

The lake has a maximum depth of 66 m, making it the deepest natural lake in Costa Rica (Horn and Haberyan, 1993). A bathymetric study by Gocke et al. (1987) showed a mean depth of 45.5 m, corresponding to a water volume of 15.12 x 10^6 m^3. Surface temperature has been observed to vary between 24.6 and 29.9 ºC, whereas the temperature of the hypolimnion at 60 m fluctuates only between 24.2 and 24.4 ºC (Gocke et al., 1987, 1990;

Haberyan and Horn, 1993). The depth of the boundary layer between the oxic and anoxic (H_2S-rich) water bodies varies between 25 m (January-February) and 20 m (May-June); about 55% (mean value) of the total lake water body is permanently anoxic (Gocke et al., 1987).

5.3. Poás volcano geochemistry

Here we show the geochemical relation of each Poás volcano geologic unit, and the geochemical variation between them through the volcano evolution. Geochemically the lavas from the different units of Poás span from basalts to dacites. The most common rock type based on the Pacerrillo & Taylor diagram (1976, Fig. 6) are basaltic-andesites and andesites. In this same diagram we observed that the lavas present two tendencies in the K_2O values which allowed us to differentiated them between calco-alcaline and calco-alcalines high in K. Using a variation diagram of TiO_2 vs MgO (Fig. 7) we showed the differentiation and mixing of the geochemical units, and its fractional crystallization as well. The variation in major oxides (TiO_2 and P_2O_5) and the trace elements Zr and Ba from each volcanic unit showed their chemical evolution of the volcanic edifice. Each volcanic unit was associated to one of the two geochemical components of Poás volcano: The Sabana Redonde Geochemical Component (SRGC) and the Von Frantzius Geochemical Component (VFGC) defined by Gazel & Ruiz (2005). The most important geochemical ranges used in the diagrams for each unit are present in the table 1.

5.3.1 Río Sarapiquí Unit

According to the chemical analyses for this unit, the rocks range from basalts to andesites. All of them have values lower that 2 % for K_2O and are located in the zone of the calc-alcaline series low in K (Fig. 6). They present low values of TiO_2 < 1 % and MgO < % 5 (Fig. 7), also the values of P_2O_5 are relatively low (0.2-0.25 %; Fig 8). This unit belongs to the VFGC and geochemically it is different from the La Paz Andesites that is overlying it.

5.3.2 La Paz Andesites Unit

The rocks of this unit range from basalts to dacites, however most are basaltic andesites (Fig. 6). This unit belongs to the calc-alkaline series with high K. The majority of the samples from this unit have high values of TiO_2 (≥ 1 %) and low to intermediate values of MgO (≤ 5 %) with a tendency to fractional crystallization of the phase of olivine, pyroxene, plagioclase and magnetite (Fig. 6). It also present values > 0.3 % of P_2O_5 and ranges from 600 to 1000 ppm of Ba and 175 to 200 ppm of Zr (Fig 7). This unit belongs to the SRGC being different geochemically from the Rio Sarapiqui Unit (below) and Achiote Unit (similar age).

5.3.2 Tiribí Formation

The chemical composition of this ignimbrite spans a wide range, where basaltic andesite lapilli are found along with andesites, but the trachyandesites are the ones that predominate. This unit belongs to the calc-alkaline series with high K. The majority of the samples have high values of TiO_2 (> 1 %) and low values of MgO (≤ 4 %) and P_2O_5 < 0.5 %). They can be differentiated very

well from the Poás lavas by comparing the values of trace elements like Sr with ranges from 200-900 ppm versus 400-750 ppm for Poás and Rb with ranges between 50-150 ppm versus 10-75 ppm for Poás (Pérez et al. 2006). It is not included in any of the Poás geochemical components.

5.3.3 Río Cuarto Lavas Unit

Geochemically, this unit consists only of basaltic andesites that belong to the calc-alkaline, high-K series. (Fig. 6). These lavas have high values of TiO_2 (>1 %) and values of (4 to 5%) of MgO (Fig. 7) and 0.2- 0.3 % in P_2O_5 with ranges from 600-800 ppm of Ba and 130-150 ppm of Zr (Fig. 8).It belongs to the SRGC.

5.3.4 Achiote Unit

Geochemically, this unit consists of rocks that range from basalts to andesites, in the calc-alkaline series low in K (Fig. 6). This is a main difference between the La Paz Andesites lavas that are enriched in K_2O. Achiote unit presents values < 1% de TiO_2 and low to intermediate of MgO <5.5% (Fig. 4) and < P_2O_5 0.3 % also ranges from 500 to 600 ppm of Ba and 75 to 130 ppm of Zr (Fig. 7). This unit is geochemically associated with the VFGC.

5.3.5 Poasito Unit

This unit is in the High-K, calc-alkaline series with compositions that range from basaltic andesite to andesite (Fig. 6). TiO_2 contents are ≥ 1 % (Fig. 7). Like Tournon (1984) and Prosser & Carr (1987), Gazel & Ruiz (2005) mentioned there is a stong chemical affinity between the aphyric andesites from Poasito Unit and the porphyiritc lavas from the La Paz Andesites Unit. Furthermore there is a different composition compared to the

Achiote Unit which is not so high in K_2O and TiO_2 (Fig 7). The values of Zr for this Unit are in the range of 150-250 ppm while the values for Ba are > 500 ppm to 1100 ppm (Fig. 8). We associated this unit to the SRGC.

5.3.6 Sabana Redonda

Geochemically, this unit ranges from basalts to andesites of the calc-alkaline, high-K series (Fig. 6) This unit shows the highest values of TiO_2 from Poás, MgO (3 to 4 %) (Fig. 7) and values for P_2O_5 from 0.2 to 0.3 %. In the same way that the La Paz Andesites and Poasito units, Sabana Redonda, presents the highest values in Zr (140 to160 ppm), Nb (12 to 17 ppm) and values between 600 ppm to 800 pmm for Ba (Fig. 8)

5.3.7 Cerro Congo Unit

The samples from this unit vary from basalts to andesites in the low to normal K, calc-alkaline series (Fig 6). The percentage of MgO ranges from 2 to 6 %., but the values of TiO_2 are < 1 % (Fig. 7). This unit has P_2O_5 contents between 0.2 and 0.3 %. Trace elements contents, like Ba (400-700 ppm), Nb (5-20 ppm) and Zr (500-200ppm) (Fig. 8), are lower than the ones present in the La Paz Andesites, Poasito and Sabana Redonda units. This unit is geochemically associated with the VFGC.

5.3.8 Von Frantzius Unit

The lavas from this unit range from basaltic andesites to dacites, in the Low-K, calc-alkaline series (Fig. 6) with some samples that tend to be normal and even high K. The values of K_2O do not rise above 2.5 %, TiO_2 contents are < 0.8 % and MgO varies

between 1% and 6 %) (Fig. 7) while the values for are P_2O_5 < 0.3. In trace elements like Sr, they present values of 500 to 800ppm and Rb that ranges from 20 to 75 ppm (Fig. 8). Gazel and Ruiz (2005) defined the VFGC based on the geochemical characterization of this unit.

5.3.9 Poás Summit Unit

To characterize this unit and due to geochemical differences within, it was divided in two sub-units (Poás Summit Main crater and Botos sub-unit).

5.3. 9.1 Poás Summit Botos Sub-unit

The geochemical behavior of this sub-unit is very heterogeneous, with rocks that vary from basalts to dacites and with representatives of both the high and low K series (Fig. 6). They are also very variable in TiO_2 and MgO. Due to these differences it was divided in Poás Summit Botos (High Ti) and Poás Summit Botos (Low Ti) The samples that have high contents of magnesium > 7 % also are low in (< 52 %) in SiO_2 making them true basalts. The values of P_2O_5 are also variable with samples that present values of < 0.3 %, while others are above this number. The Ba values are between 450 to 950 ppm and for Zr the range from 75 to 175 ppm (Fig. 8). The sub-unit Poas Summit Botos (High Ti) belongs to the SRGC while the Poás Summit Botos (Low Ti) belongs to the VFGC.

5.3. 9.2 Poás Summit Main Crater Sub-unit

In contrast to the Botos subunit, the Main Crater subunit has no basalts but it ranges from basaltic andesites to dacites. Another difference between the samples from this unit and

Botos is that the Main Crater lavas are all in the low-K, calc-alkalineseries (Fig. 6). Finally, there is a unimodal distribution of TiO_2 with all values < 1% (Fig. 7). Similarly, all values of P_2O_5 Ba, Zr and Nb are low in comparison to other units. This differentiates the Main Crater Sub-unit from units like La Paz Andesites and Poasito Units. This unit belongs to the VFGC.

5.3.10 Bosque Alegre Unit

Based on earlier chemical analyses, we present a wider appraisal of the maar formation. There are few petrographic and chemical analyses available of the Hule area (Fig. 9 and Table 4). There are 4 analyses from the Hule intra-maaric cones and lavas (McBirney and Willians, 1965; Tournon, 1984; Prosse and Carr, 1987; Malavassi, 1991) and one from the juvenile andesitic pumice of the Hule tephras (Soto, 1999). There are other samples from this area, although without precise locations (Malavassi, 1991), of which five appear to be from the intra-maaric cone-lavas, one from the silica-rich andesites of Hule tephra, and two from the walls of the maar.

The rocks classify as low to medium in K in the calc-alkaline series, ranging from basalts to andesites (Fig 9). Two samples (150 and 182 in table 4) from unknown localities (Malavassi, 1991) may be from the maar wall, and are also plotted in the diagram for comparison. They fit in the basalt-andesite trent defined ny the intr-maar rocks and pyroclastic flows and partilly cover the compositional gap in between these rocks. Based on the geochemistry of the rocks from Poás massif, Ruiz et al. (2010) defined the VFGC and the SRGC. According to the geochemistry of the Bosque Alegre Unit (deposits from the Hule maar and itra-maar cones), it is part of the VFGC. Some of the characteristics

present in these lavas are: the levels of TiO2 < 1%, P2O5 contents < 0.2 %, low values for trace elements like Ba, Nb and Zr compared to the SRGC, which presents higher values of these elements (Fig. 9).

5.3.11 Poas Lapilli Tuff

Based on geochemistry and the distribution from materials of the Poás Lapilli tuff Unit, Gazel & Ruiz (2005), associated the products of this unit with the Botos crater because there are chemical differences with the main crater. According to Gazel & Ruiz (2005) the materials of this unit have major elements contents similar to the geochemistry of the Sabana Redonda Unit; TiO_2 (0.9-1 %), Fe_2O_3 (9-10%) and CaO (< 6.5 %).

6. Geologic history of Poás volcano

In the last 700 ka, the Poás volcano has risen over materials that came from the protocordillera, aphyric lavas from fissure eruptions and ignimbrite layers from the Barva volcano. All through different episodes of effusive, explosive, and erosive activity intersperse between the different units that currently made the edifice of this composite volcano. Each of these volcanic units has unique characteristics and diverse origins. Some units, like Poasito and Sabana Redonda, have origins related to extension processes in the volcano-tectonic fracture in the south part of Poás. Other units, like La Paz Andesites, Achiote and Poás Summit, have mainly effusive activity and virtually all erupted from a common central vent, typical activity of a composite volcano. On the northern flank of the Poás volcano, over the same volcano-tectonic fracture, two volcanic cones are located, the Von Frantzius and Cerro Congo, which grew from effusive and

explosive phases. During thousands of years they have been eroding constantly, with high erosive peaks likely associated with seismic activity from strike slip faults on the flanks of the volcano. Finally, on the north side of the study area, three explosive craters formed as maars and deposited the units, Bosque Alegre and Kopper (Río Cuarto), which broke up the previous lava surfaces, leaving their explosive materials around them. The genesis of the Laguna Hule maar likely occurred in these phases: first there was an aperture phase, the result of the phreatic explosions (here the lavas from Congo are projected). Next, there was a Strombolian phase. The sequence continued with phreatomagmatic explosions with pumice flows that buried artifacts dated at 6.1 Ka. After the maar created the tuff ring, a basaltic magma built the two piroclastic cones by a strombolian explosions and contemporaneous lava eruption creating small lava flows about 2.8 ka ago (Alvarado et al., 2011).

7. Geochemistry evolution of Poás volcano

The presence of two geochemical components in the lavas from Poás was reported in Gazel & Ruiz (2005). In that paper two parental magmas were defined. The Sabana Redonda Component (SRGC) (TiO_2 > 1 %) and the Von Frantzius Component (VFGC) (TiO_2 < 1 %) the rest of the data were modeled as the result of the mixing of these two types of magma. The new data from the paper Ruiz et al. (2010) confirmed the existence of these components and now we know that they are present in other Poás units. The lavas with a trend to the SRGC belong to the High-K, Calc-Alkaline series (Fig. 6). This component is present in La Paz Andesites, Río Cuarto Lavas, Poasito and some lavas from Botos crater. On the other hand, the units where the VFGC is present are located in

the Low-K, Calc-Alkaline series (Fig. 6). These units are: Main Crater, Von Frantzius, Achiote, Bosque Alegre Cerro Congo, and some lavas from Botos crater.

The two magmatic series differ in several geochemical components and cannot be related to each other by crystal fractionation. The variation diagram (Fig. 7) shows the effects of crystal fractionation where it is evident that there are two independent fractionation series, one high in TiO_2 (SRGC) and the other relatively depleted (VFGC). (The vectors show the direction of change expected from crystal fractionation in different stages.)

The ranges of major elements (TiO_2, P_2O_5) and trace elements (Zr and Ba) through time (Fig. 8) show the geochemical evolution of the Poás Volcano during the last 600 ka. This plot has a logarithmic scale to graph the ages of the units with a range from almost 600 ka and to less than 2 ka. The ages used for this diagram are the age ranges for each unit. For example, for the Botos Crater the range extends from 54 ka to 0.1 ka; the real ranges are shown in (Fig. 8). Additionally, in this graph (Fig 8), only effusive units were shown. There are hiatuses between units that will have to explain. Even though this graph is just a preliminary approach to this problem and more geochronology and geochemistry are needed, some observations can be made from it. There are units with similar age ranges that present different geochemical behaviors and, in general, opposite to each other (e.g La Paz Andesites and Sarapiqui-Achiote, Río Cuarto Lavas and Achiote, Botos high in TiO_2 and Botos low high Ti O_2). This behavior presented in the diagrams show the existence of the two magmatic components from Poás since the Paleo-Cordillera phase. There is a decrease with time for TiO_2 and P_2O_5 from the oldest unit, La Paz Andesites, followed by Achiote and finishing with the Poás Summit unit. However, between them

there are units with high values for these elements (e.g. Poasito and Sabana Redonda). Again, this confirms the presence of two different geochemical components that are independent and that came out from different vents (e.g., Sabana Redonda and Poás Summit Main Crater), as well as the same vent (e.g., Botos high and low in TiO_2) (Fig 8).

8. Discussion and conclusions

The first complete geologic map of the Poás volcano was presented by Ruiz et al. (2010), here was presented the newer version (Fig. 2). A stratigraphic reconstruction was completed using new information from the geologic campaigns in of 2008 and 2009 resulting in (Fig. 3).

The volcanic units that form the Poás volcano have ages below 700 ka. Through its volcanic evolution its lavas show the presence of two geochemical components: The Sabana Redonda Geochemical Component (TiO_2 > 1 %) and the Von Frantzius Geochemical Component (TiO_2 < 1 %), the former is related with processes that requires a relatively lower degree of partial melting, produced primarily by a decompression mechanism, which may be related to the extension generated within the Poás volcano-tectonic fracture, while the later represents magmas produced primarily by flux melting, related to subduction (Cameron et al., 2002).

The fact that these magmatic components on some occasions are clearly separated and on other occasions share and mix between the same vents, suggests that on some occasions the magmatic chambers have been separate and on other they have served to mix these magmatic components to generate intermediate compositions (Fig. 6, 7 and 8). This

magmatic process is not exclusive for Poás as similar geochemical behavior has been observed in the Irazú volcano (Alvarado et al., 2006).

9. References

Alvarado, G.E., 1984. Aspectos petrológicos-geológicos de los volcanes y unidades lávicas del Cenozoico Superior de Costa Rica.- 183 págs. Univ. Costa Rica [Tesis de Lic.].

Alvarado, G.E., 1985. Mapa geológico para el P.H. Toro II. - En: Piedra, J., Vega, O.C., Alvarado, G. & Lezama, G., 1985. Informe geológico-geotectónico de avance a la prefactibilidad. P.H. Toro II. Vol. 1 y 2; Vol 1: 156 págs. + anexos A y B.

Alvarado, G.E., 2009. Los volcanes de Costa Rica: Geología, historia, riqueza natural y su gente. - 3ª edición, XXXII + 16 laminas + 335 págs. Ed. Univ. Estatal a Distancia, Costa Rica.

Alvarado, G.E. & Climent, A., 1985. Informe sismológico para la etapa de avance a la prefactibilidad. - En: Piedra, J., Vega, O.L., Alvarado, G. & Lezama, G: Proyecto Hidroeléctrico Toro II, 46 págs. ICE, San José [Inf. Interno].

Alvarado, G.E. & Carr, M.J., 1993. The Platanar-Aguas Zarcas volcanic centers, Costa Rica: spatial-temporal association of Quaternary cal-alkaline and alkaline volcanism. - Bull. Volcanol. 55: 443-453.

Alvarado, G.E. & Salani, F.M., 2004. Tefroestratigrafía (40 000-2000 a.P.) en el sector Caribe de los volcanes Barva, Congo y Hule, Cordillera Central, Costa Rica. - Rev. Geol. Amér. Central, 30: 59-72.

Alvarado, G.E., Carr, M.J., Turrin, D.B., Swicher III, C.C., Schmincke, H.-U. & Hudnut, K.W., 2006. Recent volcanic history of Irazú volcano, Costa Rica: Alternation and mixing of two magma batches, and pervasive mixing.- In Rose, W.I., Bluth, G.J.S., Carr, M..J., Ewert, J., Patino, L.C., & Vallance, J. (eds.): Volcanic hazards in Central America, Geol. Soc. Amer. Spec. Pap. 412: 259-276.

Borgia, A., Burr, J., Montero, W., Morales, L.D. & Alvarado, G.E., 1990. Fault propagation folds induced by gravitational failure and slumping of the Central Costa Rica Volcanic Range: Implications for large terrestrial and Martian volcanic edifices. - J. Geophys. Res. 95:14357-14382.

Cameron, B.I., Walter, J.A., Carr, M.J., Patino, L.C., Matias, O. & Feigenson, M.D., 2002. Flux versus decompression melting at stratovolcanoes in southeastern Guatemala. - J. Volcanol. Geotherm. Res. 119: 21-50.

Campos, L.A., Castro, L., Gazel, E., Montes, N., Murillo, S., Ramírez, S., Ruiz, P. & Sequeira, M., 2004. Geología, geomorfología, amenazas naturales del Cantón de Poás, Alajuela.- 60 págs. Univ Costa Rica, San José [Inf. Campaña Geol.].

Carr, M.J., 2002. CAGeochem database.-http://www.rci.rutgers.edu/~carr/,consulta junio 2009.

Carr, M.J., Alvarado, G.E., Bolge, L., Linsay, F., Milidakis, K., Turrin, B., Feigenson, M. & SWISHER III, C., 2007. Element fluxes from the volcanic front of Costa Rica and Nicaragua. - Geochem. Geophys. Geosyst., 8 Q06001. DOI: 10.1029/2006GC001396

Casertano; L., Borgia, A. & Cigolini, C., 1983. El volcán Poás, Costa Rica: Cronología y características de la actividad. – Geof. International, 22: 215-236

Cigolini, c., Kudo, A.M., Brookins, D.G. & Ward, D., 1991. The petrology of Poás Volcano lavas: basalt-andesite relationship and their petrogenesis within the magmatic arc of Costa Rica. - J. Volcanol. Geotherm. Res., 48: 367-384.

DeMets, C., R. G. Gordon and D.F. Argus., 2010., Geologically current plate motions. Geophysical Journal International 181 (1), pp. 1-80 doi: 10.1111/j.1365-246X.2009.04491.x

Echandi , E., 1981. Unidades volcánicas de la vertiente N de la cuenca del río Virilla. - 123 págs. Univ Costa Rica, San José [Tesis Lic.].

Fernández, M., 1969. Las unidades hidrogeológicas y los manantiales de la vertiente norte de la cuenca del río Virilla.- Investigaciones de aguas subterráneas en Costa Rica. - Informe Técnico 27, 56 págs.

Gans, P.B., Macmillan, I., Alvarado, G. E., Pérez, W & Sigarán, C., 2002. Neogene evolution of the Costa Rican Arc. - Abstr. Geol. Soc. Amer. 2002 Annual Meeting, Denver , October 2002.

Gazel, E. & Ruiz, P., 2005. Los conos piroclásticos de Sabana Redonda: Componente magmático enriquecido del volcán Poás, Costa Rica. - Rev. Geol. Amér. Central, 33: 45-60.

Gazel, E., Alvarado, G.E., Obando, J. & Alfaro, A., 2005. Evolución magmática del arco de Sarapiquí, Costa Rica. - Rev. Geol. Amér. Central, 32: 3-13

Gazel E. Carr M. J., Hoernle K., Feigenson M. D., Szymanski D., Hauff F. and Van Den Bogaard P., 2009: Galapagos-OIB signature in southern Centraal America: Mantle refertilization by arc-hot spot interaction Geochem. Geophys. Geosyst.10,doi 10.1029/2008GC002246

Goss, A. R., and Kay S. M., 2006: Steep REE patterns and enriched Pbisotopes in southern Central American arc magmas: Evidence for forearc subduction erosion? Geochem. Geophys. Geosyst., 7, 111 B09206, doi:10.1029/2005GC001163.

Hannah, R.S., Vogel, T.A., Patino, L.C., Alvarado, G.E., Pérez, W &, Smith, D.R., 2002. Origin of silicic volcanic rocks in Central Costa Rica: a study of a chemically variable ash-flow sheet in the Tiribi Tuff. – Bull. Volcanol. 64: 117-133.

Herrstrom, E. A., Reagan M. K. and Morris J. D., 1995: Variations in lava composition associated with flow of asthenosphere beneath southern Central America, Geology, 23, 617-620, DOI:10.1130.

Hoernle K., ABT, D. L., Fisher K. M., Nichols, H., Hauff F., Abears G. A., Bogaard, P. Van Den, Alvarado G. Protti, M., and Stauch W., 2008: Arc paralel flow in the mantle wedge beneath Costa Rica and Nicaragua, Nature, 451, 1094-1097 doi: 10.1038/nature06550

Krushensky, R.D & Escalante, G., 1967. Activity of Irazú and Poás volcanoes, Costa Rica, Nov.1964/Jul. 1965. - Bul. Volcanol. 31:75-84.

Kussmaul, S., 1988. Comparación petrológica entre el piso del valle central y la cordillera central de Costa Rica. - Ciencia y Tecnología 12(1-2): 109-116.

Kussmaul, S. & Sprechmann, P., 1982. Estratigrafia de Costa Rica (América Central) II: Unidades litoestratigráficas ígneas. – Actas V Congreso Latinoamericano de Geología, Buenos Aires, I: 73-79.

Kussmaul, S., Paniagua, S. & Gaínza, J., 1982. Recopilación, clasificación e interpretación petroquímica de las rocas ígneas de Costa Rica. - Inf. Sem. IGN, 1982(2): 17-79.

Malavassi, E., 1991: Magma sources and crustal processes at the terminous of the Central American Volcanic Front.- 435 págs., Univ de Santa Cruz, California [Tesis PhD].

Malavassi, E., GILL, J.B. & TRIMBLE, D., 1990. Nuevas dataciones radiométricas del alineamiento volcánico de Poás (Costa Rica): Contribución a la evaluación de peligros volcánicos. - VII Congreso Geológico de América Central, 19-23 de noviembre de 1990, San José, Costa Rica, Programas y Resúmenes de Ponencias: s.p..

Marshall, J.S. & Idleman, B.D., 1999. $40Ar/^{39}Ar$ age contraints on Quaternary landscape evolution of the central volcanic arc and Orotina debris fan, Costa Rica. - Abstr. GSA Annual Meeting, Nº 06426.

Marshall, J.S., Idleman, B.D., Gardner, T.W. & Fisher, D.M., 2003. Landscape evolution within a retreating volcanic arc, Costa Rica, Central America . - Geology, 31(5): 419-422.

Mcbirney, W., & Williams, H., 1965. Volcanic history of Nicaragua. - Univ. Calif. Publ. Geol. Sci., 55: 1-65.

Melson, W. G., Sáenz, R., Barquero, J. & Fernández., 1988. Edad relativa de las erupciones del Cerro Congo y Laguna Hule. - Boletín Vulcanología, Univ Nacional, Heredia, 19: 8-10.

Montero, W., Soto, G.J., Alvarado, G.E. & Rojas, W., 2010. División del deslizamiento tectónico y transtensión dentro del macizo del volcán Poás, Costa Rica.-Rev. Geol. Amér. Central (en este volumen).

Montes, N., 2007. Clasificación de los suelos a partir de sus propiedades físicas, mecánicas e hidráulicas y su relación con el potencial de infiltración, en el sector occidental del cantón de Grecia, Alajuela. - 97 págs. Univ. Costa Rica, San José [Tesis Lic.].

Paniagua, S., 1985. Geoquímica de los elementos traza de las vulcanitas del Cenozoico superior de la región central de Costa Rica. - Rev. Geol. Amér. Central, 2: 33-62.

Patino, L. Carr, M.J., Feigenson, M.D.,2000. Local and regional variations in Central America arc lavas controlled by variations in subducted sediment input. - Contrib. Mineral. Petrol. 138, 265-283, doi:10.1007/s004100050562.

Peccerillo, A. & Taylor, S.R., 1976. Geochemistry of Eocene calc-alkaline volcani rocks from the Kastamonu area, northen Turkey: Contributions to Mineralogy and Petrology, v.58, p.63-81.

Peraldo, G. & Montero, W., 1999. Sismología histórica de América Central. - 347 págs. Ed. IPGH, México.

Pérez, W., 2000. Vulcanología y petroquímica del evento explosivo del Pleistoceno Medio (0,33 Ma) del Valle Central, Costa Rica.- 170 págs Univ. de Costa Rica, San José [Tesis Lic.].

Pérez, W., Alvarado, G.E. & Gans P., 2006. The 322 ka Tiribí Tuff: stratigraphy, geochronology and mechanisms of deposition of the largest and most recent ignimbrite in the Central Valley, Costa Rica. – Bul. Volcanol. 69: 25-40.

Prosser, J.T., 1983. The Geology of Poás Volcano, Costa Rica. - 165 págs. Dartmouth College, Hanover, New Hampshire [Master Thesis].

Prosser, J.T. & Carr, M.J., 1987. Poás Volcano, Costa Rica: Geology of the summit region and spatial and temporal variations among the most recent lavas. - J. Volcanol. Geotherm. Res. 33:131-146.

Ranero, C. R., A. Villasen˜or, J. Phipps Morgan, and W. Weinrebe (2005), Relationship between bend-faulting at trenches and intermediate-depth seismicity, Geochem. Geophys. Geosyst., 6, Q12002, doi:10.1029/2005GC000997.

Red Sismológica Nacional (RSN: ICE-UCR), 2009. El terremoto de Cinchona del jueves 8 de enero de 2009. -Rev. Geol. Amér. Central, 40: 91-95.

Rojas, L., 1993: Estudio geológico-geotécnico de un sector del P. H. Laguna Hule. - 42 págs. - Univ. Costa Rica, San José. [Inf. Campaña Geol.].

Russo, R. M., and Silver P. G., 1994: Trench-parallel flow beneath the Nazca plate plate from seismic anisotropy, Science, 263, 1105-1111, doi:10.1126/science 263.5150.1105

Rymer, H., Cassidy, J., Locke, C.,A., Barboza, M., V., Barquero, J., Brenes, J. & Van Der Laat, R.,2000: Geophysical studies of recent 15-year eruptive cycle at Poás Volcano, Costa Rica. Journal of Volcanology and Geothermal Research Vol 97 425-442.

Rymer, H., Locke, A.A., Borgia, A., Martinez, M., Brenes, J., Van DeR Laat, R., Willians, J., 2009: Long-term fluctuations in volcanic activity: implications for future enviromental impact. Terra Nova, Vol 21 Num 4, 304-309

Salani, M. F. & Alvarado G.E., 2010. El maar poligenético de Hule (Costa Rica). Revisión de su estratigrafía y edades. Rica.-Rev. Geol. Amér. Central, 43: 97-118.

Soto, G.J., 1994. Volcanología Física. - En: DENYER, P. & KUSSSMAUL, S. (comps.) Atlas Geológico del Gran Área Metropolitana. – Ed. Tecnol. Costa Rica: 131-146.

Soto, G.J., 1999. Geología Regional de la Hoja Poás (1:50 000) Instituto Costarricense de Electricidad: 1 hoja. – En: ALVARADO, G.E. & MADRIGAL, L.A. (Eds.): Estudio Geológico-Geotécnico de Avance a la Factibilidad del P.H. Laguna Hule. – 30 págs. ICE, San José [Inf. Interno].

Soto, G.J. & Alvarado, G.E., 1989. Procesos volcánicos asociados con el agua subterránea. El caso de los volcanes Arenal y Poás, Costa Rica. – Memoria del III Congr. Nac. Recursos Hídricos, nov. 1989, San José, 249-261.

Soto, G.J & Arredondo, S.G., 2007. Chronostratigraphic summary of Barva Formation (Costa Rica). - Abstract volume, Worshop to integrate Subduction Factory and Seismogenetic Zone Studies in Central America, junio 18-22, 2007, Heredia,

Costa Rica, p.103 (en cibersitio http://www.nsf-margins .org/Costa Rica2007/index.html)

Soto, G., Pérez, W. & Arredondo, S., 2008. ¿Cuán extensa y voluminosa es la Formación Tiribi, Costa Rica? Nuevos hallazgos y reinterpretaciones. - IX Congreso Geológico de América Central, San José, julio 2008 [Resumen].

Soto, G.J., Alvarado, G.E., Salani, F.M., Ruiz, P. & HUrtado De Mendoza, L., 2010. The Hule and Río Cuarto maars, Chapter One: The beginning. - IAVCEI Commission of Volcanic Lakes, 7th Workshop on Volcanic Lakes Costa Rica, 10-19 March 2010, Scientific Programme and Abstracts: 37.

Stuiver, M. & Reimer, P.J., 1993. Extended ^{14}C database and revised CALIB radiocarbon calibration program. - Radiocarbon, 35: 215-230.

Thorpe, C.A., Locke, G.C. &. Brown, P.W. 1981. Magma chamber below Poás volcano, Costa Rica. - J. Geol. Soc. 138: 367-373

Tournon, J., 1984. Magmatismes du Mesozoique a l'actuel en Amérique Centrale: l'exemple de Costa Rica, des ophiolites aux andésites. - Mém. Sc. Terre Univ. Pierre et Marie Curie, París, 84-49, 335 págs.

Van Der Plicht, J., Beck, J.W., Bard, E., Baillie, M.G.L., Blackwell, P.G., Buck, C. E., Friedrich, M., Guilderson, T.P., Hughen, K.A., Kromer, B., Mccormac, F.G., Bronk Ramsey, C., Reimer, P.J., Reimer, R.W., Remmele, S., Richards, D.A., Southon, J.,R Stuiver, M & Weyhenmeyer, C.E., 2004: NotCal04-Comparasion/Calibration ^{14}C Records 26-50 cal kyr BP. - Radiocarbon, 46(3): 1225-1238.

Williams, H., 1952. Volcanic history of the Meseta Central Occidental , Costa Rica . - Univ. California Pub.Geol. Sc. 29(4): 145-180.

Figure captions

Figure 1

Digital elevation map of Costa Rica, with an inset map of the Central American Volcanic front and its tectonic setting. Main volcanoes from Costa Rica are show in grey triangles. Active volcanoes also show a plume: From northwest to southeast, Rincón de la Vieja, Arenal, Poás, Irazú and Turrialba. Red rectangle denotes close-up to study area shown in Figure 2. Bathymetry is from Ranero et al. (2005).

Figure 2

Geologic map of Poás Volcano, Based on Based on Prosser 1983; Alvarado & Climent 1985; Borgia et al., 1990; Rojas 1993; Alvarado y Carr 1993; Soto 1999; Campos et al.,2004; Gazel & Ruiz 2005, Montes 2007 and Ruiz et al ., 2010.

Figure 3

Crono-stratigraphic column of the Poás units. The main and subordinated lithology are presented and its geographical position (north or south) from the main crater. The color of the units is the same from the geologic map in figure 2.

Figure 4

Hule maar. a) Interpretation of the geological features. b) DEM from LiDAR images from april 2009. c) Aerial photo taken on April 2009. d) Sketch of geologic profile (A-B-C).

Figure 5

Río Cuarto maar. a) Interpretation of the geological features. b) DEM from LiDAR images from april 2009. c) Aerial photo taken on April 2009. d) Sketch of geologic profile (A-B).

Figure 6

Rock classification diagram for the lithologic units of Poas volcano based on Paccerillo & Taylor (1976). Major elements (oxides) in %.

Figure 7

Variation diagram between % of major elements of TiO_2 and MgO. The ranges from geochemical components show its differentiation and mix. The vectors show the crystal fractionation, while the dash lines the percentages from each geochemical component

Figure 8

Variation of major elements TiO_2, P_2O_5 and traces Zr and Ba during the Poás volcano evolution. Major elements in %, trace elements in ppm.

Figure 9

Rock classification diagram for rocks from volcanic arc (based on Pacerillo and Taylor, 1979) for the Bosque Alegre Unit (Hule maar deposits and intra-maar cones), and variation of TiO2 and Zr in function of Mg for series characterization. Major elements in %, trace elements in ppm.

Figure 1

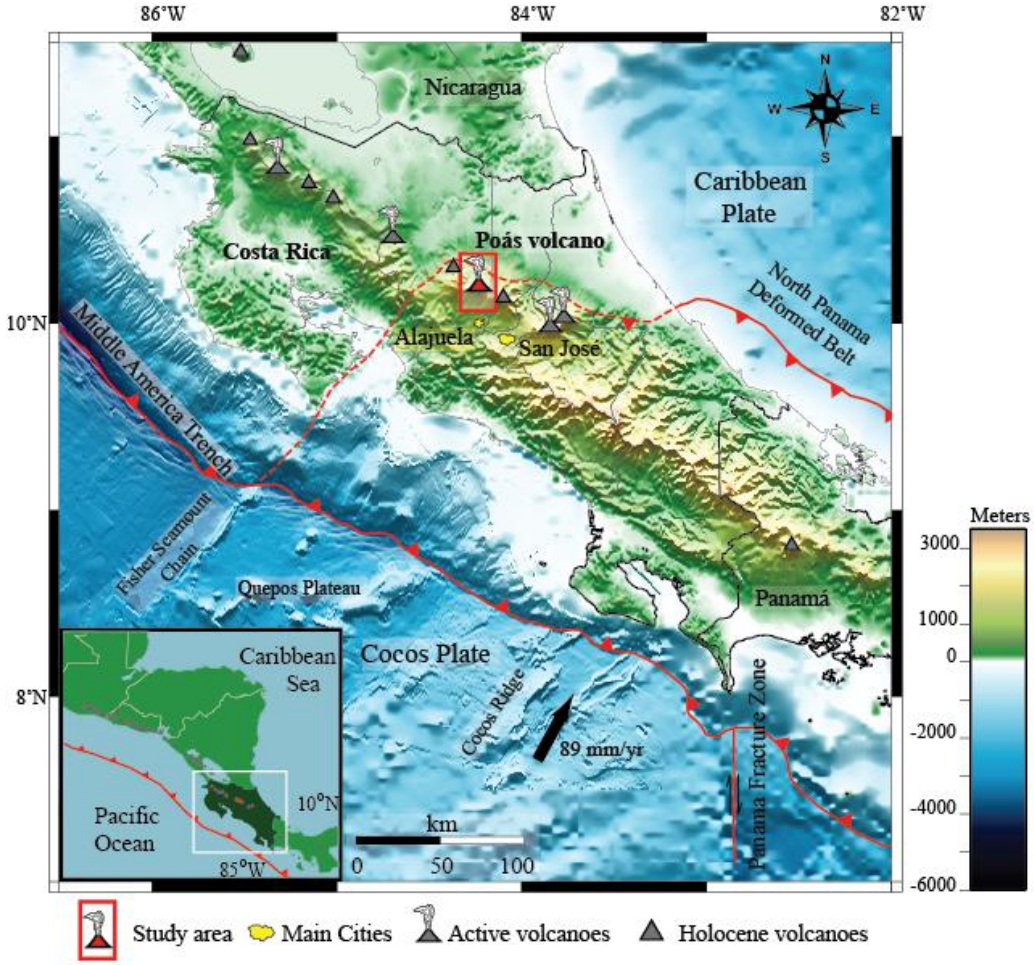
86°W
84°W
82°W
10°N
8°N
Nicaragua
Costa Rica
Poás volcano
Alajuela
San José
Caribbean Plate
North Panama Deformed Belt
Middle America Trench
Fisher Seamount Chain
Quepos Plateau
Cocos Plate
Cocos Ridge
89 mm/yr
Panamá
Panama Fracture Zone
Caribbean Sea
Pacific Ocean
10°N
85°W
km
0
50
100
N
W
E
S
Meters
3000
1000
0
-2000
-4000
-6000
Study area
Main Cities
Active volcanoes
Holocene volcanoes

Figure 2

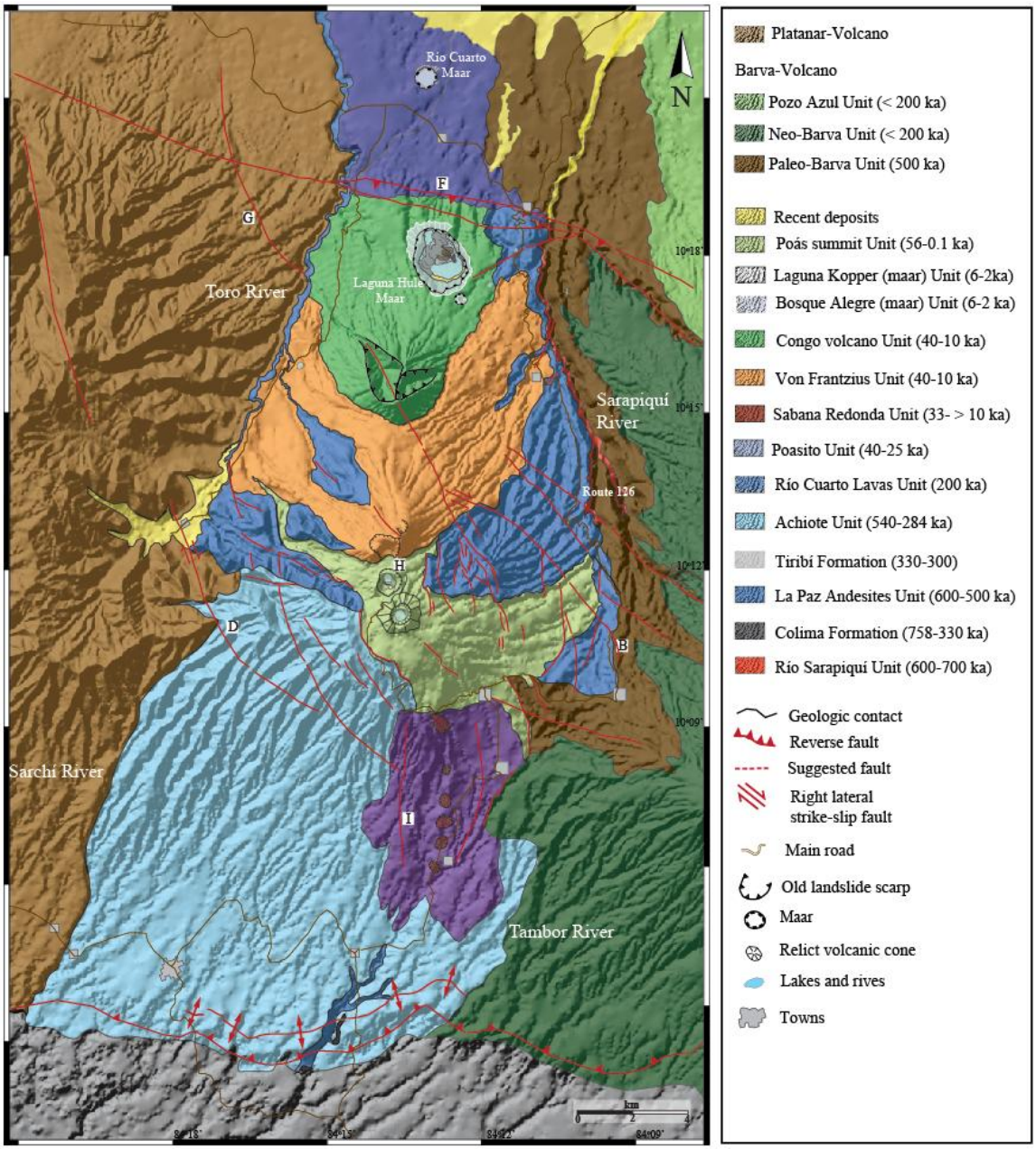
Rio Cuarto Maar
N
F
G
Toro River
Laguna Hule Maar
Sarapiquí River
Route 126
H
D
B
Sarchí River
I
Tambor River
km
0
2
4
Platanar-Volcano
Barva-Volcano
Pozo Azul Unit (< 200 ka)
Neo-Barva Unit (< 200 ka)
Paleo-Barva Unit (500 ka)
Recent deposits
Poás summit Unit (56-0.1 ka)
Laguna Kopper (maar) Unit (6-2ka)
Bosque Alegre (maar) Unit (6-2 ka)
Congo volcano Unit (40-10 ka)
Von Frantzius Unit (40-10 ka)
Sabana Redonda Unit (33- > 10 ka)
Poasito Unit (40-25 ka)
Río Cuarto Lavas Unit (200 ka)
Achiote Unit (540-284 ka)
Tiribí Formation (330-300)
La Paz Andesites Unit (600-500 ka)
Colima Formation (758-330 ka)
Río Sarapiquí Unit (600-700 ka)
Geologic contact
Reverse fault
Suggested fault
Right lateral strike-slip fault
Main road
Old landslide scarp
Maar
Relict volcanic cone
Lakes and rives
Towns

Figure 3

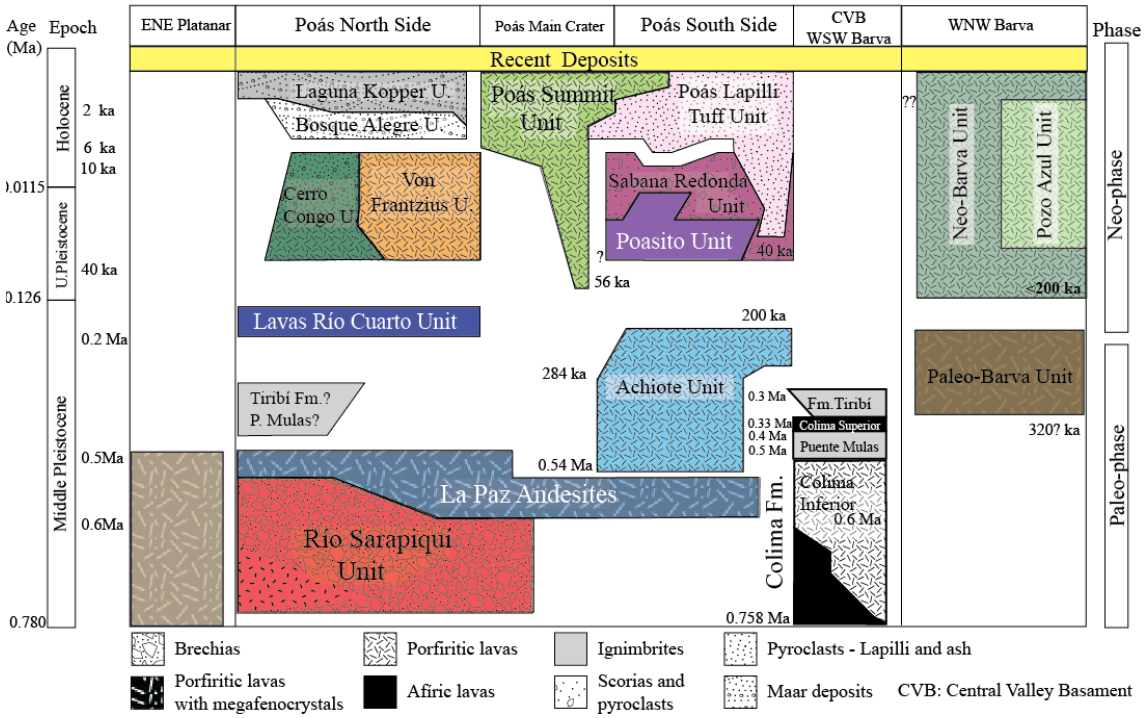
Age (Ma)
Epoch
ENE Platanar
Poás North Side
Poás Main Crater
Poás South Side
CVB WSW Barva
WNW Barva
Phase
Recent Deposits
Holocene
2 ka
6 ka
10 ka
0.0115
U.Pleistocene
40 ka
0.126
Middle Pleistocene
0.2 Ma
0.5Ma
0.6Ma
0.780
Laguna Kopper U.
Bosque Alegre U.
Cerro Congo U.
Von Frantzius U.
Poás Summit Unit
Poás Lapilli Tuff Unit
Sabana Redonda Unit
Poasito Unit
40 ka
56 ka
??
Neo-Barva Unit
Pozo Azul Unit
<200 ka
Neo-phase
Lavas Río Cuarto Unit
200 ka
284 ka
Achiote Unit
0.3 Ma
0.33 Ma
0.4 Ma
0.5 Ma
0.54 Ma
Tiribí Fm.?
P. Mulas?
Fm.Tiribí
Colima Superior
Puente Mulas
Colima Inferior
0.6 Ma
La Paz Andesites
Río Sarapiqui Unit
Colima Fm.
0.758 Ma
Paleo-Barva Unit
320? ka
Paleo-phase
Brechias
Porfiritic lavas
Ignimbrites
Pyroclasts - Lapilli and ash
Porfiritic lavas with megafenocrystals
Afiric lavas
Scorias and pyroclasts
Maar deposits
CVB: Central Valley Basament

Figure 4

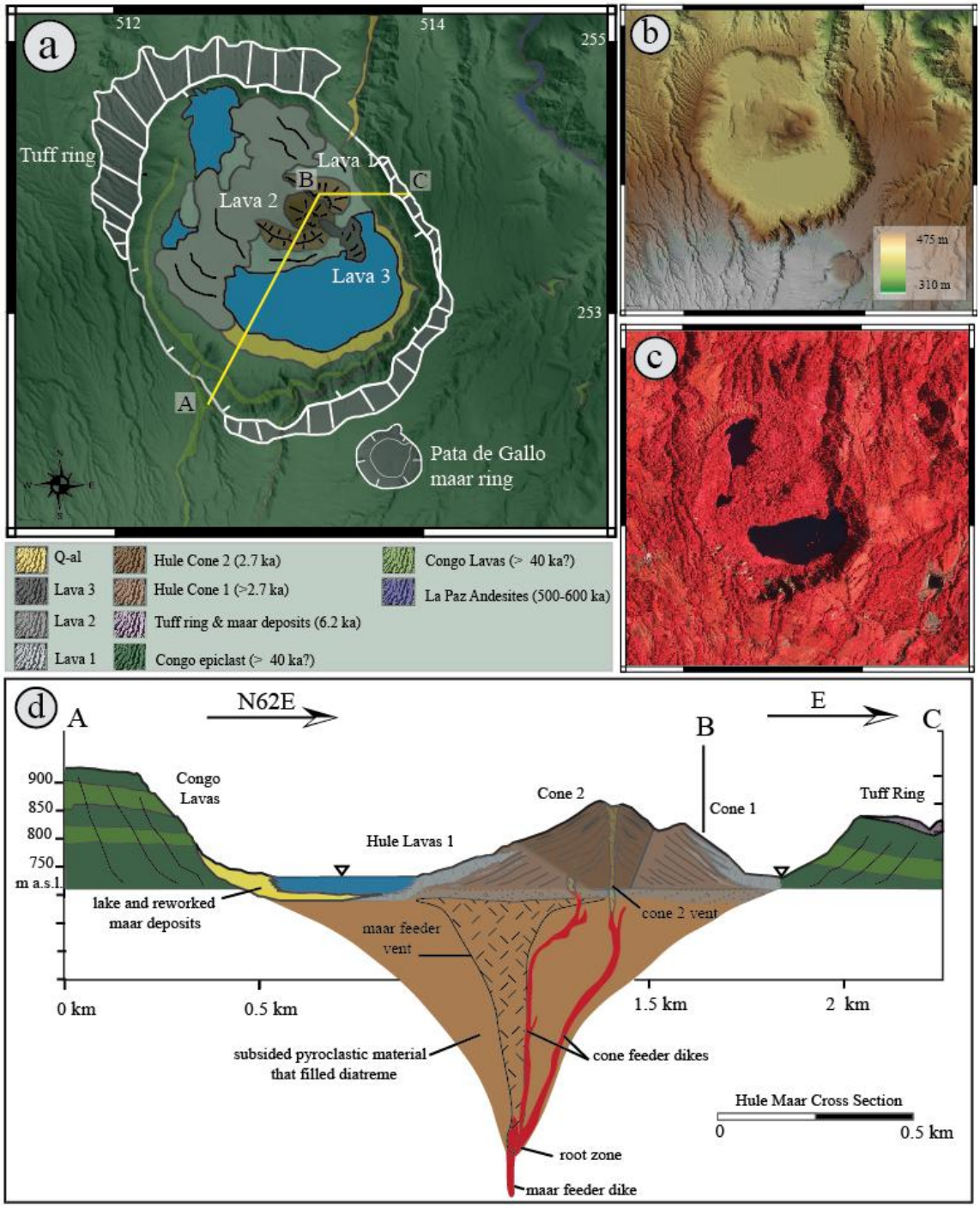
a
512
514
255
253
Tuff ring
Lava 1
Lava 2
Lava 3
A
B
C
Pata de Gallo
maar ring
b
475 m
310 m
c
Q-al
Lava 3
Lava 2
Lava 1
Hule Cone 2 (2.7 ka)
Hule Cone 1 (>2.7 ka)
Tuff ring & maar deposits (6.2 ka)
Congo epiclast (> 40 ka?)
Congo Lavas (> 40 ka?)
La Paz Andesites (500-600 ka)
d
A
N62E
B
E
C
900
850
800
750
m a.s.l.
Congo
Lavas
Hule Lavas 1
Cone 2
Cone 1
Tuff Ring
lake and reworked
maar deposits
maar feeder
vent
cone 2 vent
0 km
0.5 km
1.5 km
2 km
subsided pyroclastic material
that filled diatreme
cone feeder dikes
Hule Maar Cross Section
0
0.5 km
root zone
maar feeder dike

Figure 5

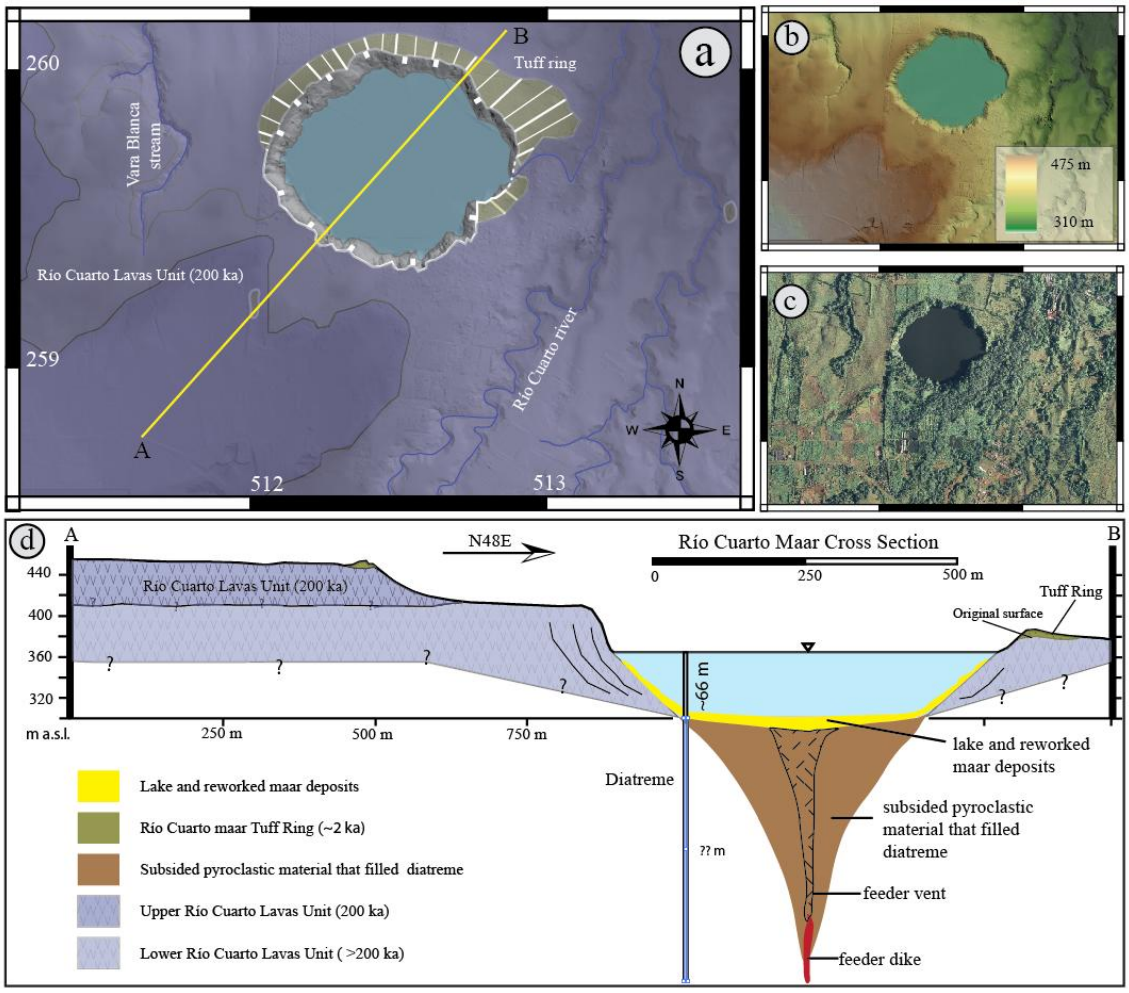
a
B
Tuff ring
260
Vara Blanca stream
Río Cuarto Lavas Unit (200 ka)
259
Río Cuarto river
A
512
513
N
W
E
S
b
475 m
310 m
c
d
A
B
N48E
Río Cuarto Maar Cross Section
0
250
500 m
440
400
360
320
m a.s.l.
250 m
500 m
750 m
Río Cuarto Lavas Unit (200 ka)
Tuff Ring
Original surface
~66 m
Diatreme
?? m
lake and reworked maar deposits
subsided pyroclastic material that filled diatreme
feeder vent
feeder dike
Lake and reworked maar deposits
Río Cuarto maar Tuff Ring (~2 ka)
Subsided pyroclastic material that filled diatreme
Upper Río Cuarto Lavas Unit (200 ka)
Lower Río Cuarto Lavas Unit (>200 ka)

Figure 6

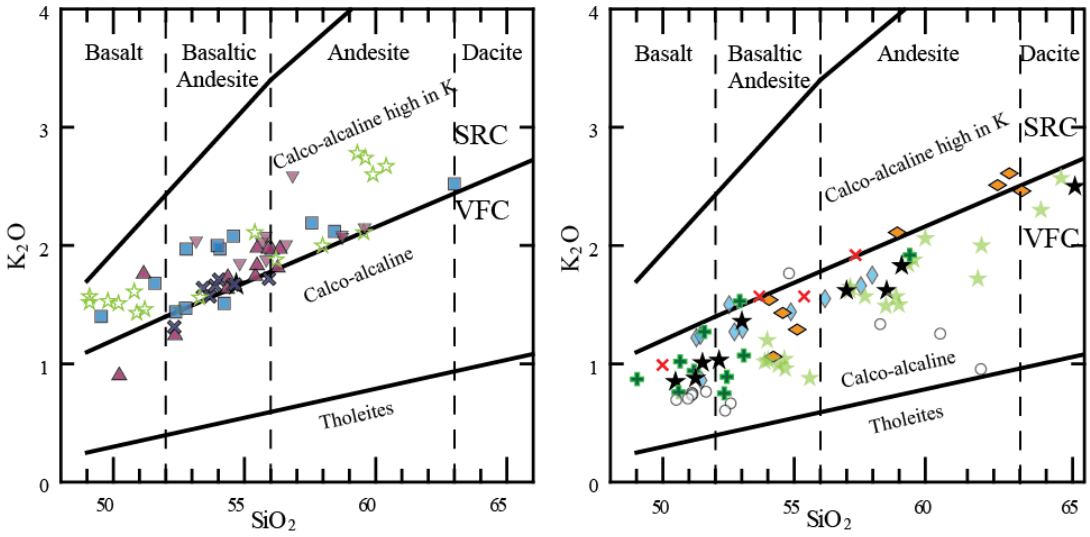

SRGC = Sabana Redonda Geochemical Component

VF = Von Frantzius Geochemical Component

- Poás Summit (Botos high Ti)
- Sabana Redonda Unit
- Poasito Unit
- Lavas Río Cuarto Unit
- La Paz Andesites Unit
- Poás Summit (Main Crater)
- Bosque Alegre Unit
- Poás Summit Unit (Low Ti)
- Von Frantzius Unit
- Cerro Congo Unit
- Achiote Unit
- Río Sarapiquí Unit

Figure 7

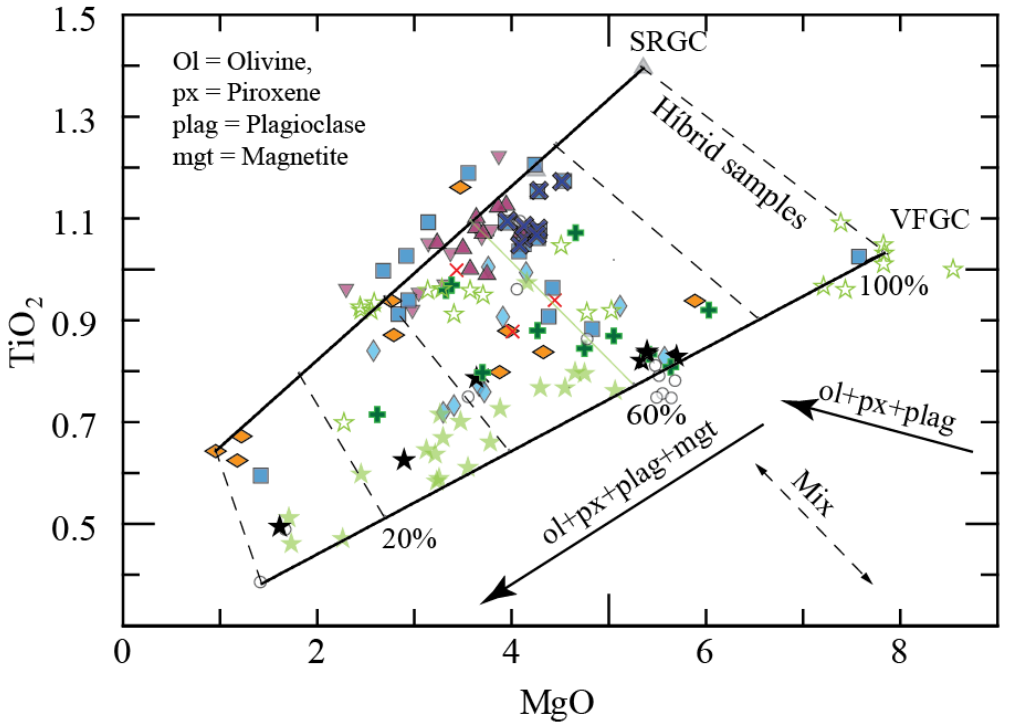

SRGC = Sabana Redonda Geochemical Component VF = Von Frantzius Geochemical Component

- ☆ Poás Summit (Botos high Ti)
- ▲ Sabana Redonda Unit
- ▼ Poasito Unit
- ✖ Lavas Río Cuarto Unit
- ■ La Paz Andesites Unit
- ★ Poás Summit (Main Crater)
- ○ Bosque Alegre Unit
- ★ Poás Summit Unit (Low Ti)
- ◆ Von Frantzius Unit
- ✚ Cerro Congo Unit
- ♦ Achiote Unit
- × Río Sarapiquí Unit

Figure 8

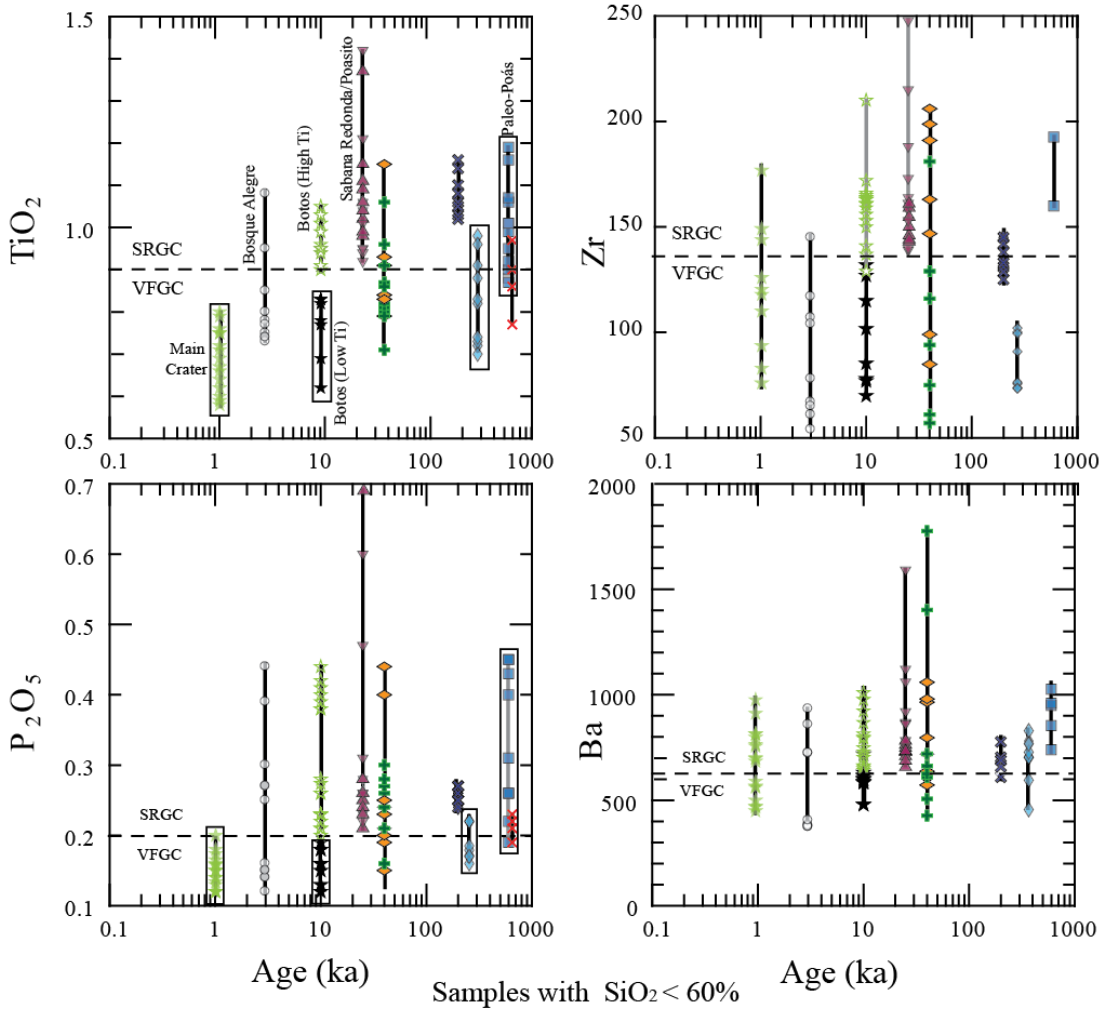
TiO2
P2O5
Zr
Ba
SRGC
VFGC
Main Crater
Bosque Alegre
Botos (High Ti)
Botos (Low Ti)
Sabana Redonda/Poasito
Paleo-Poás
Age (ka)
Age (ka)
Samples with SiO2 < 60%

Figure 9

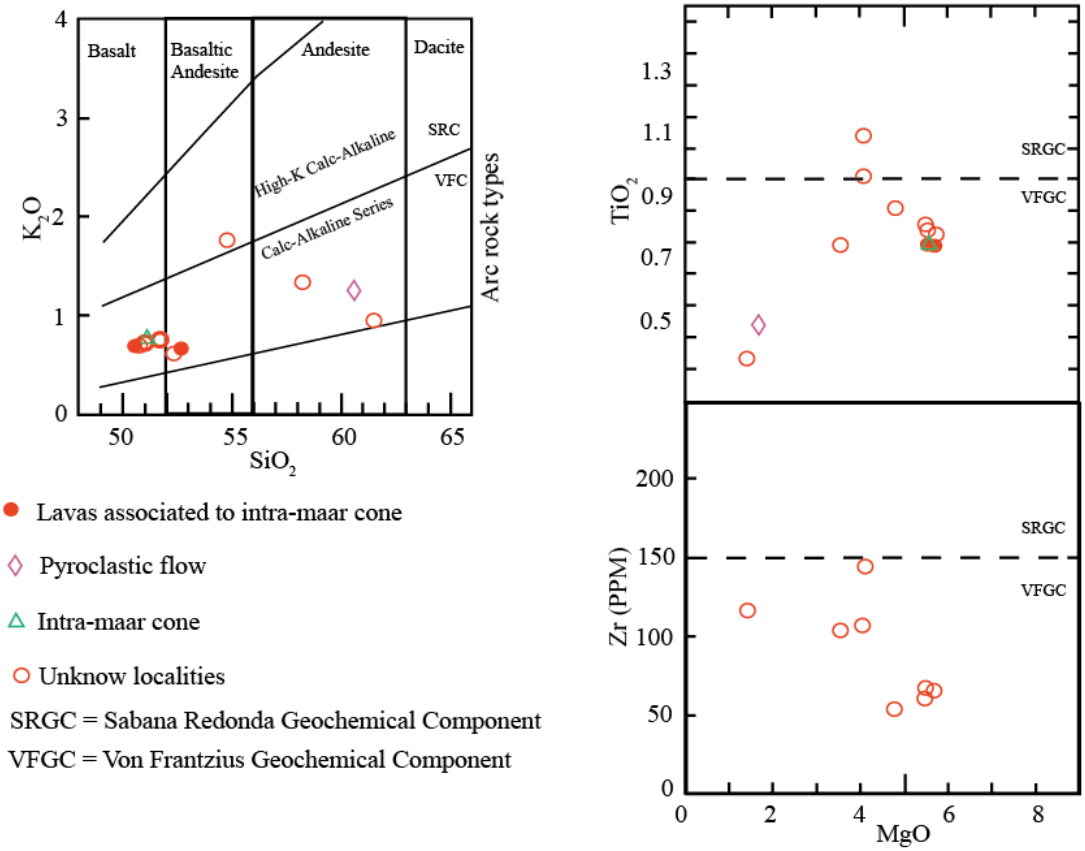
Basalt
Basaltic Andesite
Andesite
Dacite
SRC
VFC
High-K Calc-Alkaline
Calc-Alkaline Series
Arc rock types
K2O
SiO2
TiO2
SRGC
VFGC
Zr (PPM)
MgO
Lavas associated to intra-maar cone
Pyroclastic flow
Intra-maar cone
Unknow localities
SRGC = Sabana Redonda Geochemical Component
VFGC = Von Frantzius Geochemical Component

Table 1.

Age of geologic units of Poás volcano.

Unit	Method	Age (ka)	Reference and comments
Fm. Colima	$^{40}Ar/^{39}Ar$	758-330	Marshall & Idleman (1999) Marshall et al. (2003) Gans et al. (2003)
La Paz Ande U.	$^{40}Ar/^{39}Ar$	514 ± 24 527 ± 6 610 ± 36	Gans, com. oral (2004)
Achiote U	$^{40}Ar/^{39}Ar$	283 ± 15	This study
	$^{40}Ar/^{39}Ar$	538 ± 15	This study
Tiribí Fm.	$^{40}Ar/^{39}Ar$	322 ± 2	Pérez et al. (2006)
Lavas Río Cuarto U.	$^{40}Ar/^{39}Ar$	201 ± 30	Carr et al. (2007)
Congo U.	^{14}C	35.6 ± 0.6	Malavassi et al. 1990, calibrated in this study with Van der Plicht et al. (2004). possible age of its first events
Von Frantzius U.	$^{40}Ar/^{39}Ar$	41 ± 2	Gans, com. oral (2004)
	^{14}C	> 46.60	This study: the lahars above Von Frantzius in the northeast flank are older than this age.
Sabana Redonda U.	^{14}C	40.04+1.37-2.40	This study calibrated with Van der Plicht et al (2004)
Poás Summit U (Botos)	^{14}C	8.330 ± .070-0.160	Prosser & Carr (1987), calibrated and re interpreted by (1999)
	^{14}C	10.890 ± 0.300	Malavassi et al. 1990, calibrated in this study with CALIB REV 5.0.2*
	^{14}C	11.360 ± 0.250	Malavassi et al. 1990, calibrated in this study with CALIB REV 5.0.2*
	$^{40}Ar/^{39}Ar$	56 ± 4	This study
Bosque Alegre U.	^{14}C	6.2	Melson et al. (1988) y Soto (1999), re-interpreted by Alvarado & Salani (2004, 2009)
	^{14}C	2.79 ± 0.070-0.020	Malavassi et al. 1990
Poás Lapilli U.	^{14}C	40-3.3 ± 1	Prosser & Carr, 1987

*: RADIOCARBON CALIBRATION PROGRAM, CALIB REV5.0.2, ©1986-2005 por M Stuiver & PJ Reimer, disponible en: http://calib.qub.ac.uk/calib/calib.html

Table 2. Petrographic composition of the Poás volcano geologic units.

Sample code	Coordinates	Microscopic Description	Classification	Unit/ Formation
N5-27-7-04	509479 E 227279 N	Fluidal texture. Matrix (88 %) with fiame glass and flow textures and shards. Phenocrysts (4 %): Plagioclase (3%) idiomorphic and hipidiomorphic. Clinopyroxene (1 %) hipidiomorphic. Vesicles: (8 %) elongated and following flow direction.	Ignimbrite	Tiribí Formation
PO-01	518350 E 243350 N	Phaneritic porphyritic texture. Matrix: (72 %) Hyalopilitic texture with microlites of plagioclase. Phenocrysts: (28 %). Plagioclase: (15 %) megaphenocrysts idiomorphic - hipidiomorphic (2-3 cm). Olivine: 4% hipidiomorphic - xenomorphic with iddingsite. Clinopyroxene (8 %) hipidiomorphic, magnetite (1 %).	Basaltic-Andesite	La Paz Andesites Unit
R4-1/7/01-2	509881 E 260814 N	Aphanitic porphyritic texture. Matrix (94 %), Texture hyaline flow, folds and preferential direction along the long axis of phenocrysts and the matrix. Phenocrysts (6 %). Plagioclase (3-4%) idiomorphic, augite (2%) hipidiomorphic and olivine (1%).	Andesite with olivine	Lavas Río Cuarto Unit
ATN-58	503517 E 234834 N	Porphyritic hipocrystaline texture. Matrix: (80%) Intersertal texture, microlites of plagioclases in a irregular network of, augites. Phenocrysts: (20%), Plagioclases: (17%) hipidiomorphic to xenomorphic weathered, 3 x 1.6 mm. Olivine: (3%), hipidiomorphic to xenomorphic phenocrysts with iddingsite, 0.4 x 0.3 mm.	Andesite with olivine	Achiote Unit
PO-8	513400 E 233900 N	Porphyritic hipocrystaline texture. Matrix: 95 % with hyaline texture flow aspect. Phenocrysts: 5 % glomero-crystals.of plagioclases: (2%) idiomorphic. Clinopyroxene (2 %), hipidiomorphic, magnetite (1 %).	Basaltic-Andesite	Poasito Unit
SR-26704-2	513360 E 233770 N	Scoriaceous texture microlites of plagioclases in a glassy black matrix. Phenocrysts of plagioclase (1%) hipidiomorphic to idiomorphic with a max size of 0,1 mm. elongated vesicles 35 %	Vesicular bomb	Sabana Redonda Unit
C-25-3-27.45	515328 E 251361 N	Porphyritic hipocrystaline texture. Matrix: 75 % intersertal texture, microlites of plagioclase in an irregular network. Phenocrysts: (25%) Plagioclase (20%) hipidiomorphic to xenomorphic 3 x 1.6 mm. Olivine: (3%), in phenocrysts hipidiomorphic to xenomorphic with iddingsite. Clinopiroxeno (2 %) idiomorphic.	Andesite	Von Frantzius Unit
VP	511506 E 242019 N	Porphyritic holocrystaline texture. Matrix (60 %) microlites of plagioclase and augites. Phenocrysts (40 %). Plagioclase (30 %) idiomorphic. and hipidiomorphic 15 mm. Augite (4 %) idiomorphic 10 mm. Magnetite (5 %) hipidiomorphic. Olivine (1 %) hipidiomorphic to xenomorphic.	Andesite	Poás Summit (Main Crater)
PO-13-8-9-1	514538E 251368N	Porphyritic hipocrystaline texture. Matrix (97 %) Texture hyaline flow. Phenocrysts: 3 % in cluster. Plagioclases: (1%) idiomorphic. Clinopiroxeno (1 %), hipidiomorphic, magnetite (1 %).	Andesite	Cerro Congo Unit

Table 3. Geochemical composition ranges of the geologic units that are part of the Poás volcano edifice.

Geologic Unit	SiO_2	Al_2O_3	MgO	K_2O	Na_2O	TiO2	P_2O_5	Sr	Rb	Zr	Ba	Geochemical Component	Age range
Río Sarapiquí	51.4-58.9	17.4-20.7	3.4-4.4	1.0-2.0	2.9-3.2	0.8-1.0	0.20-0.23					VFGC	>0.6 Ma
Andesitas La Paz	51.5-63.5	16.7-20.1	1.4-4.8	1.3-2.5	2.5-4.0	0.6-1.2	0.19-0.47	487-733	36-58	131-193	635-854	SRGC	0.6-0.5 Ma
Formación Tiribí	50.3-56.6	18.7-20.0	1.3-4.1	1.2-2.2	2.7-3.5	0.8-1.3	0.30-0.50	200-900	50-150			NA	0.332 Ma
Lavas Río Cuarto	52.9-55.2	16.7-18.2	3.9-4.5	1.3-1.7	2.5-3.1	1.0-1.2	0.24-0.28	496-541	36-47	125-145	509-777	SRGC	0.2-0.15? Ma
Achiote	51.3-59.6	16.9-21.0	2.6-5.6	0.9-1.8	2.6-3.4	0.8-1.0	0.17-0.27	471-651	13-37	75-145	455-829	VFGC	0.54-0.20? Ma
Poasito	51.9-60.3	15.9-17.9	2.3-3.9	1.9-2.6	3.0-3.8	0.9-1.4	0.23-0.61	500-713	42-67	139-259	702-1591	SRGC	40?-25? ka
Sabana Redonda	52.1-56.9	16.6-18.6	3.2-5.4	0.9-2.0	2.7-3.3	1.0-1.4	0.21-0.70	508-582	16-57	143-161	657-781	SRGC	40-10? ka
Cerro Congo	49.6-59.8	14.7-21.0	2.6-6.0	0.8-2.2	2.4-3.3	0.7-1.1	0.16-0.30	552-746	13-40	57-129	427-662	VFGC	40-10? ka
Von Frantzius	54.3-63.7	17.2-19.6	1.0-5.9	1.1-2.7	2.6-4.1	0.6-0.9	0.15-0.44	499-804	20-73	85-206	572-1059	VFGC	40-10? ka
Poás Summit (Botos high Ti)	50.0-61.0	15.9-18.5	2.3-8.5	1.4-2.9	2.5-3.5	0.9-1.1	0.20-0.45	362-741	24-79	102-210	598-1010	SRGC	54-8 ka
Poás Summit (Botos low Ti)	51.8-65.7	16.9-19.1	1.6-5.7	0.9-2.5	2.2-3.5	0.5-0.9	0.12-0.23	451-615	16-48	70-156	480-1243	VFGC	54-8 ka
Poás Summit Main	54.3-66.1	16.2-19.4	1.7-5.1	0.9-2.6	2.3-3.7	0.5-0.8	0.12-0.20	428-697	18-71	76-177	472-976	VFGC	<1 ka
Bosque Alegre	51.3-62.6	16.8-20.9	1.4-5.7	0.6-1.8	2.2-3.9	0.4-1.1	0.12-0.44	510-789	13-50	54-145	374-933	VFGC	6 ka
Lapilli Poás	53.4-55.3	17.4-18.4	3.9-4.5	1.1-1.5	2.7-2.8	0.9-1.0	0.12-0.23	536-559	22-44	106-136	494-610	SRGC	>40 ?-10 ka

SRGC: Sabana Redonda Geochemical Component

VFGC: Von Frantzius Geochemical Component

Table 4. Geochemical composition of Bosque Alegre Unit.

Sample	PO2	P001	2	3	P09	69	123	68	244	150	592	182	141
SiO_2	51.13	50.54	51.18	52.61	62.29	51.56	51.67	51.13	50.98	54.83	52.4	58.31	61.64
TiO_2	0.75	0.73	0.82	0.74	0.48	0.77	0.78	0.8	0.85	1.08	0.95	0.74	0.38
Al_2O_3	19.64	18.83	18.89	18.44	18.14	19.16	18.97	19.18	19.05	16.64	20.74	17.85	19.46
FeO	8.99	5.35	5.11	5.16	5.58	-	-	-	-	-	-	-	-
Fe_2O_3	-	4.62	4.01	4.12	-	-	-	-	-	-	-	-	-
Fe_2O_3T	-	-	-	-	-	10.14	9.96	10.28	11.36	10.32	11.41	8.26	6.05
MnO	0.18	0.19	0.17	0.17	0.18	0.17	0.17	0.18	0.18	0.17	-	0.15	-
MgO	5.55	5.55	5.33	5.47	1.67	5.64	5.48	5.44	4.74	4.06	4.04	3.54	1.42
CaO	9.61	9.39	9.61	9.43	6.15	9.61	9.49	9.8	9.69	8.22	7.76	7.03	6.24
Na_2O	2.89	2.35	2.57	2.47	3.9	2.46	2.57	2.33	2.3	2.66	2.2	2.65	3.56
K_2O	0.75	0.69	0.94	0.66	1.28	0.74	0.76	0.73	0.7	1.76	0.6	1.33	0.95
P_2O_5	0.16	0.3	0.24	0.44	0.27	0.14	0.16	0.14	0.15	0.27	0.25	0.12	0.39

Chapter 2

Destruction of Poás volcano

This chapter resulted in one submitted paper:

Ruiz, P., Carr M.J., Alvarado G.E., Soto G.J., Mana S, Feigenson M.D.& Sáenz L.F. Coseismic landslide susceptibility analyses using LiDAR images and GIS: Coseismic landslide susceptibility analyses using LiDAR images and SIGs: The case of Poás volcano, Costa Rica, Central America. (Gomorphology), in revision.

Abstract

A landslide susceptibility model for Poás volcano was created in response to the most recent event that triggered landslides in the area (the M_w 6.2 Cinchona earthquake 1-8-2009). This earthquake was the sixth event related to destructive landslides in the last 250 yr in this area and it severely affected important infrastructure. Our study consisted of three phases 1) A post Cinchona earthquake landslide inventory which was made based on a set of high resolution LiDAR images and includes 4846 landslides. 2) A susceptibility to slide model, based on the Mora-Vahrson method http://www.eird.org/deslizamientos/pdf/eng/doc9195/doc9195-contenido.pdf, our landslide inventory, and a new modeling of earthquake triggering indicator based on the attenuation of the peak ground acceleration of the event, and 3) The evaluation of the methodology used, which for the Cinchona case resulted in an overlap of the actual landslides and the higher susceptibility zones of ~ 97%. From the four landslide

susceptibility models run in this study (the Cinchona earthquake, the M_w 5.5 Sarchí earthquake 1912, and two hypothetical earthquakes one on the Angel fault with M_w 6.0 and the other on the San Miguel fault with a magnitude of M_w 7.0), we determined that the Toro and Sarapiquí river canyons, the non-vegetated corridor located west from the main crater of Poás and the areas where the La Paz andesites Unit are located are always the zones with highest susceptibility to slide values. Meanwhile, the northern part of the study area, where the Río Cuarto Lavas unit outcrops presented always the lowest susceptibility values due to the low slope angles and low weathering level of its rocks.

1. Introduction

Volcanic edifices in Central America are exposed to high mean annual precipitation (3000-6000 mm/yr^{-1}), intense weathering, hydrothermal alteration, elevated erosion rates, and fluctuating temperatures (18-30^{o}C) typical of the tropics. These factors make them extremely susceptible to mass wasting events, which have produced damage and high death tolls in the past. The most common triggers of landslides in the area are: heavy rain (e.g., Casitas volcano Nicaragua by- Hurricane Mitch in 1998, described by Kerle and van Wyk de Vries 2001), earthquakes M_w >5.5 (e.g., Guatemala, 1976; San Salvador, El Salvador, 2001; Cinchona, Costa Rica, 2009, Bommer and Rodriguez 2002, Evans and Bent 2004, and this study) or a combination of both. Moreover, the region is known to have a disproportionally high number (at least an order of magnitude) of landslides triggered by earthquakes compared with other regions of the world (Keefer 1984, Rodriguez et al. 1999, Bommer and Rodriguez 2002 and this study). Central America is a highly populated area with ~42 million people, and many of the major cities (e.g.,

Guatemala City, Tegucigalpa, San Salvador, Managua and San José) are located near active volcanoes and/or active seismic zones (Small and Neumann 2001, Fig.1a).

Since a large number of inhabitants live near areas at risk of coseismic landslides, the study of this phenomenon based on high quality data is important to facilitate effective hazard mitigation strategies. This study focuses on the coseismic landslides generated during the M_w 6.2 earthquake of January 8, 2009 in Costa Rica, called the Cinchona earthquake (Fig. 1b and 1c). This is an excellent opportunity to study in detail one of the most recent coseismic landslide events in the region, due to the collection of a set of high quality airborne light detection and ranging (LiDAR) images obtained three months after the earthquake, together with field work immediately after the event. Our work is pioneering in the region and in the application of this technology to study coseismic landslides on the flanks of an active volcano.

Previous work on the coseismic landslides triggered by the Cinchona earthquake include: a) an aerial mapping of the landslides that occurred within the walls of the main active crater of Poás volcano (GVN, 2009), b) the geologic description of the area affected by landslides on route 126 on the eastern side of Poás volcano (Méndez et al., 2009), c) the effect of the earthquake on the road slopes near Poás volcano based on a geotechnical approach (Laporte 2009 a, b); and d) a sedimentological account of the mudflows related to this seismic event, including a preliminary map of the landslides in the Poás massif (Alvarado, 2010).

Due to the location of several hydropower projects around the area that account for 7.2 % of the total electricity production of the country, the Costa Rican Institute for Electricity

(ICE) had performed several seismological and earthquake hazard studies before the occurrence of the Cinchona event. However, no previous studies taking into account the possibility of coseismic landslides occurring in the area had been done. After the effects of the Cinchona earthquake (see below), the necessity of a study of this kind became evident.

The main objective of this work is to do a coseismic landslide susceptibility analysis of the study area in which we correlate the main factors that influence the generation of coseismic landslides induced by the Cinchona earthquake around Poás volcano and the data obtained here from our landslide catalog. The principal factors that influence the generation of landslides studied here are: type of lithology, weathering degree, slope angle, precipitation rates, ground moisture, and attenuation of the peak ground acceleration. The correlations found here, together with the historical data from past earthquakes and the most recent neotectonic studies near Poás volcano (Montero et al., 2010) are applied to estimate areas and volumes affected in past events and to determine which localities would be the most affected by landslides in future earthquakes.

1.1 Study area

The study area, shown by the black polygon in figure 1c, represents the area covered by the LiDAR images. It has a total perimeter of 94 km and encloses an area (A_{ts}) of 519 km^2. It is bordered by the coordinates $10^o7'$ - $10^o21'$north latitude and $84^o18'$ - $84^o07'$ west longitude. It covers the mesoseismic area where most of the landslides triggered by the Cinchona earthquake occurred, including the entire north flank and part of the southern flank of Poás volcano, the northwest slope of Barva volcano and part of the northeast flank of Platanar volcano.

1.2 Tectonic setting of Costa Rica and around Poás volcano

Costa Rica is located at the southern end of the subduction zone between the Cocos and Caribbean plates. The former is subducting to the northeast underneath the latter at a rate of ~83 mm-yr^{-1} in the northwestern part of Costa Rica (DeMets et al., 2010, Fig. 1a-b). The majority of earthquakes in Costa Rica are associated with subduction, the Panama Fracture Zone (PFZ), the North Panama Deformed Belt (NPDB) and crustal faults located in the interior of the country (Fig. 1b). The latter are historically the ones responsible for generating more destruction and induced landslides (Mora and Mora 1994 and Climent et al. 2009).

Platanar, Poás and Barva volcanoes are located in the Central Volcanic Range (CVR), the magmatic product of the subduction, which is partly cut by a belt of neotectonic faults named Central Costa Rica Deformed Belt (CCRDB) (Fig. 1b and 1c), defined and described by Marshall et al. (2000), Montero (2001) and Montero et al. (2010). In this zone of the country, most of the tectonic structures are right lateral faults with a northwest strike and left lateral faults with northeast strike, in which both systems present vertical components as well.

The most important tectonic structures near Poás volcano are the faults mapped in figure 1c called Alajuela, San Miguel, Carbonera, Ángel, Volcán Viejo-Aguas Zarcas, Venecia, the Poás Summit Fault System and the Volcano-Tectonic Fracture of Poás (VTFP) (Alvarado et al., 1988, Borgia et al., 1990, Soto 1999, Gazel and Ruiz 2005 and Montero et al., 2010). Based on Montero et al. (2010) the faults that affect Poás volcano could be controlled by an interaction between the regional tectonic stress and volcanic processes

(Fig. 1b and 1c). In Table 1, we present a summary of the main features of these faults and their historical activity.

1.3 Historical coseismic landslides in Costa Rica and around Poás volcano

Mass wasting triggered by earthquakes has been a recurrent phenomenon in Costa Rican history. Between 1772 and 2011, at least 19 earthquakes (M_w > 5.5) generated landslides within the Costa Rican territory, being one of the main causes of infrastructure damage from earthquakes and, since 1950, causing more human losses than the direct effects of the earthquake shaking (Mora 1985, 1989, Mora and Mora, 1994, Peraldo and Rojas 2000, Bommer and Rodríguez, 2002, Climent et al. 2009; and this study Fig. 1b and 1c, and Table 2). Only four of these 19 earthquakes that have induced landslides in Costa Rica were originated by subduction, while the rest were generated by upper crustal faults resulting into a ratio similar to the one obtained for all the Central America region by Bommer and Rodriguez, (2002) (Fig. 1b-and 1c and Table 2). Ten of these shallow (depth < 23km) earthquakes occurred near volcanic centers, three in the Guanacaste Volcanic Range (GVR) affecting Miravalles and Tenorio volcanoes and seven in the CVR generating landslides on Platanar, Poás, Barva and Irazú volcanoes (Fig. 1b). Historically, the volcanic massif of Poás volcano has been the most affected by coseismic landslides, since four of these landslide generating earthquakes occurred within the edifice of the volcano and two nearby. The Cinchona earthquake is the most recent case (Fig. 1c).

1.4 The Cinchona earthquake and its impact

The Cinchona earthquake occurred on January 8, 2009 at 13:21:34 local time (UTC- 6 h) with a magnitude of M_w 6.2. It was located only 6.5 km east from the active main crater

of Poás volcano, with a hypocentral depth of 4.5 km (RSN: ICE-UCR, 2009, Fig. 1c.). The maximum intensity reported was IX (Modified Mercalli Intensity scale, MMI) near the epicenter (Fig. 2). However, intensities of VIII-VII were dominant in the mesoseismic area (Fig. 2). The peak ground acceleration (PGA) measured was (0.67 g) at a hypocentral distance of 15 km (Fig. 2b).Field observations though suggest that values close to 1 g were reached in places near the epicenter (RSN: ICE UCR, 2009, Rojas et al., 2009, Climent and Moya 2009).

Based on the location and focal mechanism (Fig. 1c), Rojas et al. (2009) determined that the origin of the event was the rupture of 72 km^2 of the Ángel dextral strike-slip fault. No superficial rupture was found near the fault trace. However, this earthquake triggered thousands of landslides all around Poás, Barva and Platanar volcanos.

The effects caused by the coseismic landslides include environmental damage (mainly destruction of primary tropical rainforest, soil erosion and silting of rivers), damage to housing, public services, road network, agriculture, dairy cattle, tourism and casualties (29 out of 30 were caused by landslides) (Méndez et al., 2009 and this study). The total losses in infrastructure from the earthquake were calculated at more than US$ 100 million (RSN: ICE-UCR, 2009).

1.5 Geology and geomorphology setting of the affected region

Here we summarize the main features of the three volcanic edifices (Poás, Barva and Platanar) that were affected by the Cinchona coseismic landslides. In figure 3a we present the new geological map for the study area with the location of each coseismic landslide studied for our catalog. In table 3 we summarize the most important geologic and

geomorphologic features of each volcanic unit that was affected by the coseismic landslides. More stratigraphic details, geochemical and geochronological data of these volcanoes and their units can be found in Prosser and Carr (1987), Alvarado and Carr (1993), Soto (1999), Gazel and Ruiz (2005), Alvarado et al. (2009), Ruiz et al. (2010).

1.5.1 Platanar volcano

Platanar volcano (dormant) is located in the northwestern end of the CVR, about 15 km northwest of the active crater of Poás volcano (Fig. 1c). It is formed by at least one eroded caldera (Chocosuela) infilled by two young (< 0.4 Ma) volcanic centers: Platanar and Porvenir volcanoes (Alvarado 2009). These volcanic centers were subdivided in eight volcanic units by Alvarado and Carr (1993) and their products correspond to basaltic and andesitic lavas, pyroclastic flows, volcanic breccias, lahars and volcanic alluvium. In addition, on the northern flank of Platanar volcano, a group of nine Quaternary monogenetic cones called Aguas Zarcas Cinder Cones are located along a NNW trend extending ~10 km (Fig. 1c).

1.5.2 Barva volcano

The summit of this dormant andesitic composite complex is located 10 km southeast from the active crater of Poás volcano (Fig 1c). It has at least a dozen eruptive centers on its summit and several satellite cones on its northern and southern flanks (Soto, 1999, Alvarado 2009). Similar to Poás, and other volcanoes from the CVR, Barva has been subdivided into two extensive units that define the last two temporal phases, Paleo (800?-240 ka) and Neo-Barva (< 240 ka) (Soto, 1999). The products from the Paleo-Barva temporal phase are grouped into a volcanic unit called (Paleo-Barva Unit), while the products from the Neo-Barva temporal stage are divided in two units: Neo-Barva and

Pozo Azul. Segments of these three units are located within the study area and were affected by coseismic landslides (Fig. 3). More volcanic units have been mapped on Barva (i.e. Arredondo and Soto, 2006), but here we are focusing only on the ones that are located within the study area.

1.5.3 Poás volcano

Poás volcano is one of the five currently active volcanoes in Costa Rica (Fig. 1b) and is located between the Platanar and Barva volcanic centers (Fig. 1c). It was formed by the stacking of volcanic rocks during at least three principal stages (Proto-Paleo-Neo) occurring over almost one million years (Soto 1994, Soto 1999 and Ruiz et al. 2010).

Poás volcano is bounded by the canyons of the Sarapiquí river on the northeast side and Toro river on the northwest side (Fig. 1c). These rivers present narrow (~400 m wide) and profound (~250 m high) canyons with internal slopes that vary from high (45^{o}-60^{o}) to extremely high (75^{o}-89^{o}) slopes. On the southern flank, the rivers that mark the limit of the volcano are Sarchí in the southwest and Tambor in the southeast, though their river valleys are not as deep nor as wide as their counterparts on the northern flank (Fig. 1c).

1.6 Orographic regions and climatic conditions around Poás volcano

The territory of Costa Rica is cut by a magmatic range that divides the country into two orographic regions: the northeastern region (Caribbean slope) and the southwestern region (Pacific slope). These regions have significant differences in aspects that might play a significant role in the generation of landslides such as: mean temperature, type of vegetation cover, hydrology and climate, including precipitation rates (PNUD-IMN-MINAET 2009). Since the volcanoes of the CVR are part of this orographic division,

their slopes are affected differently depending on which side they are located. In general, the Platanar, Barva and Poás volcanoes are located in a tropical climate zone with annual mean temperature variations of 8^{o}C and mean temperature of 19^{o}C (Peel et al., 2007). Since the study area extends to the north and to the south from the summit of these volcanoes, then is affected by two climate zones based on the Köppen climate classification. The northern part of the study area (Caribbean slope) corresponds to a warm humid climate zone (A_f) meaning that there is variable precipitation every month and no dry season with a mean annual precipitation between 4000 and 6000 mm (Peel et al., 2007 and IMN 2008 a, b). The southern part of the study area (Pacific slope) is characterized by a tropical rain forest climate in spite of a short dry season in a monsoon type cycle zone (A_m) with a mean annual precipitation between 3000 and 4000 mm (Peel et al., 2007 and IMN 2008 a, b). The rainfall season in the Pacific slope extends from May to November. In table 4 we present the rainfall data for one year prior to the Cinchona earthquake from four meteorological stations near the study area, two of them located in the Pacific slope of Poás volcano, one near Poás summit and one in the Caribbean slope.

1.7 Land cover and soil type

Based on aerial photos obtained with the LiDAR images we define and measure five different types of land cover in the study area. These types of land cover are: primary tropical rain forest, secondary tropical rain and/or gallery forest, crops and/or farming areas, no vegetation cover areas, and water bodies (Fig. 4).

Most of the primary tropical rain forest is located within the limits of the Poás Volcano National Park (Fig. 4). The secondary forests areas correspond to zones that have

naturally recovered after being used for pasture, other zones are teak forests for industrial uses, private reforestation areas and gallery forest in the river and stream valleys. The most important activities in the crop and farming areas are pastures for dairy cattle, plantations of coffee, sugarcane and cinchona (this last plant, the source of quinine, gave the name to the town that was destroyed by the earthquake and subsequently gave its name to this event). The zones without vegetation cover are located primarily in the main active crater of Poás volcano and in a corridor 4 km long by 2 km wide west from it that, which due to the prevailing wind direction, has been exposed through years to of acid rain and acid gas emissions from the fumarole vents located inside the main crater. Also in the northern sector of the study area there are rock quarries with lavas completely exposed. The water bodies correspond mostly to crater lakes (Poás main crater, Botos, Hule and Laguna Río Cuarto) and artificial reservoirs from the hydroelectric projects within the zone (Table 5, Fig. 4).

The study area comprises soils of the type known as andisols, which have a high content of allophone clay that is the main product of the decomposition of volcanic ash in wet areas (PNUD-IMN-MINAET 2009). The allophone is a very unstable clay that gives to andisols special features such as a well defined structure which facilitates a good drainage but at the same time tends to retain a lot of the humidity. They have a low bulk density, low plasticity and low cohesion. Close to the volcanic craters, the andisols tend to have a texture that is more sandy and coarse, while in the intermediate zones its texture is more like silt and in the lower altitude zones, its texture is mostly clay.

In situ studies made after the Cinchona earthquake in different slopes of the study area showed soils with high humidity contents (as high as 82-108%), and Atterberg liquid limit values (LL) close to the unit (71-143%) (Laporte, 2009a, b).

2. Methodology

The methodology used here to create a coseismic landslide susceptibility model for the study area is a combination of heuristic and statistic methods divided in three phases, a) the creation of a landslide catalog for the most recent coseismic landslides in the area, b) the application of a heuristic model based on the Mora-Vahrson approach (Mora et al., 1992, Mora et al., 1993, 1994) with some modifications and c) the evaluation of the methodology used.

2.1 Coseismic landslide catalog for the Cinchona earthquake

The set of high resolution LiDAR used here to create our coseismic landslide catalog were acquired during an airborne survey in April 2009 by STEREOCARTO S.L. with an ALS50-II Leica system. The resolution of these LiDAR images is three points per m^2, which were used to create a digital elevation model (DEM) with a resolution of 50 cm in the x and y axes, and 15 cm the z axis.

Using the existing geological information of the area (Alvarado and Carr 1993, Soto 1999, and Ruiz et al., 2010), field observations after the earthquake and the new high resolution DEM, we created a variety of thematic maps (land use, slope, geology, and temporal phase of the volcanic units), each one with its corresponding histograms to show correlations between the theme and the occurrence and areas striped by the coseismic landslides from the Cinchona earthquake. Our results were normalized based on the % of the total study area that every parameter (land cover, slope, geology, and others) presented.

The new DEM allowed us to refine some geological contacts and interpretations previously presented in the geologic map by Ruiz et al. (2010). Based on field observations of the new outcrops produced by the landslides, we assigned a level of weathering (unweathered, slightly, moderate, badly, very badly and extremely weathered) to each volcanic unit (table 3). Due to their geomorphologycal characteristics, the Bosque Alegre and Laguna Kooper units are very similar and because most of the landslides occurred within the crater walls of these two maars, for this study we grouped these units into a single unit called, maar unit (Fig. 3).

To map the coseismic landslides from the Cinchona earthquake and create our catalog, the aerial photos taken during the acquisition of the LiDAR data were overlapped to the DEM and then each landslide was drawn over these composite images. To facilitate the mapping of the landslides, we use photos that had a false-color that is a combination of near infrared, red and green light in which the vegetation is bright red, while areas stripped by the landslides appear in the brown and dark gray ranges. The use of this false-color was more convenient than the true-color images in which it was sometimes difficult to spot the limits of the landslides. Using commercial software packages (GLOBAL MAPPER 10.0, SURFER 9.0, ROCKWORKS 14.0 and Arc Map 10) to process the images, we obtained different parameters (geographical location, slope angle, bearing of the flow, length, maximum and minimum heights, perimeter and area) directly for each landslide.

The areas measured from each mapped landslide correspond to the zone disturbed by each event. In this study we considered the disturbed zone as the sum of the detachment and deposition areas. Using the mapped landslides we created a slope failure map that

was superposed on some of the thematic maps previously mentioned to better understand the relationship between each factor and the distribution and size of the landslides.

The geographical location (latitude and longitude) for each landslide was assigned from the midpoint of the crown of each feature. The bearing of each flow was also measured from this same point. Comparing each landslide's geographical location and the thematic maps, each event was cataloged based on their position according to: orographic region (Pacific slope or Caribbean slope), land cover, volcanic edifice (Platanar, Barva or Poás), geologic unit, temporal volcanic phase (Paleo or Neo-phase) and slope angle ranges.

Based on the aerial photos, oblique pictures and field work each landslide was identified and classified using the classification of Varnes (1978) and Skinner and Porter (1992). We distinguished rock fall, slide/earth flows, slump, and debris flows, according to their type of movement and rock, soil or a combination of both according to the type of material that was removed. We also identified if the material removed entered directly or not into the drainage system (rivers and streams).

Since the study area does not have any previous LiDAR images, the measurements of the removed volume by the coseismic landslides (V_{ls}) could not be obtained directly from the actual images. Instead we used equation (1) from Parker et al. (2011) and the parameters for global relationships ($\alpha = 0.146$ and $\gamma = 1.332 \pm 0.005$) defined by Larsen et al., 2010 to obtain a volume estimation for the Cinchona event.

$$V_{ls} = \sum_{i}^{n} \alpha A_i^{\gamma} \quad (1)$$

We compared some of our parametric results (area, volume and landslides magnitude) with the coseismic events from the world catalog of Malamud et al., 2004. Our volume results for this comparison were obtained using equation (2) from Hovius et al. (1997) with $\varepsilon = 0.005 \pm 0.002$ to be in agreement with the method used by Malamud et al. (2004).

$$V = \varepsilon A_L^{1.50} \quad (2)$$

Because the LiDAR images were taken three months after the earthquake, they were not adequate to spot landslides in areas without vegetation cover due to the lack of noticeable differences between the failure slopes and the surroundings slopes. The region affected by this situation was the main crater of Poás volcano and the corridor located western from it (Fig. 4). Most of the landslides mapped in the main crater where done via aerial and oblique pictures taken days after the earthquake, some reported in GVN (2009). Based on the number and size of these intra-crater landslides, the steep slopes $>45^o$ and the proximity to the epicenter ~ 8 km we estimated a number of ~93 landslides by km^2 for the non-vegetated corridor. It is also possible that we missed mapping some landslides in various river valleys and especially the Toro river canyon because of the steep slope and tree shadows in the aerial pictures. Therefore our coseismic landslide database has an error of about 200 events, this number of small events could account for about 0.32 km^2 of the total area removed by the landslides in this study. This value was added to the sum of the areal error that each landslide presented from our measurements (0.5 % of the landslide area from each event). The error obtained for the volume was also calculated for each landslide based on the equation used (1 or 2) and the value estimated for the landslides that we miss mapping.

To compare our results with other worldwide coseismic catalogs we used the Malamud et al. (2004) data and plot (total volume of landslides triggered versus earthquake moment magnitude). Although this is a log-log plot it has a reasonably good power law dependence of the total landslide volume on the earthquake's moment magnitude. We added information to each earthquake in this plot to evaluate the geological (rock type), geophysical (earthquake type and depth) and climatic (mean annual rainfall rate) conditions in order to understand better the differences in the volumes obtained between events of similar moment magnitude.

2.2 Coseismic landslide susceptibility model

The coseismic landslide susceptibility model for Poás volcano is essentially based on the methodology proposed for the slope instability hazard method (Mora et al., 1992, Mora et al., 1993, 1994). Our model though, presents some differences from this method, which are summarized here: a) we use slope angle ranges instead of ranges for topographic gradient by unit area as proposed by Mora et al. (2002), b) the lithological susceptibility (S_l) was determined based on statistical data of the two temporal phase units (see below) and not geotechnical data, being this statistical approach in agreement with van Westen and Soeters' (2000) methodology, c) we use only one possible trigger mechanism (earthquakes), since our model is applied only for coseismic landslides and not landslides triggered by excess of rain, d) for the trigger event, we used weighted values derived from a formula for peak ground acceleration attenuation (PGAa) for crustal earthquakes (depth < 25 km) in Costa Rica, instead of values derived only from the maximum Modified Mercalli Intensity. Therefore, our method defines the slope susceptibility to

slide (H) as the product of the slope's intrinsic susceptibility (Susc) and the earthquake trigger mechanism (Earthq Trig) (equation 3).

$$H = (Susc) * (Earthq\ Trig) \quad (3)$$

Where the slope's intrinsic susceptibility is defined as the product of the lithological susceptibility (S_l), the slope angle susceptibility (S_s) and the ground moisture susceptibility (S_h) (equation 4).

$$Susc = (S_l * S_s * S_h) \quad (4)$$

The lithological susceptibility (S_l) quantifies the influence of the different geologic units in the generation of landslides. To obtain the weight values for this factor, we first grouped the units based on their temporal phases (Paleo and Neo), and their weathering level (Table 3). Although the Rio Cuarto Lavas Unit belongs to the Paleo temporal phase units, because its weathering level is nil to slightly weathered for the lithological susceptibility analysis, we used it as if it belonged to the Neo-phase units. Once all the units are grouped, and then based on the frequency and density of coseismic landslides from the Cinchona inventory for each temporal phase unit we obtained a value for their lithological susceptibility using the equations (5 to 9).

$$S_l = \frac{d1}{d2} + \frac{f1}{f2} \quad (5)$$

Where,

$$d1 = \frac{\text{Area stripped by landslides for each temporal phase unit}}{\text{Area of each temporal phase unit}} \quad (6)$$

$$d2 = \frac{\text{Total area stripped from landslides (21.98 km2)}}{\text{Total study area (519 km}^2\text{)}} \quad (7)$$

$$f1 = \frac{\text{Number of landslide in each temporal phase unit}}{\text{Area of each temporal phase unit}} \quad (8)$$

$$f2 = \frac{\text{Total number of landslides (4846)}}{\text{Total study area (519 km}^2\text{)}} \quad (9)$$

To obtain the values for the factor slope angle susceptibility S_s we created a slope angle map from the DEM based on the LiDAR data, similar to the one created for the landslide inventory. However, in this case we created a grid based on an interpolation of a point every 30 m that resulted in one data point per meter, instead of one data point every 0.5 m, to facilitate the data handling in the following steps of the methodology. The classification used to create this slope angle map is based on van Zuidam (1986) it has seven angle ranges (0^o, 0.1 – 4^o, 4 -8^o, 8 - 16^o, 16 - 35^o, 35 - 55^o and >55^o), to which weights from 0 to 6 were assigned based on Mora et al. (2002) classification.

The value of the S_h represents the prevalent ground moisture in the study area and was derived from a simple hydrologic balance based on the methodology used by Mora et al. (1992). Our hydrologic balance was made using the rainfall data of seven meteorological stations located within the study area for a time period between 1959 and 2002 (Paniagua and Soto 1986, ICE 2008 and this study). To obtain the weights for S_h we analyzed the data (mm/month) from each station and a monthly value from 0 to 2 was assigned respectively (< 125 mm = 0, 125 – 250 mm = 1 and > 250 mm = 2). Afterwards, the sum of the 12 monthly values for each station was associated to a S_h weight (0 to 5) following the classification from Mora et al. (1992) respectively (0 - 4 = 1, 5 - 9 = 2, 10 - 14 = 3, 15 - 19 = 4 and 20 - 24 = 5).

The calculation of the earthquake trigger factor is derived from a process that begins with the calculation of the peak ground acceleration attenuation (PGAa) of the earthquake that generated the landslides, the Cinchona earthquake in this case. For this step, we used the peak ground acceleration attenuation equation from Schmidt (2010) for crustal earthquakes in Costa Rica (equation 10). In which the cb variables are constant (cb1 = 0.15454, cb2 = 0.48743, cb3 = 1.03269, cb4 = 3.83891, cb5 = 0.21489 and cb6 = 0.11115), Mw = the earthquake moment magnitude, d = hypocentral distance, and the values for s and h depend on the type of soil where the formula is applied. Based on Schmidt (2010), the soil classification that corresponds to our study area presents homogeneous values of s=1 and h=0.

$$\log_{10}(\mathrm{PGAa}) = cb1 + cb2 * (M_w) + cb3 * \log_{10}\sqrt{(d^2+cb4^2)} + s * cb5 + h * cb6 \quad (10)$$

The PGAa values obtained from equation 10 for each point of the grid of the study area were grouped into the ranges proposed for each grade of the MMI scale following Wald et al. (1999) and Linkimer (2008). Finally, to transform the PGAa associated value ranges into the weight values proposed by Mora et al., 1992 for the Earthq Trig, we used an equation obtained by us for this study from an empirical regression with a logarithmic best fit.

$$\text{Earthq Trig} = 1.2597 \ln(\mathrm{PGAa}) - 1.2517 \quad (11)$$

The values of the slope susceptibility to slide obtained from the application of equation 3 were grouped in five different ranges. These ranges were obtained by dividing in five equal intervals the value obtained by multiplying the maximum value of each of the intrinsic susceptibility factors and the trigger event for the study area. Then, to each range

we assigned a classification of susceptibility, from (very low, low, moderate, high and very high). These same values and classification ranges obtained are used for all the models tested in the study area and can be applied only to this zone. Based on (Mora et al., 1992) we can expect to have landslides in zones with a hazard susceptibility level of moderate, high and very high.

2.3 Evaluation of the methodology

The evaluation of the methodology is a measurement of the degree of overlap between the coseismic landslides from Cinchona earthquake catalog and the zones from the susceptibility to slide map that have H values of moderate, high and very high. The number of coseismic landslides that occurred within these ranges was divided by the total number of landslides from the catalog. To obtain a relationship based on landslide density, we divided the total area stripped by the coseismic landslides by the total area covered by the moderate, high and very high hazard zones.

3. Data and results

In this section, we first report the results from our post-Cinchona earthquake landslide inventory. The total number of landslides (N_{Lt}) measured here was 4846, if we include the number of landslides missed during the mapping we obtain a total number of 4946 ± 100 events, however our distribution results are based only in the sampled landslides. A simple statistical approach was used to study the collected data of landslides from the LiDAR images. Our analysis includes the landslide frequency and landslide density within the areas of the analyzed factors (orographic regions, type of land cover, volcanic units, temporal phase, slope angle and distance from the epicenter). In a second section of

our coseismic inventory we present the morphometric parameters obtained including type of landslides, area, and volume to later compare the Cinchona results to data from other world earthquakes that generated landslides.

In separate sub-sections, we present the results of the landslide susceptibility to slide model of the study area and the evaluation of our methodology by recreating the Cinchona earthquake. Finally, we present the results of testing our model in three scenarios. First with a simulation of a historical event in the southwest of the study area, and later, two hypothetical earthquakes, one located in the northwest sector of the study area and other in the east side of Congo volcano.

3.1 Post-Cinchona earthquake landslide inventory

3.1 .1 Landslide distribution by orographic regions (Caribbean-Pacific)

Although the epicenter of the Cinchona earthquake is located ~4 km northern from the border line between the Pacific slope and the Caribbean slope of Poás volcano (Fig. 4a), most of the landslides (95 %) are located in the Caribbean side (Table 4 and Fig. 4). This irregular distribution could be explained based on different factors like geology, slope angle, and soil saturation between these two orographic regions. In the following sections we analyzed in detail all these factors, while here we focus in the differences in precipitation rates between the two slopes, using it as an indirect measurement of soil saturation in the study area.

During November and December of 2008, Costa Rica was directly affected by at least seven atmospheric events (five cold fronts, one low pressure system and one trade wind system) and was indirectly affected by the Paloma Hurricane (IMN, 2008 a, b). These

events generated precipitation rates above average for these months, in three regions of the country (Northern, Caribbean and Central) (IMN-CR 2008 a, b). Based on the rainfall data of the stations close to the study area (table 4), historical accounts since 1961 (PNUD-IMN-MINAET, 2009), and additional information from IMN (2008 a, b) we determine that the surplus of rain for November and December 2008 in the study area was between 15 % and 50 %. This surplus was more obvious in the Pacific slope and near the summit of Poás volcano than in the Caribbean slope, because normally by November-December the Pacific slope of the Poás volcano is already influenced by dry season conditions, while the Caribbean side usually experiences its maximum amount of rain during the year.

By January 8th when the Cinchona earthquake occurred, the Pacific slope was already showing the normal conditions of the beginning of the dry season, while the Caribbean slope was experiencing the typical high amounts of rain during that time of the year. The total accumulated rain measured in La Selva de Sarapiquí meteorological station (~25 km northward of the epicenter, Fig. 1c, Caribbean slope) 12 months previous to the Cinchona earthquake was 3994 mm. The same station recorded 435 mm of rain one month before the event (Table 4). Meanwhile, the meteorological station located in San Rafael de Poás (~15 km southward of the epicenter Fig. 1c, Pacific slope) recorded 4796 mm for the year previous the earthquake but only 13 mm for the month before the event (Table 4). Therefore, the level of the ground water table was shallower near the summit and especially in the Caribbean slope. On the Caribbean side a high ground water table could have influenced the slopes failures. However, on the Pacific slope this is unlikely.

3.1.2 Landslide distribution by type of land cover

The majority and the most extensive landslides occurred in areas that were covered by primary tropical rain forest, which is the second most common land cover of the study area (Fig. 4). Most of this land cover is located on the Caribbean slope and near the epicenter of the earthquake (Table 5 and Fig 4). We also noted that the density of landslides that occurred in zones where the rocks are completely exposed is less reliable because a) we were not able to map all the landslides that occurred in these zones and b) their size is relatively small (Table 5 and Fig. 4).

The soils in areas covered by tropical rain forest act as sponges and retain high levels of moisture (Bonell et al 1981). Because the epicentral area got a considerable amount of rain during the whole year and especially in the two months previous to the earthquake, the dense canopy favored the generation of landslides by retaining more moisture in the soils. Other cases of widespread stripping of saturated superficial materials and jungle cover from steep slopes by coseismic landslides in other humid tropical areas are: New Guinea 1935 and 1970 (Marshall 1937 and Pain 1973), Panama 1976 (Garwood et al., 1979) and Ecuador 1987 (Schuster 1996). It is well known that forest and vegetation cover can prevent landslides and erosion, however due the high peak ground acceleration near the epicenter (0.67 to about 1g) the expected protective effect of the forest cover was not observed, at least close to the epicenter (0 to 5 km)

3.1.3 Landslide distribution by volcanic edifice

The volcanoes from the CVR that were affected by the Cinchona landslides were Poás, Platanar and Barva. Because the epicenter was located on the north flank of the Poás volcano, the edifice of this volcano was the most affected, presenting the majority and

biggest landslides of the study area (Table 6 and Fig. 3). Barva volcano was the second most affected and Platanar volcano was the least affected having the fewest and smallest landslides (Table 6 and Fig. 3). Although the study area encloses more area of Poás volcano and only portions of the Platanar and Barva volcanoes (Table 6 and Fig. 3), the occurrence of landslides on these last two edifices outside the limits of the study area was reduced and mainly located on steep slope zones near their summits.

3.1.4 Landslide distribution by volcanic unit

Based on the detailed geologic map of the study area (Fig. 3), we conducted a more careful analysis of the incidence and area affected by the landslides based on which volcanic unit they occurred in. From the three volcanoes affected by the event, a total of 13 volcanic units presented landslides (Table 7 and Fig. 3). From N_{Lt}, the three volcanic units with higher landslide frequency are: La Paz Andesites Unit, Paleo-Barva Unit and Poás Summit Unit. Because the epicenter of the earthquake was located almost between the La Paz Andesites and the Poás Summit units (Fig. 3) the high frequency of landslides on these units is understandable. Furthermore, other factors like steep slopes (see below), high weathering level, hydrothermal alteration and the presence of several active faults on the La Paz Andesites unit (Fig. 3) could also play an important role in the high frequency of landslides on this unit. The Paleo-Barva Unit is located close to the epicenter as well and it has a weathering level similar to La Paz Andesites unit, these might be the main reasons to explain its high landslide frequency too (Table 7 Fig. 3).

The three volcanic units that presented the most extensive landslides are: La Paz Andesites, Congo volcano and Von Frantzius units (Table 7 and Fig. 3). The differences between the frequency and the areal approaches can be explained by the fact that in

Congo volcano and Von Frantzius units there were more events of the type known as debris flows than in Paleo Barva and Poás Summit units. Debris flow events tend to cover more area than the less complex slide/earth flows or slumps events because they travel farther distances.

Although the Platanar unit had a significant number of landslides they were relatively small and their contribution in the total area affected by landslides is relatively small, especially if we compare it to the Congo volcano Unit that presented a similar frequency of landslides but had landslides that were much bigger and stripped about nine times more area (Table 7 and Fig. 3).

3.1.4 Landslide distribution by volcanic temporal phase units (Paleo-Neo)

Because of the stratigraphic control we had on the Platanar, Barva and especially on the Poás volcanic units based on Ruiz et al. (2010), we were able to compare the occurrence of landslides from two major temporal units (Paleo-Stage units: older than 0.2 My or Neo-Stage units: younger than 0.2 My) (Table 8 and Fig. 5). This approach was done because of the significant differences in geomorphology and weathering level between these age groups (Fig. 5 and Table 3). From N_{Lt}, 65% occurred in Paleo temporal stage units, while the remaining 35% occurred in Neo temporal stage units (Table 8 and Fig. 5a-e). However, some of the landslides that occurred in the Neo stage units were relatively big and the area relationship between the Paleo and Neo stage units is not as disproportionate as the frequency of landslides (Table 8 and Fig. 5a-e).

3.1.5 Landslide distribution by slope angle

The study area is characterized by having slope angles that range from 0 to 90^{o} (Fig. 6a). By using ranges of 15^{o}, we obtain six different slope angle sub-ranges. The area covered by these sub-ranges in the study zone decreases as the slope angle values increase (Table 9 and Fig. 6a). As might be expected, steep slopes generate a high frequency of landslides. However the frequency of landslides shown by Cinchona earthquake presented an apparent Gaussian distribution with the highest number of landslides in the slope ranges between (30^{o} and 59^{o}) (Table 9 and Fig. 6b, c). This apparent Gaussian distribution is the result of not having large enough areas covered by slopes with angles > 60^{o}. This makes the estimated landslide frequency for these slope bins less reliable. Otherwise, the landslide frequency strongly increases with slope. Meanwhile the small areas of landslides that occurred in slopes with angles < 30^{o} is understandable since these low angle slopes are less susceptible to slide and are located far from the epicenter. There is a relationship between the landslides that occurred in slopes with angles > 75 and the type of material that they involved, since most of them removed only rock (see below).

3.1.6 Types of landslides and types of material that they involved

From the N_{Lt}, 53% presented translational movement (slides/earth flows), 35% were rotational events (slumps), 10 % corresponded to debris flows and only 0.4 % were recognized as rock fall events (Fig. 5f-h and Table 10). This last type of landslides were located as expected in areas where the bedrock is completely exposed and where the slopes are very steep > 60^{o}. The remaining 1.6% of landslides could not be recognized because they occurred next to roads that were stabilized by machinery just weeks after the earthquake before the LiDAR images were taken.

We determined that most of the landslides involved displacements of andisols. Besides the typical characteristics of these soils previously described, the soils here also include recent ashes (brown tuffs), and older ashes (orange and yellowish tuffs). In some cases a combination of soils and rocks also occurred in the displacement of material. Alvarado (2010) reported that some of the debris flows included lava blocks (mostly boulders) and mega clasts of ignimbrite blocks as big as 5 m x 4 m x 9 m. Just a few of the coseismic landslides removed only rock and they were located within the walls of the main crater of Poás volcano and in some areas of the Toro river canyon where columnar lavas are exposed in cliffs as high as ~50 m and with slopes angles > 75^{o}.

3.1.7 Distance to the epicenter

From N_{Lt} about 49 % are located within a radius of 5 km from the epicenter of the earthquake (Fig. 7a). The attenuation of landslide density in five kilometer windows from the epicenter exhibits a logarithmic trend from the epicenter to as far as ~21 km (Fig. 7a and b). Outside the study area, small and isolated landslides occurred as far as 35 km from the epicenter in places with steep slopes, primarily in river valleys and near the summits of Barva and Platanar volcanoes.

3.1.8 Area and volume removed from the coseismic landslides

The total disturbed area from the landslides that we measured (A_{Lt}) in the study area was 22.14 ± 0.27 km^2, an area equivalent to ~ 2020 soccer fields with the maximum official dimensions. The disturbed area most likely was removed in less than 8.2 seconds, which was the duration of the strong movement of the earthquake in the mesoseismic area (Climent and Moya 2009), resulting in an average of 2.7 km^2 per second.

Single landslide areas ranges from 10.91 m^2 to more than 671,700 m^2 with an average of 4,500 m^2. As shown in figures 4, 5, 6 and 7c the largest landslides did not occur close to the epicenter, but are actually located between 4 km and 18 km from it. Most of these large landslides are debris flows that occurred in the Congo volcano and Von Frantzius cones (Neo-temporal Units). Debris flows accounted for 36% of the total slope failure area measured in this study (Table 10 and Fig. 5f-h.). The Congo volcano and Von Fratzius cones are characterized by steep slopes between (30^o and 60^o) covered by a thin layer of volcanic soils no greater than five meters with fresh lava flows underneath (Table 3). These lava flows worked as sliding surfaces for the debris flows that traveled for several kilometers and affected large areas.

We estimate that the landslides from Cinchona earthquake produced ~ 0.24 ± 0.0013 km^3 - 0.39 ± 0.1017 km^3 of erodible material (depending on the equation (1) or (2) used to calculate the volume). By analyzing the aerial pictures, we also determined whether the material removed from the landslides entered directly into the drainage system (rivers and streams) or if it was deposited on the volcano's flanks without direct access to river valleys or streams. From N_{Lt} only ~20 % of the landslides did not enter directly into the drainage system leaving almost all these materials just meters away from where it came from, since the size of most of these landslides were small they only account from a volume between 0.047 $km^3$and 0.0087 km^3. The remaining 80 % of the landslides occurred in the river valleys walls and/or in the river headwaters which have direct access to the streams. Alluvial processes will eventually carry these materials out from the volcanoes and transport them into different basins.

However this does not mean that all the material removed by the landslides that entered into the drainage system was transported outside the volcano. An exception could be the mud flows, but not even these events rapidly remove all the material that mobilized. Alvarado 2010 estimated a minimum volume between 2.5 x 10^{-3} km^3 and 3.5 x 10^{-3} km^3 of material that got out from the volcanic system through the mud flows (lahars) that occurred minutes and days after the earthquake.

Using a volume of 0.3 km^3 per event, a 50 yr return period for earthquakes (Mw >5.5 - 6) and 20 km length of arc segment, we calculated a mass flux from coseismic mass wasting of ~ 300 ± 150 km^3/km/Myr, a rate comparable to estimates of magma flux at arc volcanic systems (Holbrook et al., 199, Clift and Vannuchi 2004 and Carr et al., 2007). The same recurrence interval yields an average erosion rate due to landslides of 0.19 to 0.75mm/yr given an area of 519 km^2. However estimations of the amount of material that remain in the edifice are still needed.

3.1.9 Comparison of the Cinchona event with other coseismic worldwide events

Using the equations for landslide event magnitude (m_L) proposed by Malamud et al. (2004) based on the (N_{Lt}) or the (A_{LT}) we got values for m_L of 3.68 and 3.85 respectively for the Cinchona earthquake. By comparing our (m_L) results with an analogous event (Mammonth Lakes, CA, USA earthquake, 1980) which had the same moment magnitude (M_w 6.2), a similar focal mechanism solution (right lateral slip) and focal depth (8 km) (Julian and Sipkin 1985 and Malamud et al 2004), we realized that if the m_L is compared based on total number of landslides, the Cinchona event result is very similar to the Mammoth Lakes event which had a N_{Lt} of 5253 (Malamud et al. 2004). However if the m_L is compared based on the total area affected by the landslides our result differs

significantly because the Cinchona earthquake removed a total landslide area at least one order of magnitude greater than the Mammoth Lakes event. The same amount of difference is noticeable between these events in the binary plot of earthquake moment magnitude versus volume removed (Fig. 8). With additional information included to the original plot from Malamud et al. (2004), we found that there are significant differences in the mean annual precipitation rates between the region of Poás volcano (3000 and 6000 mm) and Mammonth Lakes (1000 and 2500 mm) that could help to explain the area and volume differences. These rainfall rates at Poás are sufficient to produce a high level of moisture in the soils that as we observed in this landslide catalog, facilitated the generation of debris flows events which contributed to about 36% of the total area stripped in the Cinchona event (Table 10). Meanwhile the occurrence of this type of landslides is not considered normal in higher latitude zones with lower rainfall levels. We also suggest that the intense weathering and thick regolith soils at volcanic edifices in tropical regions could help to explain why the Poás's landslides removed more material than the Mammonth Lakes event.

By using the difference between the expected volume removed for a 6.2 M_w magnitude earthquake (best fit line) and the results obtained here for the Cinchona earthquake in the plot earthquake moment magnitude versus volume removed (Fig.8), we created a range where the other five historic events near Poás volcano from table 2 may be located. Based on what we observe in this study, we differentiated the historical earthquakes that had same moment magnitude using their differences in location (Pacific or Caribbean slope) and time of the year when they took place. The events located in the north and central region of the Poás volcano are going to present higher frequency, density and volume

removed by the landslides than the ones located in the southern flanks and that occurred between January and May which corresponds to the dry season.

3.2 Coseismic landslides susceptibility model for the Poás volcano

The results and analyses of the slope's intrinsic susceptibility factors (S_l, S_s and S_h,), the earthquake trigger event (Earthq Trig) and the susceptibility to slide (H) are presented in this sub section. These results are presented in maps and tables within the maps (Fig. 9 and 10) showing the ranges and weight values used for each factor in our susceptibility model. The maps were created using a grid of ~ 1100 pixels per km^2 in which each pixel presents the values obtained from each factor from the equations (3 to 11), to fill the spaces between pixels, a triangulation with linear interpolation was applied for each map.

3.2.1 Lithological susceptibility (S_l)

Because of the differences in frequency and density of coseismic landslides observed in the Cinchona event between the Paleo and Neo phase and described in the previous sub section units, we selected these two temporal phase units to obtain the lithological susceptibility factor for the study area. By doing a statistical approach following the equations (5-9) we obtained that the S_l for the Paleo-phase units is 2.22 while and that for the Neo-phase units this factor presents a value of 1.72 (Fig. 9a). The first weight value covers 49.35 % of the study area and the second weight value 50.65%.

3.2.2 Slope angle susceptibility (S_s)

The results for this factor were obtained directly by first transforming the altitude values from the LiDAR based DEM into the slope angle ranges suggested by Van Zuidam (1986). Then each slope angle value was grouped and transformed into the S_s weights

values from 0 to 6 based on Mora et al. (2002) classification (Fig. 9b). From the slope angle susceptibility map (Fig. 9b) we observed that the distribution for each class of the range of values for Ss is: (0 = 0.05%, 1 = 6.30%, 2 = 10.90 %, 3 = 21.22 %, 4 = 40.18%, 5 = 19.03 % and 6= 2.32%).

3.2.3 Ground moisture susceptibility (S_h)

Based on the simple hydrologic balance executed for this study following the methodology proposed by Mora et al. (1992), we observed that our study area presents only two zones for ground moisture susceptibility which are $S_h = 4$ and $S_h = 5$. The distribution of the zones affected by these two ranges is not proportionate since about 97 % of the study area presents values for $S_h = 5$ (Fig. 9c). As mentioned before the Caribbean side of the CVR presents higher rainfall rates than the Pacific side. The Fraijanes meteorological station (FRA) located on the Pacific slope (Fig. 9c and Table 11) is the only station from the seven studied here that showed the significant differences between the Pacific and the Caribbean rainfall rates based on our hydrologic balance. This station has a short dry season between the months of January to April and the amount of rain in this time period never exceeded 150 mm/month, meanwhile the rest of the stations had values between 150 and >250 mm/month during the entire year (Table 11).

3.2.4 Earthquake trigger (Earthq Trig)

The result for this factor was obtained using the methodology proposed in this study (equations 10 and 11). The main idea of this new methodology consists in using data from the earthquake (location, depth, moment magnitude) that generated the landslides and transform that data into weight values for the earthquake trigger factor. The main

difference from previous susceptibility models is that the final result is not a unique value, based on the maximum intensity for the study area in the last 100 years. In contrast our result is a range of values that attenuate from the source of the event following a similar trend described by the attenuation of the peak ground acceleration values that were calculated with the data from the earthquake.

Using the Cinchona earthquake data, M_w = 6.2 and depth = 4.5 km in the equation 10, we obtained a maximum value for the PGAa = 392.92 m/s^2 that correspond to the earthquake epicenter location, therefore by using the equation 10 to calculate the PGAa for each pixel location (latitude-longitude) in our map grid, we obtained different values for the PGAa that decrease as the pixels are located away from the epicenter and in this way we were able to model the attenuation of the PGA in the study area. The lowest value for PGAa obtained using equation 10 within the study area was (92.52 m/s^2). Thus the PGAa values obtained for the Cinchona event gave us a range from 392.92 to 92.52 m/s^2. Using the ranges for the relationship between peak ground acceleration and the Modified Mercalli Intensity scale from Linkimer (2008) for MMI < VII and Wald et al. (1999) for MMI > VII we obtained the earthquake trigger values that depend on the values of MMI following the classification from Mora et al., 1992. Based on the range of values of PGAa for the Cinchona event, we got intensities from VIII to VI and trigger weight values that attenuate from 6 to 4. Using equation 11, we obtained the relationship between the peak ground acceleration attenuation ranges and these trigger values. Therefore, we were also able to obtain a specific value for the earthquake trigger factor for each pixel in the study area, modeling in this way the attenuation of earthquake trigger factor and making our susceptibility model more realistic (Fig. 9d).

3.2.5 Slope susceptibility to slide (H)

Following the equation (3), we obtained the slope susceptibility to slide values by multiplying the intrinsic susceptibility factors by the earthquake trigger values of Cinchona event. The values obtained for each of the three factors of the intrinsic susceptibility to slide could be considered fixed for the study area, unless they are obtained using a different methodology. The only factor that could change in the area is the trigger event as it depends on the earthquake location and its magnitude. By using the maximum possible value for each of the four factors used to calculated H we obtained the upper limit for the range values of H, the lower limit is = 0 and this happens only if the slope angle of a certain place is zero. Therefore, the range limits for H and their classification in the study area using our susceptibility to slide model with its corresponding classification following the same five categories proposed by Mora et al. (2002), are: 0 - 93.24 = very low, 93.24 - 186.48 = low, 186.48 - 279.72 = moderated, 279.72 - 372.96 = high and 372.96 - 466.2 = very high. Using these categories we created a landslides hazard map for the Cinchona event (Fig. 10a), which shows the relative hazard. It does not quantify the absolute hazard.

In the landslide hazard map for the Cinchona event (Fig. 10a), the areas classified as very low correspond to 10.10% of the total area and are mostly located in the north sector of the study area where the Rio Cuarto Lavas Unit is situated. Factors like distance from the epicenter, low slope angles values and unweathered rocks determinate the low susceptibility to slide values for this region. The areas classified as low susceptibility correspond to 33.72 % of the study area and are located in the lower flanks of the Congo volcano and Von Frantzius Units and southern sector of the Botos cones. Most of the

study area corresponded to the classification moderate (45%), nearly all the area covered by the Paleo-phase units and the steep zones of the Neo phase Units have this zonation or higher. The distribution of the high and very high zones are 10.70% and 0.48% of the total area, and are almost exclusively located in the sector where the La Paz Andesites Unit (Paleo phase) is located, this includes the epicentral area and the river canyons of the Sarapiquí and Toro rivers.

3.3 Methodology evaluation

Considering that coseismic landslides normally occur in zones classified as moderate, high and very high susceptibility to slide, we performed a statistical analysis to evaluate our methodology. The area from our model where we expect slides comprises 291.57 km^2~ 56% of the total study area. From the Cinchona landslide catalog, we found that 97.10% of coseismic landslides studied are located within the moderate to very high susceptibility to slide zones. If we do the same kind of analysis but just for the zones classified as high or very high susceptibility we obtained that from N_{Lt}, 48.95 % are located within these higher susceptibility zones, which comprise only about 11% of the total study area. The ratio between the area stripped by the Cinchona landslides (21.98 km^2) and the area that resulted from our model as moderate high and very high susceptibility to slide (~ 293 km^2) is 0.075. This means that our susceptibility model can determinate satisfactorily the zones where the landslides are going to occur but, there is not a good correlation between the size of the area stripped by landslides and the area of the high susceptibility zones.

Some of the Cinchona coseismic landslides located in the very low and low susceptibility to slide zones are located on road cuts and/or crops and farming areas. This analysis

suggests that human activities that generated changes in the original topography might have influence the occurrence of these landslides.

There is a discrepancy between the PGA obtained from accelerometers (658.0 m/s^2) within the study area for the Cinchona earthquake and the maximum value for PGAa obtained using the equation 10 with the data from the same earthquake (392.92 m/s^2). This difference is reflected in an incongruity of one degree in the MMI values between the ones reported for the study area after the earthquake (RSN: ICE-UCR, 2009) and to the ones associated in our model. Therefore, the trigger values that we used could be considered to be also one degree lower than what they are supposed to be, if we based the earthquake trigger on the PGA measured and not the calculated with the equation 10.

These differences between the values for the PGA measured within the study area and the values obtained with equation 10 could be explained by the fact that the equation 10 is a general equation used to calculate the peak ground attenuation for crustal earthquakes in Costa Rica that does not include the type of faulting that produced the earthquake. Therefore, directivity and site effects could affect the PGA values measured, making them higher than the calculated values.

We decided to use the PGA values obtained from equation 10 and not the relatively limited measured data, to be consistent and use only values from our calculations, since we also propose to use this new methodology to recreate historical earthquakes and estimate future earthquakes that lack measured PGA data.

3.5 Use of the coseismic landslide susceptibility model in other events near Poás volcano

Here we present the results obtained using our coseismic landslide susceptibility model in three other events near the area of Poás volcano. In the first case we recreate an historical event that generated landslides by using the earthquake data from Montero et al. (2010) for the 1912 earthquake (Table 3) which was located in the southwest sector of our study area (Fig. 10b). In the second case we create a hypothetical earthquake located in the northern flank of Congo volcano (Fig. 10c) between the Ángel and the Venecia faults (Fig. 3). Finally, in the third case we created an earthquake located on east flank of Congo volcano (Fig. 10d) that could be associated with an earthquake from the San Miguel fault.

3.5.1 The Sarchí earthquake (June 12-1912, 5.5M_w, depth 18 km)

This earthquake was relocated by Montero et al. (2010) in the southern flank of Poás volcano and associated to the Carbonera fault (Fig. 10b). Most of the infrastructure damage and coseismic landslides reported for this event (Peraldo and Montero 1994) were located in the southwestern flank of Poás volcano outside of our study area. However, our model is in agreement with the historical reports (Peraldo and Montero 1994) that mention how the region, located close to the springs of the Sarchí and Anonos rivers, and their valleys were affected by coseismic landslides. Also our model shows that in the northern sectors from the epicenter there are zones that could be affected by landslides. However, because these zones were isolated at that time, there are no specific reports of the occurrence coseismic landslides there. The distribution of the susceptibility to slide zones for this case was (Fig. 10b): the areas classified as very low correspond to 25.80%, the zones classified as low susceptibility correspond to 61.15 % and only 13.05

% of the study area corresponds to a moderate susceptibility to slide. There are no zones classified as high and very high zones (maybe some high zones outside the study area). The areas classified as moderate susceptibility to slide are located close to the epicenter, specifically the zone of the non-vegetated steep corridor located west from the Poás main crater, also some patches in the Platanar northeastern flank and the river canyons of the Sarapiquí and Toro rivers (Fig. 10b). Due to the location of this earthquake in relation to our study area (almost at the southwestern edge) we are missing the data that this event could generate outside our limits especially on the Platanar volcano and southwestern flank of Poás volcano.

3.5.2 Hypothetical earthquake case: extension of Ángel fault (6.0 M_w, depth 10 km)

Based on the historical ruptures for the local faults and the seismic hazard of the study area proposed by Montero et al. (2010), the Ángel fault could have an extension to the northwest that that could rip and produce a shallow earthquake with magnitude between 5.5 and 6.0 M_w. For this hypothetical case we ran our model for an earthquake located on the northwestern flank of Congo volcano, between the traces of the Ángel and Venecia faults (Fig. 10c), with a focal depth of 10 km and M_w = 6.0. The distribution of the susceptibility to slide zones in the study area for this case was (Fig. 10c): the areas classified as very low correspond to 13.73%, low = 44.89% =, moderate = 37.34% and only 4.04% corresponded to high susceptibility, no areas were classified as very high susceptibility. The high susceptibility zones are mostly located in the Toro and lower part of the Sarapiquí river canyons, additionally the northeast flank of Platanar could be severely affected by landslides. Since the Congo volcano and von Frantzius summit cones were classified as moderate susceptibility, and based on what we observed from the

Cinchona event, the landslides type that could occur in these cones are debris flows which could affect severely the lower areas and river valleys.

3.5.3 Hypothetical earthquake case: San Miguel fault (7.0 M_w, depth 10 km)

There are no historical records of activity of the San Miguel fault; however because of its length and fault type it could have the potential to produce one of the worst possible scenarios in our study area. We modeled an earthquake produced by this fault with a depth = 10 km, M_w = 7.0 and an epicenter located east of Congo volcano (Fig. 10d). The results of our susceptibility to slide model are: only 6.84 % of the study area was cataloged with very low susceptibility, 23.95% low, 47.47% moderate, 20.28 % high and 1.46 % very high (Fig. 10d). This means that about 70 % of the study could be affected by landslides, and only the low angle slopes located north of the study area will be safe. The occurrence of an event like this could be a potentially very dangerous situation even for zones located as far as 20 km or more from the epicenter (Fig. 10d). The Toro and Sarapiquí rivers canyons, the summit of Congo volcano, and the zones where La Paz Andesites unit are located could be the zones most affected by coseismic landslides from this earthquake.

4. Discussion

The combination of the detailed data obtained from the LiDAR images to create the Cinchona earthquake coseismic landslides catalog, the analyses of the intrinsic susceptibility factors of the study area, and the new methodology proposed here to model the earthquake trigger event provide a broad framework to create the first coseismic susceptibility to slide model for the Poás volcano. The fact that our susceptibility to slide model was able to recreate satisfactorily the distribution of the Cinchona coseismic

landslides allow us to venture to use it for modeling other events. Since we might reasonably expect future earthquakes in the study area to produce landslides having characteristics similar to those triggered by the Cinchona earthquake, we tested our model for two hypothetical events and one historical event.

The morphometric data from the Cinchona coseismic landslides catalog provided useful insights into how the frequency, the sizes and types of coseismic landslides are related to the differences in weathering level and age of the geologic units of the study area. The geological units grouped as the Paleo-temporal phase are predisposed to present higher frequency of coseismic landslides than the Neo-temporal phase units. However, we discovered that since the most common type of landslide occurring on the Neo-phase units is debris flow, the size and area disturbed by these type of coseismic landslides is prone to be considerable on the Neo-phase units, especially on the Congo volcano and Von Frantzius units.

Data from the Cinchona coseismic landslides catalog also provided different causes to explain the distribution and style of the coseismic landslides on the study area. It is interesting to note how the differences in rainfall rates between the Caribbean and Pacific slopes prior to the event might have affected these parameters. The Caribbean slope had about ~408 mm of rain more than the Pacific slope one month before the earthquake, in addition to a previously intense rainy season (Table 4). Therefore, the surface soils of the Caribbean side were saturated at the time of the earthquake, thanks to the combination of the surplus of rain and the volcanic soils characteristic. Meanwhile, due to the decrease in rainfall on the Pacific side one month prior the earthquake, the same situation of high moisture in the soils did not occur on this slope of the Poás volcano, explaining the low

frequency of landslides on this side. The saturated soils in the Caribbean side might also explain why some of the earthquake-induced slope failures on this side were very fluid. From our observations we determine that these slope failures commonly started in the head streams of the different river basins, and as thin slips, which rapidly turned into very fluid debris flows (lahars) that traveled through the river valleys, using the smooth surface of the fresh lava flows as a slide plane and affecting the river valley walls all the way until lower altitudes, where the flows lost their energy and were able to spread out.

The morphometric data also indicate the range of slope angles on which the coseismic landslides occurred. The majority of the triggered landslides occurred on slopes ranging from 30 to 60^{o} (Fig. 6). Although some coseismic landslides occurred on much more gentle slopes, we observed that some of them where located in places affected by human activities like road cuts and/or farming zones. We propose here, that a site effect and a reverse pendulum effect took place in the vicinity of the epicenter explaining the high frequency of landslides in this area. Most of the coseismic landslides occurred in areas where the land use was primary tropical rain forest and secondary and/or gallery tropical rain forest (Fig. 4) because the epicenter of the earthquake was located near the limits of the Poás Volcano National Park where the vegetation cannot be modified by human activities and that the gallery forests since they are by default located in zones with steep slopes.

In Costa Rica, landslide triggered by earthquakes with MMI from IX to VII may cause at least one landslide per km^2 in an area between 1000 km^2 and 90 km^2 (Mora and Mora, 1994). However, we observed here for the Cinchona event that in the study area only 348 km^2 had at least one landslide per km^2, this number may be greater if we include regions

outside the limits of the study area where isolated landslides occurred but it will still way lower than the 1000 km^2 proposed by Mora and Mora (1994). The same intensities may cause an area between 6 to 90 km^2 to present a destruction rate of 60% (Mora and Mora 1994). However, this was not the case for the Cinchona event in which we found only 1 km^2 with that rate of destruction, 18 km^2 presented rates between 30 % and 59 % of destruction, 27 km^2 had rates between 15% and 29 % and 308 km^2 with <15% destroyed. The zones with a destruction >15% are located close to the epicenter and/or in zones with steep slopes, like Congo volcano. The possible explanation of this difference is that since the Cinchona earthquake was so shallow (4.5 km depth) its energy dissipated very fast, creating a much smaller impacted area.

The comparison of the Cinchona coseismic landslide catalog with another catalog from a similar magnitude, depth and focal mechanism earthquake but located in a dryer location (Fig. 8), showed similarities in the number of landslides generated by the shaking, but significant differences in the areas and volumes affected. The rainfall differences and the occurrence of debris flows in the Cinchona case might explain these differences. These factors may also explain what Keefer (1984), Rodriguez et al. (1999), Bommer and Rodriguez (2002) demonstrated before, that coseismic landslides in Central America affect more area (at least an order of magnitude) compared to other world regions.

The use of our new methodology to model the attenuation of the of trigger earthquake events allowed us to include data in the susceptibility to slide model that before was left aside and that is strongly related to occurrence of landslides. The use of the epicenter location, moment magnitude, focal depth and the application of an equation that follows the same graph as the attenuation of the peak ground acceleration of the earthquake

provided a better and more realistic landslide distribution. Furthermore, the possibility of changing the parameters mentioned before for different earthquakes opened the possibility to test multiple scenarios. However, the addition of the fault type energy distribution in our model could improve it even more.

5. Conclusions

The use of LiDAR images to create the Cinchona coseismic landslide catalog allowed us to obtain detailed measurements and valuable insights into the characteristics and causes of the coseismic landslides that occur on Poás volcano.

The distribution of the Cinchona coseismic landslides was the result of a combination of key factors that coincided with the earthquake's epicenter location, these factors are: a) The age (> 0.5 Ma) and therefore the erosion and highly weathering level of the rocks and soils from the paleo-phase units, b) the steep slopes of the la Paz Andesites unit, and c) the high moisture level of the soils in the Caribbean slope of the Poás volcano.

The Cinchona earthquake caused about 4946 ± 100 landslides that striped an area of 22.14 ± 0.27 km^2 and removed a total volume between 0.24 ± 0.0013 to 0.39 ± 0.10 km^3. The occurrence of debris flows was relevant in the Cinchona event, because this type of landslides contributed for about 37% of the total area striped by landslides and the largest debris flows were mostly originated from the Neo-phase units. We demonstrated here that an earthquake in a tropical setting can generate approximately the same number of landslides than an equivalent earthquake located in a subtropical dryer region but, the landslides from the first case will strip more area, due to the differences in the ground moisture that allows the generation of debris flows in the tropical and more humid zones.

The used of the new DEM based on the LiDAR images and our landslide catalog allow us to determinate in great detail the values for the intrinsic susceptibility factors (lithology, slope and ground moisture) of the study area. The new methodology proposed here to obtain the earthquake trigger event values and then its application to obtain the susceptibility to slide zones from an earthquake resulted in high congruence (97%) for the Cinchona event. Because of this high congruence and since the intrinsic susceptibility factors are fixed for our study area, we felt confidence enough to change the epicenter location and other earthquake characteristics (M_w and depth) to model three additional events.

From the four models run in this study we found that the Toro and Sarapiquí river canyons are zones that always are going to have high susceptibility to slide values, because of their high slope angles and due to the lithology present on their walls (Paleo-phase units). Other places that also present high susceptibility values are the non-vegetated corridor located west from the main crater of Poás volcano and the areas where the La Paz andesites unit is exposed.

The northern part of the study area, where the Rio Cuarto Lavas unit outcrops presented always the lowest values of susceptibility due to the low slope angles and low weathering level of its rocks. The landslides located on the very low and low susceptibility zones could be attributed to changes in the original topography by recent human activities.

The effective use of the information generated in this study by planners and developers could reduce the impact of future coseismic landslides on the population and on the important civil infrastructure located in the study area.

6. References

Alvarado G.E., Morales, L.D., Montero, W. Climent, A & Rojas W. 1988. Aspectos sismológicos y morfo tectónicos del extremo occidental de la Cordillera Volcánica Central, Costa Rica. –Rev. Geol. Amer. Central, 9: 75-98.

Alvarado G. E., Carr M.J., 1993: The Platanar-Aguas Zarcas volcanic centers, Costa Rica: spatial-temporal association of Quaternary calc-alkaline and alkaline volcanism. Bull Volcanol 55:443-453.

Alvarado, G. E 2009, Los volcanes de Costa Rica: Geología, historia, riqueza natural y su gente. 3ª edición, XXXII + 16 laminas + 330 pp. Editorial Universidad Estatal a Distancia, Costa Rica.

Alvarado G. E., 2010. Aspectos Geohidrológicos y sedimentológicos de los flujos de lodo asociados al terremoto de Cinchona (M_w 6,2) Del 8 de enero del 2009, Costa Rica. Rev. Geol. Amer. Central, 43: 67-96.

Arredondo, S.G. & Soto, G.J., 2006: Edad de las lavas del Miembro Los Bambinos y sumario cronoestratigráfico de la Formación Barva, Costa Rica. – Rev. Geol. Amer. Central, 34-35: 59-71.

Barquero R. and Peraldo, G., 1993: El temblor de Pejibaye de Turrialba del 10 de Julio de 1993: aspectos sismológicos, neotectónicos y geotécnicos. Informe interno del Instituto Costarricense de Electricidad 32 pag.

Bommer J.J, and Rodríguez C.E., 2002: Earthquake-induced landslides in Central America. Engineering Geology 63 (2002) 189-220.

Bonell M., Gilmour D.A. and Sinclair S.F., 1981: Soil hydraulic properties and their effect on surface water transfer in tropical rainforest catchment, Hydrological Sciences Bulletin, 26:1-18 http://dx.doi.org/10.1080/02626681094908 58.

Borgia, A., Burr, J., Montero, W., Morales, L. D. and Alvarado, G. E., 1990: Fault Propagation Folds Induced by Gravitacional Failure and Slumping of the Central America Costa Rica Volcanic Range: Implications for Large Terrestrial and Martian Volcanic Edifices. J. Geophys. Res. 95 (B9): 14357-14382.

Boschini I., Alvarado, G. & Rojas W., 1988: El terremoto de Buena Vista de Pérez Zeledón (Julio 3, 1983): Evidencia de una fuente sismológica intraplaca desconocida en Costa Rica- Rev Geol de Amer Central, 8: 111-120.

Carr, M J., I. Saginor, G. E. Alvarado, L. Bolge, F. Lindsay, K. Milidakis, B. Turrin, M. D. Feigenson, and C. C. Swisher III 2007, Element fluxes from the volcanic front of Nicaragua and Costa Rica, Geochem. Geophys. Geosyst., 8(6) Q06001, doi: 10.1029/2006GC001396.

CIESIN Center for International Earth Science Information Network, Columbia University; United Nations Food and Agriculture Programme (FAO); and Centro Internacional de Agricultura Tropical (CIAT). 2005. Gridded Population of the World, Version 3 (GPWv3): Population Density Grid, Future Estimates. Palisades, NY: Socioeconomic Data and Applications Center (SEDAC), Columbia University. Available at http://sedac.ciesin.columbia.edu/gpw. [Nov 2011].

Clift, P., and P. Vanucchi 2004, Controls on tectonics accretion versus erosion in subduction zones: Implications for the origin and recycling of the continental crust, Rev. Geophys., 42, RG2001, doi: 10.1029/2003RG00127.

Climent A., Moya A., 2009: Registros acelerográficos obtenidos durante el terremoto de Cinchona del 8 de enero de 2009, Costa Rica. Memoria electrónica X Congreso Nacional de Geotecnia, V Encuentro Centroamericano de Geotecnistas, 19-21 agosto, San José.

Climent A., Rojas, W., Alvarado, G.E.& Benito B., 2009: Costa Rica. – In Benito, B. & Torres , Y. (eds.) Amenaza sísmica en América Central, Entinema, Madrid 229-251.

Evans S. G., and Bent A. L., 2004 The Las Colinas landslide, Santa Tecla: a highly destructive flowslide triggered by the January 13, 2001, El Salvador earthquake, in W.I. Rose, J. J Bommer, D.L. Lopez, M.J. Carr, J.J. Major (Eds.) Natural hazards in El Salvador, special Paper, vol 375 Geological Society of America 375. 25-38.

DeMets, C., R. G. Gordon and D.F. Argus., 2010., Geologically current plate motions. Geophysical Journal International 181 (1), pp. 1-80 doi: 10.1111/j.1365-246X.2009.04491.x

Garwood, N. C., D. P. Janos, and N. Brokaw., 1979 . Earthquake-caused landslides: A major disturbance to tropical forests. Science 205(4410, 7 September): 997–999.

Gazel, E and Ruiz, P., 2005L Los Conos piroclasticos de Sabana Redonda: Componente magmático enriquecido del volcán Poas, Costa rica. Rev. Geol. Amer. Central, 33: 45-60.

GVN, 2009., Fatalities from a large earthquake; slide and minor eruption in crater. Smithsonian Institution, BGVN 34:01.

Holbrook, W. S., D. Lizarralde, S. McGeaary, N. Bangs, and J. Diebold 1999, Structure and composition of the Aleutian island arc and implications for continental crustal growth, Geology, 27, 31-34.

Hovius N., C.P. Stark, P.A. Allen 1997: Sediment flux from mountain belt derived by landslide mapping. Geology 25, 231-234.

Instituto Costarricense de Electricidad (ICE), Sector de energía UEN proyectos y servicios asociados. 2008;. Manejo de los sedimentos del embalse del P.H. Cariblanco. Inf. Interno ICE, San José, pp. 25-50.

Instituto Meteorológico Nacional-Costa Rica IMN 2008a: Boletín Meteorológico Año XXXIII Noviembre 2008 ISSN-1659-0465, 1-29.

Instituto Meteorológico Nacional-Costa Rica IMN 2008b: Boletín Meteorológico Año XXXIII Diciembre 2008 ISSN-1659-0465, 1-30.

Julian B. R., Sipkin S. A., 1985 Earthquake Processes in the Long Valley Caldera Area, California. Journal of Geophysical research, Vol 90, No B13 pp11155- 11169.

Keefer, D.K 1984: Landslides caused by earthquakes. Geological Society of America Bulletin 95, 406-421.

Kerle N., van Wyk de Vries 2001: The 1998 debris avalanche at Casitas volcano, Nicaragua investigation of structural deformation as the cause of slope instability using remote sensing. Jour of Volcanlogy and Geothernal Research vol 105 49-63 doi:10.1016/S0377-0273(00)00244-4.

Laporte, G 2009a: Taludes y sismos. Comportamiento dinámico de taludes durante el sismo de Cinchona y sus implicaciones al diseño geotécnico. Bol. Geotécnico Notisuelos, 10: 6-7.

Laporte, G., 2009b: Efectos de los sismos en el comportamiento de las laderas naturales, cortes y rellenos: caso del sismo de Cinchona X Congreso Nacional de Geotecnia y V Encuentro Centroamericano de Geotecnistas. San José, Costa Rica, 19-21 de agosto del 2009, Memoria digital, 10 pp.

Larsen, I. J., Montgomery, D. R. and Korup, O., 2010: Landslide erosion caused by hillslope material. Nature Geosci. 3, 247-251.

Linkimer, L., 2008: Relationship between peak ground acceleration and Modified Mercalli Intensity in Costa Rica. Rev Geol. Amer. Central, 38: 81-94.

Malamud B.D., Turcotte D.L., Guzzeti F., Reichenbach P. 2004 Landslides, earthquake, and erosion. Earth and Planetary Science letters 229 45-59.

Marshall, A. J. 1937. Northern New Guinea, 1936. Geographical Journal 89 (6): 489–506.

Marshall, J. S., D. M. Fisher, and T. W. Gardner., 2000. Central Costa Rica deformed belt: Kinematics of diffuse faulting across the western Panama block, Tectonics, 19, 468-492,

Méndez, J., Soto, G.J., Zamora, N., Vargas, A., Sjöbohm, L., Bonilla, E., Barahona, D., Solís, L., Kycl, P. & Baroň, I., 2009: Geología de los deslizamientos provocados por el Terremoto de Cinchona, Costa Rica (M_w 6,2; 8 de enero del 2009) en la Ruta 126 (Varablanca-San Miguel). X Congreso Nacional de Geotecnia y V Encuentro Centroamericano de Geotecnistas. San José, Costa Rica, 19-21 de agosto del 2009, Memoria digital, 22 pp.

Montero, W., 1999: El terremoto de 1924 (Ms7,0): Un gran temblor intraplaca relacionado al límite incipiente entre la placa Caribe y la microplaca de Panamá?-Rev Geol de Amer Central, 22:25-62.

Montero, W., 2001:Neotectonica de la región central de Costa Rica: frontera oeste de la microplaca de Panamá. – Rev Geol. Amer. Central, 24: 29-56.

Montero, W., Rojas, W., Boschini, I., Barquero, R., and Flores, H., 1991, Neotectonica de la región de Puriscal. Origen de la sismicidad de mayo-diciembre de 1990. – Memorias 51 Seminario Nacional de Geotecnia – Ier Encuentro Centroamericano de Geotecnistas, 4.38-4.51.

Montero, W y Alvarado, G. E., 1995: El terremoto de Patillos del 30 de diciembre de 1952 (Ms=5.9) y el contexto geotectónico de la región del volcán Irazú, Costa Rica-Rev Geol Amer Central, 18:25-40.

Montero W., Soto G. J., Alvarado G.E., Rojas W.,: 2010 Division del deslizamiento tectónico y transtensión en el macizo del volcán Poas (Costa Rica), Basado en Estudios Neotectónicos y de sismicidad histórica. –Rev. Geol. Amer. Central 43:13-36.

Mora, R., Mora S. and Vahrson, W., 1992: Microzonificación de la amenaza de deslizamientos y resultados obtenidos en el área del valle central de Costa Rica. Escala 1:286 000 Cepredenac, San José Costa Rica.

Mora, R., Chávez, J. and Vásquez, M., 2002: Zonificación de la susceptibilidad al deslizamienti: Resultados obtenidos para la Península de Papagayo mediante la modificación del método Mora & Vahrson (Mora et al., 1992). – Memoria del tercer curso internacional sobre microzonificación y su aplicación en la mitigación de desastres. Lima, Perú. 38-46

Mora, S., 1985., Las laderas inestables de Costa Rica. Rev. Geol. America Central, 3: 131-161.

Mora, S., 1989., Extend and social-economic significance of slope inestability in Costa Rica. –In: E. Brabb & L. Harrod (eds.) Landslides: Extendt and economic significance: 93-99. Ed. Balkema, Rotterdam.

Mora, S., Vahrson, G. 1993: Macro-zoning landslide hazards. Manual for zonation on Seismic Geotechnical Hazards. Japanese Geotechnical Society. Pp 58-61 and 128-136.

Mora, C., Vahrson, W.-G., 1994: Macrozonation methodology for landslide hazard determination. Bulletin of the Association of Engineering Geologist 31 (1), 49-58.

Mora, S., y R., Mora., 1994: Los Deslizamientos por el Terremoto de Limón: Factores de Control y comparación con otros eventos en Costa Rica, Rev Geol Amer. Central, vol esp Terremoto de Limón: 139-152.

Pain, C. F. 1972. Characteristics and geomorphic effects of earthquake-initiated landslides in the Adelbert Range, Papua New Guinea. Engineering Geology 6(4): 261–274.

Paniagua S. and Soto G.E.1986: Reconocimiento de los riesgos volcánicos potenciales de la cordillera central de Costa Rica. Cienc Tec. 10 (2) 49-72.

Parker, R. N. Densmore A. L., Rosser N. J.,de Michele M., Yong L., Runqiu H., Whadcoat S., Petley D. N., 2011 Mass wasting triggered by the 2008 Wenchuan earthquake greater than orogenic growth Nature Geosci. 4, 449-452.

Peel M. C., Finlayson B.L., and McMahon 2007: Updated world map of Köppen-Geiger climate classification. Hydrol Earth Syst. Sci., 11, 1633-1644.

Peraldo, G and Montero, W., 1994: Los temblores del periodo colonial de Costa Rica. 162 págs. Ed Tecnologica de Costa Rica, Cartago.

Peraldo, G. and Montero, W., 1999 Sismología histórica de América Central. -347 pags. Inst Panamericano de Geogra. Historia, México.

Peraldo, G., and Rojas E., 2000: Catálogo de deslizamientos históricos de Costa Rica, periodo 1772-1960. IGN, Inf Semestral II.

PNUD-Programa de las Naciones Unidas para el Desarrollo, IMN-Instituto Meteorológico Nacional and MINAET-Ministerio de Ambiente y Telecomunicaciones: 2009 Diagnostico Biofísico para Costa Rica. 478 pp.

Proser, J.T. & Carr, M.J., 1987. Poás Volcano, Costa Rica: Geology of the Summit Region and Spatial and Temporal Variations among the Most Recent Lavas. - J. Volcanol. Geotherm. Res., 33:131-146.

Rodríguez, C.E., Bommer, J.J., Chandler, R.J., 1999. Earthquake-induced landslides: 1980-1997. Soil Dynamics and Earthquake Engineering 18, 325-346.

Rojas, W., Montero, W., López, A., Alvarado, G., Vargas, A. and Taylor, W., 2009: In RSN: ICE-UCR: Informe del terremoto de Cinchona del jueves 8 de enero de 2009.-Univ de Costa Rica, San José: 26-44.

Red Sismológica Nacional RSN (UCR-ICE) 2009: El Terremoto de Cinchona del jueves 8 de enero de 2009. Revista Geológica de América Central, 40: 91-95.

Ruiz, P., Gazel, E., Alvarado, G.E., Carr, M.J. & Soto, G.J., 2010: Caracterización geoquímica y petrográfica de las unidades geológicas del macizo del volcán Poás, Costa Rica. - Revista Geológica de América Central, 43: 37-66.

Schmidt V., 2010. Avances para estudios del riesgo a escala regional y local: Aplicación a América Central y a la bahía de Cádiz (Sur de España). Tesis Doctoral. Univ Politécnica de Catalunya.

Schuster, R. L., Nieto, A.S., O'ouke, T.D., Crespo, E., Plaza-Nieto, G., 1996. Mass wasting triggered by the 5 March 1987 Ecuador earthquakes. Engineering Geology 42, 1-23.

Skinner, D.J. and Porter, S.C., 1992: The Dynamic Earth: an introduction to physical geology. II edition, John Wiley and Sons, Inc. New York. 570 pp.

Small C, Naumann T., 2001 The global distribution of human population and recent volcanism. Enviromental Hazards 3 pp 93-109.

Soto, G.J., 1994: Volcanología Física. – En: Denyer, P. & Kussmaul, S. (Comps.): Atlas Geológico Gran Área Metropolitana. - Editorial Tecnológica de Costa Rica: 131-146.

Soto, G.J., 1999: Geología Regional de la Hoja Poás (1:50 000). En: Alvarado, G.E. & Madrigal, L.A. (Eds.): Estudio Geológico-Geotécnico de Avance a la Factibilidad del P.H. Laguna Hule. – Inf. Interno ICE, San José, pp. 15-45.

Van Westen, C.J., and Soeters, R., 2000: Remote Sensing and Geographic Information Systems for Natural Disaster Management. In Roy, P.S., Van Westen., Jha, V.K., Lakhera, R.C and Champati Ray, P.K: Natural Disasters and their Mitigation. A Remote sesing and GIS Perpective. Indian Institute of Remote Sensing, National Remote Sensing Agency, India: 31-76

Van Zuidam, R. A., 1986: Aerial photointerpretation in terrain analysis and geomorphologic mapping. 442 pp. Smits Publishers The Hague.

Varnes, D.J., 1978. Slope movement types and processes. In: Schuster, R.L Krizek, RJ. (Eds.), Landslides: Analysis and Control-Special Report, vol. 176. Tranport Research Board, National Academy of Sciences, Washington, DC, pp. 11-33.

Wald, D. J., Quitoriona, V.,Heaton, T.H. & Kanamori, H., 1999, Relantionship between Peak Ground Acceleration, Peak Ground Velocity, and Modified Mercalli Intensity in California, Earthquake Spectra, Volume 15, No. 3.557-564.

Figure Captions

Figure 1

a) Central American Volcanic arc and its population distribution (CIESIN 2011). b) Digital elevation map of Costa Rica, volcanic fronts and its tectonic setting. Location of earthquakes associated with coseismic landslides in the last 250 yr, numbers 1-19 correspond to event code from table 2. The black rectangle denotes a close-up to western Central Volcanic Range and the study area (see Fig. 1c). Bathymetry is from Ranero et al. (2005). c) Cinchona earthquake location with Harvard (MIT) Body-Wave moment tensor solution, the letters A-I correspond to the fault code from table 1. North Panamá Deformed Belt (NPDB), Central Costa Rica Deformed Belt (CCRDB).

Figure 2

a) Modified Mercalli Intensity map from the Cinchona earthquake based on RSN: ICE-UCR, (2009), Climent and Moya (2009) and Montero et al. (2010). Peak ground accelerations (PGA) in the horizontal axis measured in the nearest stations to the epicenter based on Climent and Moya (2009).

Figure 3

a) Geologic map of Poás volcano and location of coseismic landslides from Cinchona earthquake. Letters A-I correspond to fault the code from table 1. b) Area in km^2 from each volcanic unit of the study area. c) Number of coseismic landslides per volcanic unit.

d) Stripped area (km^2) from coseismic landslides per volcanic unit. e) Stripped area from landslides per volcanic unit divided by the area of each volcanic unit.

Figure 4

a) Land cover and slope failures map. b) Area in km^2 from each land cover type. c) Number of coseismic landslides per land cover type. d) Stripped area (km^2) from coseismic landslides per land cover type. e) Stripped area from landslides per land cover type divided by the area of each land cover type. The purple line marks the limit between the northern side of CVR (Caribbean slope) and the southern side (Pacific slope).

Figure 5

a) Occurrence of landslides based on temporal phase units (Paleo or Neo). Brown column in histograms (b to f) represent the sum of the data from the Paleo Temporal units from Platanar, Poás and Barva volcanoes, the green column has the data from the Neo temporal units from Poás and Barva volcanoes. Histograms (g to f) show the frequency and area striped based on the type of landslide.

Figure 6

a) Slope angle map. b) Area (km^2) covered by slope range. c) Number of coseismic landslides per slope range. d) Stripped area (km^2) from coseismic landslides per slope range. e) Stripped area from landslides per slope range divided by the area covered by each slope range.

Figure 7

a) Number of coseismic landslides by distance from the Cinchona earthquake epicenter in 5 km windows. b and c) Area of coseismic landslides by distance from the Cinchona earthquake epicenter.

Figure 8

Comparison of Cinchona event with coseismic world catalog from Malamud et al. (2004). Bracketed numbers correspond to events near Poás volcano from table 2, the shade area is the range between the maximum and minimum estimated volume removed from these events based on what we observe in the Cinchona event. Error lines for these events are based on the difference between the Cinchona event and the average obtained from Malamud et al. (2004) (*) Mammoth Lakes earthquake (5-25-1980) data from Julian and Sipkin 1985.

Figure 9

a) Lithological susceptibility map. b) Slope angle susceptibility map. c) Ground moisture susceptibility map. d) Cinchona earthquake trigger event map.

Figure 10

a) Susceptibility map for Cinchona earthquake. b) Susceptibility map for the historical case of the 1912 earthquake. c) Susceptibility map for hypothetical earthquake produced by an extention of the Angel fault with its epicenter located on the northwestern flank of Congo volcano. d) Susceptibility map for hypothetical earthquake produced by the San Miguel reverse fault with its epicenter located on the east of Congo volcano

Figure 1

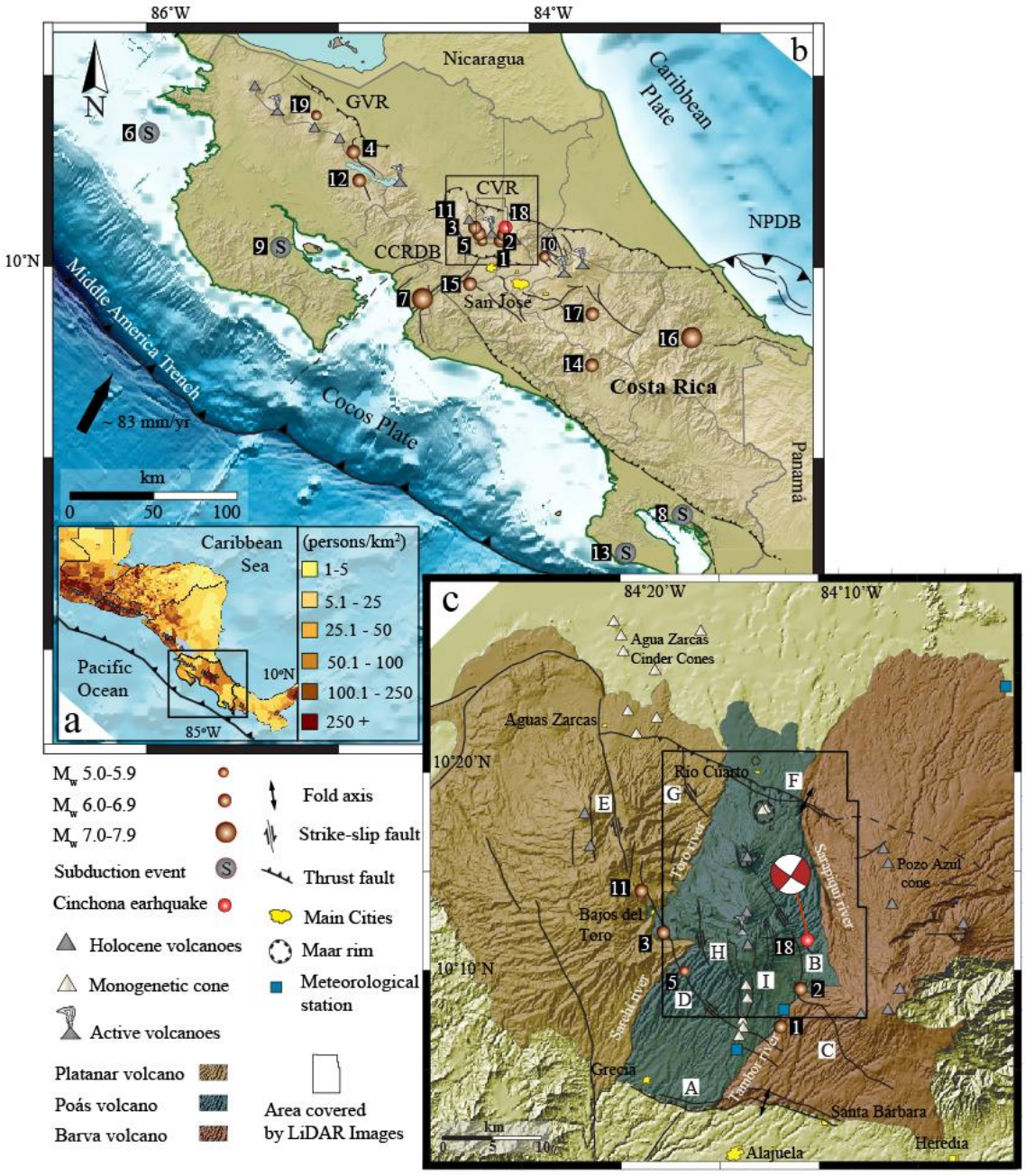
86°W
84°W
10°N
b
N
Nicaragua
Caribbean Plate
GVR
CVR
CCRDB
NPDB
San José
Costa Rica
Panamá
Middle America Trench
Cocos Plate
~ 83 mm/yr
km
0 50 100
Caribbean Sea
Pacific Ocean
10°N
85°W
a
(persons/km²)
1-5
5.1 - 25
25.1 - 50
50.1 - 100
100.1 - 250
250 +
c
84°20'W
84°10'W
10°20'N
10°10'N
Agua Zarcas Cinder Cones
Aguas Zarcas
Río Cuarto
Pozo Azul cone
Bajos del Toro
Grecia
Santa Bárbara
Heredia
Alajuela
Mw 5.0-5.9
Mw 6.0-6.9
Mw 7.0-7.9
Subduction event
Cinchona earhquake
Holocene volcanoes
Monogenetic cone
Active volcanoes
Platanar volcano
Poás volcano
Barva volcano
Fold axis
Strike-slip fault
Thrust fault
Main Cities
Maar rim
Meteorological station
Area covered by LiDAR Images

Figure 2

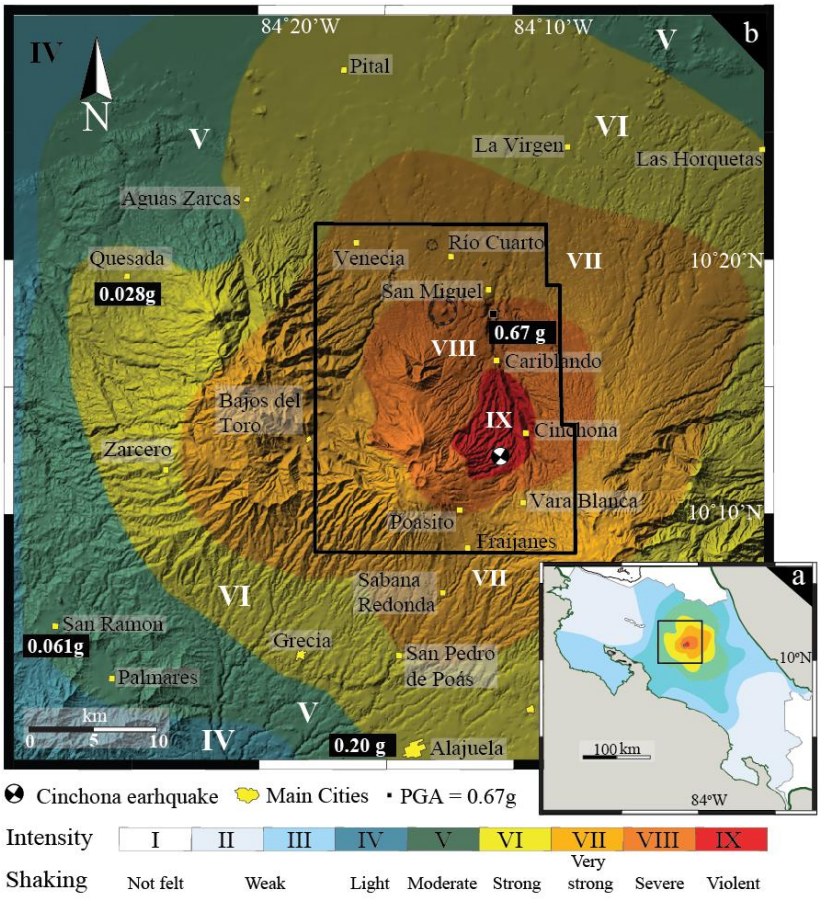
84°20'W
84°10'W
b
IV
N
V
Pital
V
VI
La Virgen
Las Horquetas
Aguas Zarcas
Río Cuarto
Venecia
VII
10°20'N
Quesada
0.028g
San Miguel
0.67 g
VIII
Cariblando
Bajos del Toro
IX
Cinchona
Zarcero
Vara Blanca
10°10'N
Poasito
Fraijanes
a
Sabana Redonda
VII
VI
San Ramon
0.061g
Grecia
San Pedro de Poás
Palmares
10°N
km
0 5 10
V
IV
0.20 g
Alajuela
100 km
84°W
Cinchona earhquake
Main Cities
PGA = 0.67g
Intensity
I II III IV V VI VII VIII IX
Shaking
Not felt
Weak
Light
Moderate
Strong
Very strong
Severe
Violent

Figure 3

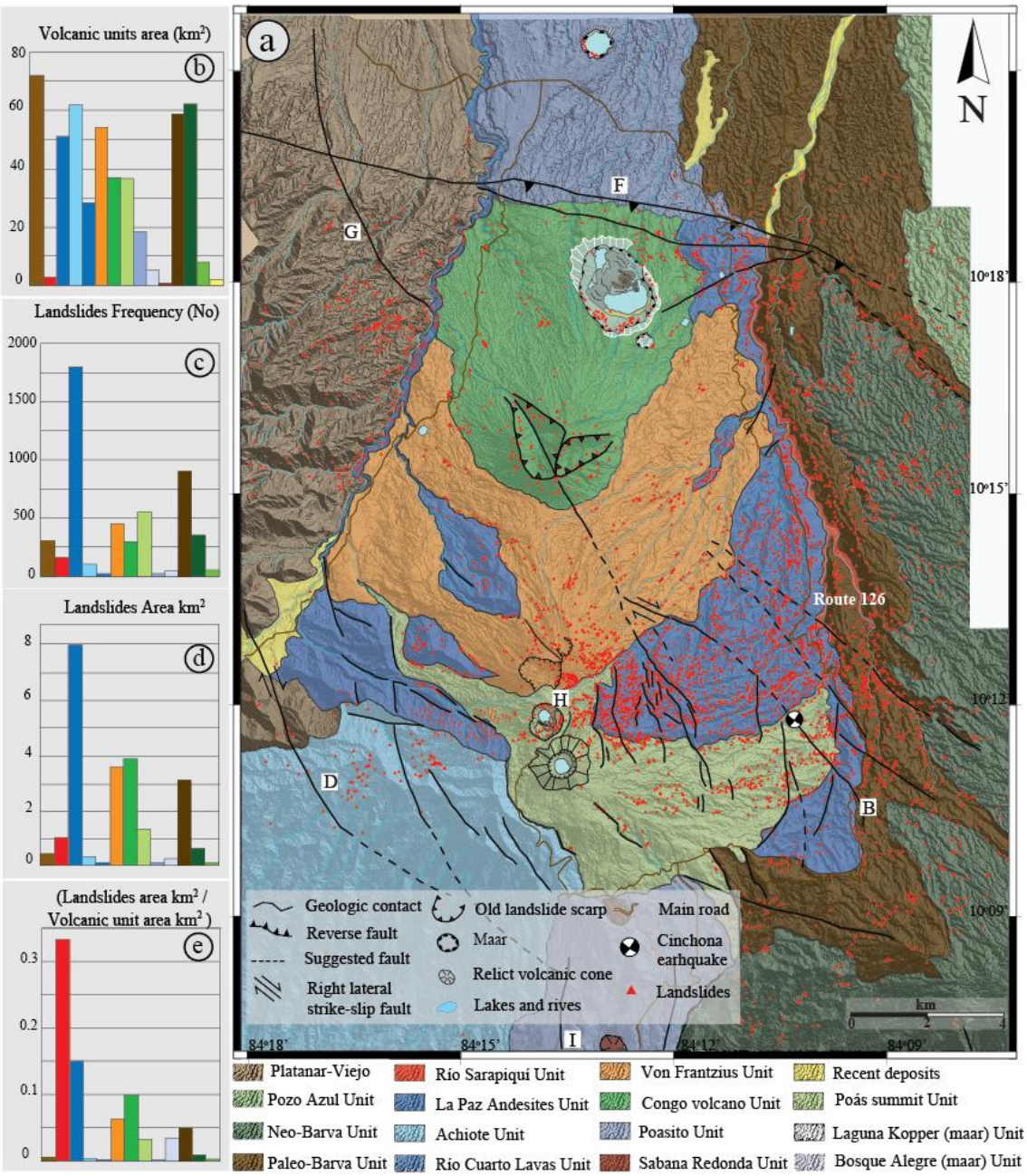
Volcanic units area (km²)
b
80
60
40
20
0
Landslides Frequency (No)
c
2000
1500
1000
500
0
Landslides Area km²
d
8
6
4
2
0
(Landslides area km² / Volcanic unit area km²)
e
0.3
0.2
0.1
0
a
N
F
G
H
D
I
B
Route 126
10°18'
10°15'
10°12'
10°09'
84°18'
84°15'
84°12'
84°09'
km
0
2
4
Geologic contact
Reverse fault
Suggested fault
Right lateral strike-slip fault
Old landslide scarp
Maar
Relict volcanic cone
Lakes and rives
Main road
Cinchona earhquake
Landslides
Platanar-Viejo
Pozo Azul Unit
Neo-Barva Unit
Paleo-Barva Unit
Río Sarapiquí Unit
La Paz Andesites Unit
Achiote Unit
Río Cuarto Lavas Unit
Von Frantzius Unit
Congo volcano Unit
Poasito Unit
Sabana Redonda Unit
Recent deposits
Poás summit Unit
Laguna Kopper (maar) Unit
Bosque Alegre (maar) Unit

Figure 4

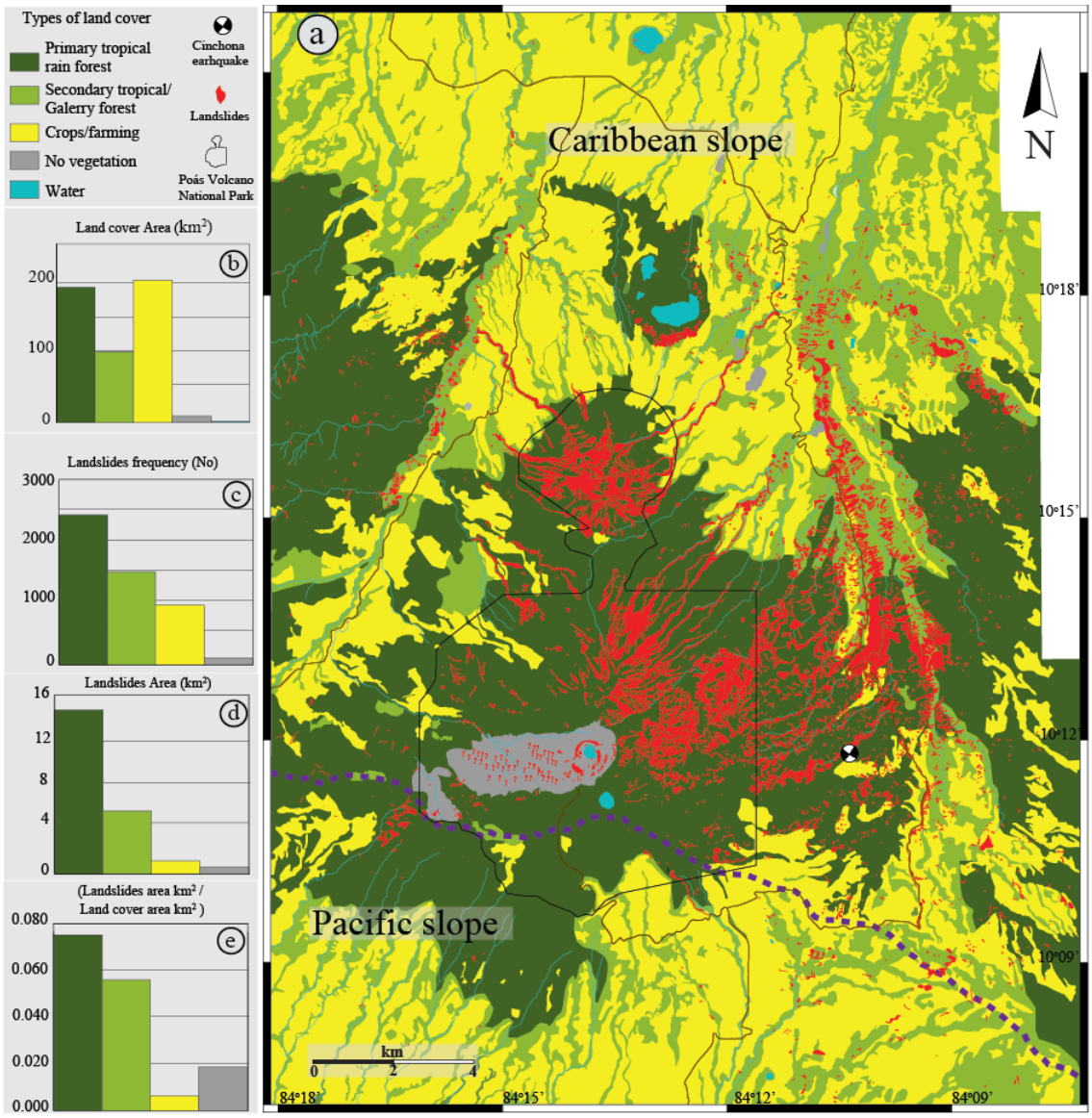
Types of land cover
Primary tropical rain forest
Secondary tropical/ Galerry forest
Crops/farming
No vegetation
Water
Cinchona earhquake
Landslides
Poás Volcano National Park
Land cover Area (km²)
b
200
100
0
Landslides frequency (No)
c
3000
2000
1000
0
Landslides Area (km²)
d
16
12
8
4
0
(Landslides area km² / Land cover area km²)
e
0.080
0.060
0.040
0.020
0.000
a
Caribbean slope
Pacific slope
N
10°18'
10°15'
10°12'
10°09'
km
0
2
4
84°18'
84°15'
84°12'
84°09'

Figure 5

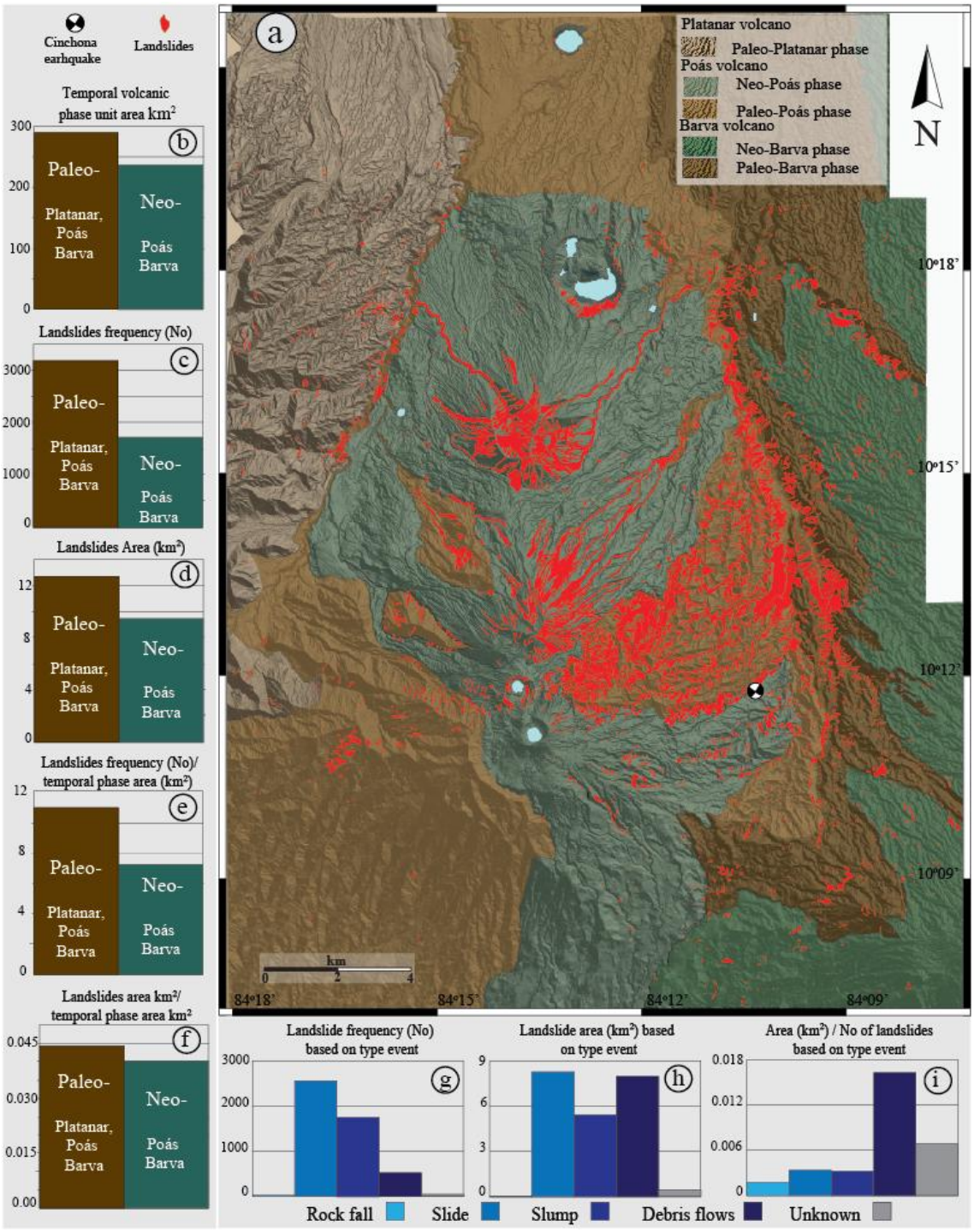
Cinchona earhquake
Landslides
Temporal volcanic phase unit area km²
b
Paleo-
Platanar, Poás Barva
Neo-
Poás Barva
300
200
100
0
Landslides frequency (No)
c
3000
2000
1000
0
Landslides Area (km²)
d
12
8
4
0
Landslides frequency (No)/ temporal phase area (km²)
e
Landslides area km²/ temporal phase area km²
f
0.045
0.030
0.015
0.00
a
Platanar volcano
Paleo-Platanar phase
Poás volcano
Neo-Poás phase
Paleo-Poás phase
Barva volcano
Neo-Barva phase
Paleo-Barva phase
N
10°18'
10°15'
10°12'
10°09'
km
0
2
4
84°18'
84°15'
84°12'
84°09'
Landslide frequency (No) based on type event
g
Landslide area (km²) based on type event
h
Area (km²) / No of landslides based on type event
i
Rock fall
Slide
Slump
Debris flows
Unknown

Figure 6

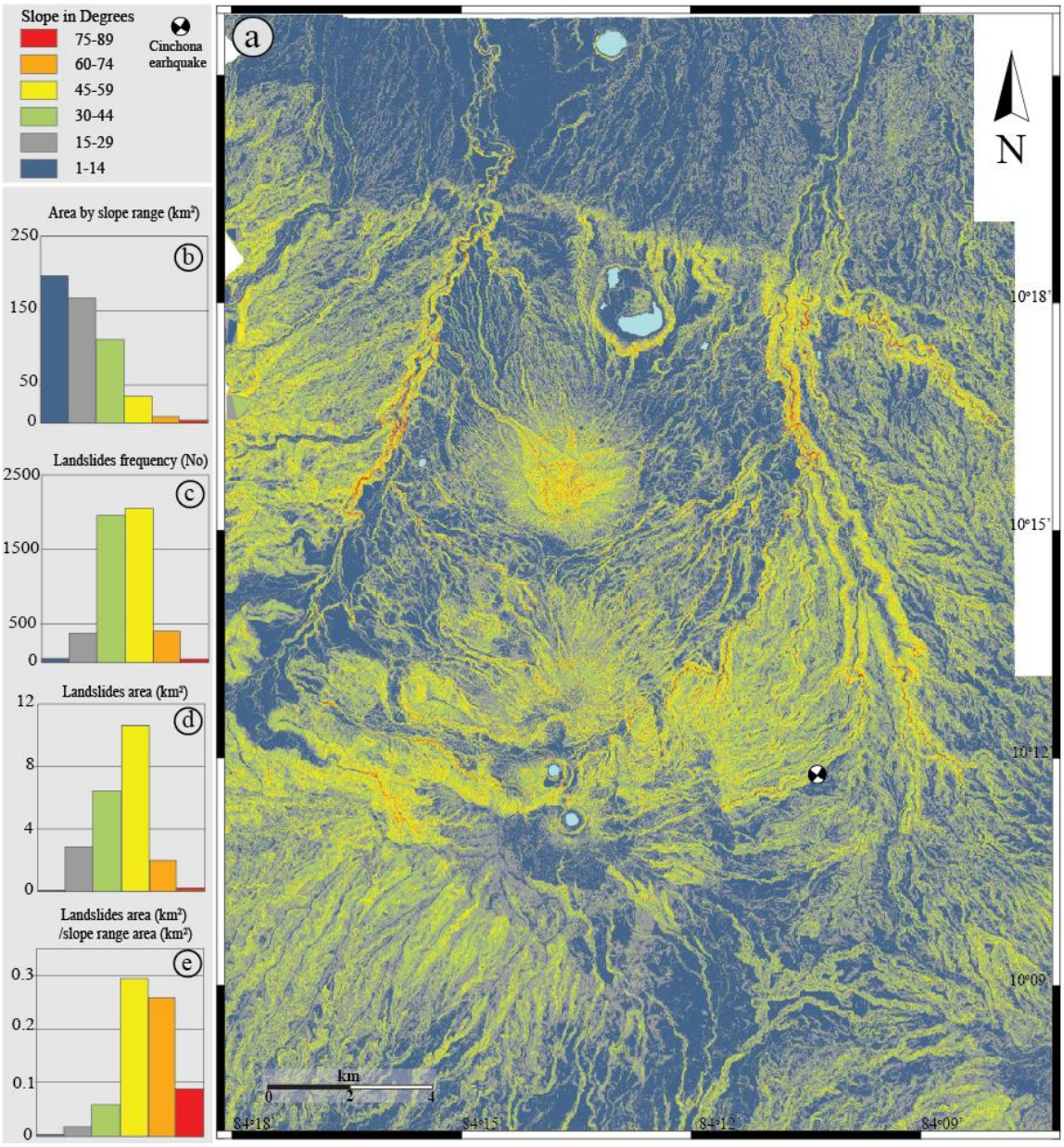
Slope in Degrees
75-89
60-74
45-59
30-44
15-29
1-14
Cinchona earhquake
Area by slope range (km²)
b
250
150
50
0
Landslides frequency (No)
c
2500
1500
500
0
Landslides area (km²)
d
12
8
4
0
Landslides area (km²) /slope range area (km²)
e
0.3
0.2
0.1
0
a
N
10°18'
10°15'
10°12'
10°09'
km
0
2
4
84°18'
84°15'
84°12'
84°09'

Figure 7

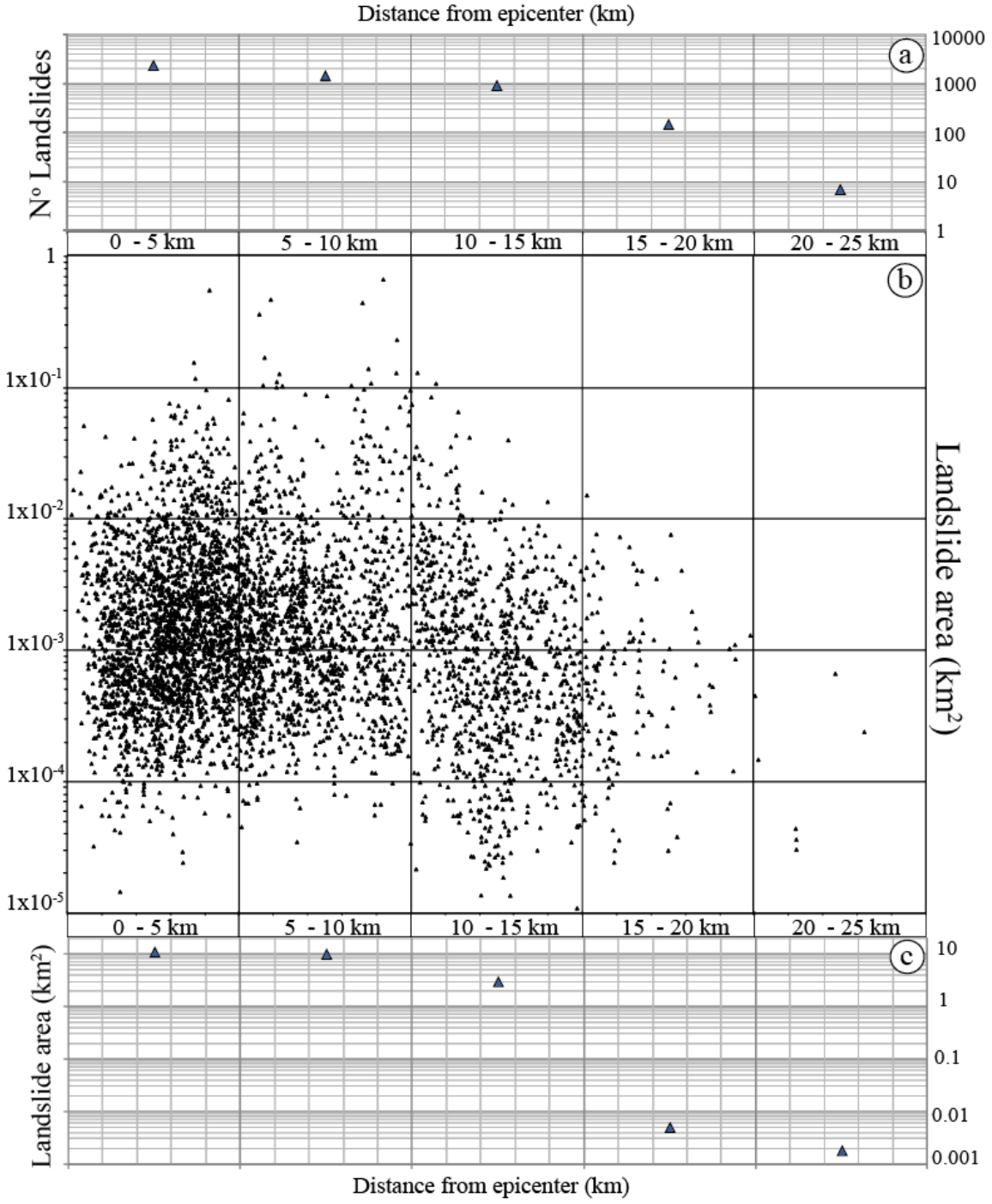
Distance from epicenter (km)
N° Landslides
a
10000
1000
100
10
1
0 - 5 km
5 - 10 km
10 - 15 km
15 - 20 km
20 - 25 km
b
1
1x10-1
1x10-2
1x10-3
1x10-4
1x10-5
Landslide area (km2)
c
10
1
0.1
0.01
0.001
Distance from epicenter (km)

Figure 8

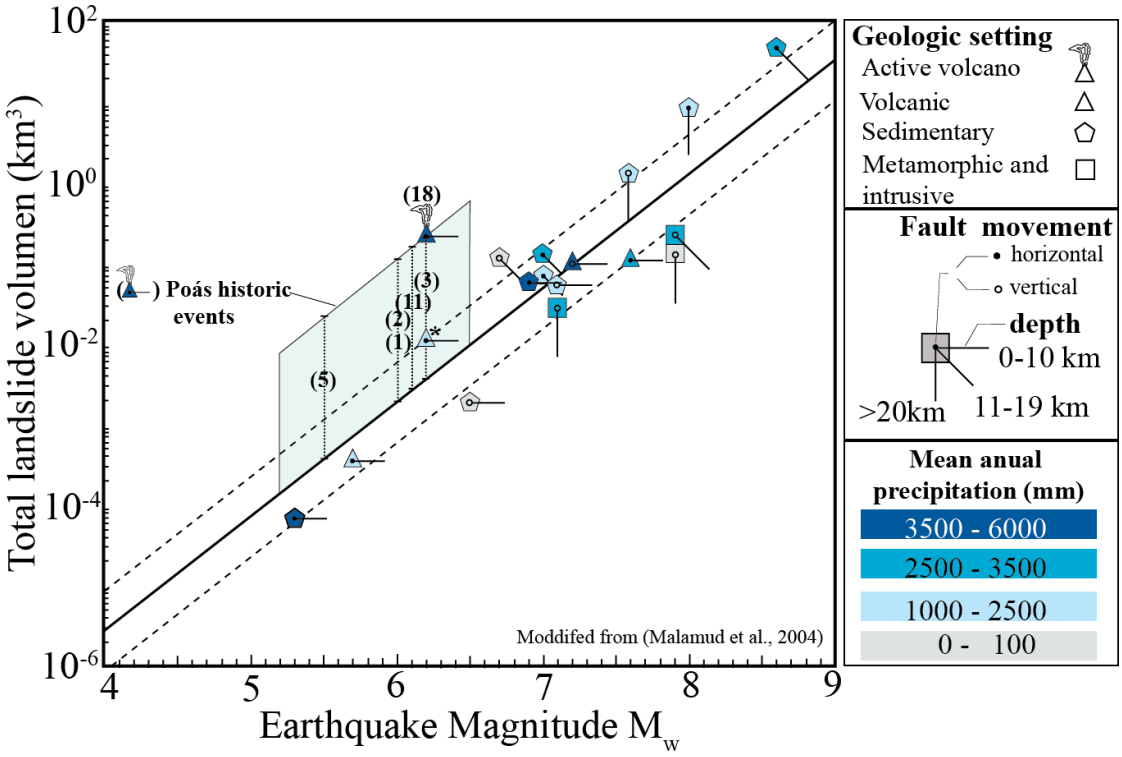
Total landslide volumen (km3)
Earthquake Magnitude Mw
Moddifed from (Malamud et al., 2004)
(18)
(3)
(11)
(2)
(1)
(5)
( ) Poás historic events
Geologic setting
Active volcano
Volcanic
Sedimentary
Metamorphic and intrusive
Fault movement
horizontal
vertical
depth
0-10 km
11-19 km
>20km
Mean anual precipitation (mm)
3500 - 6000
2500 - 3500
1000 - 2500
0 - 100

Figure 9

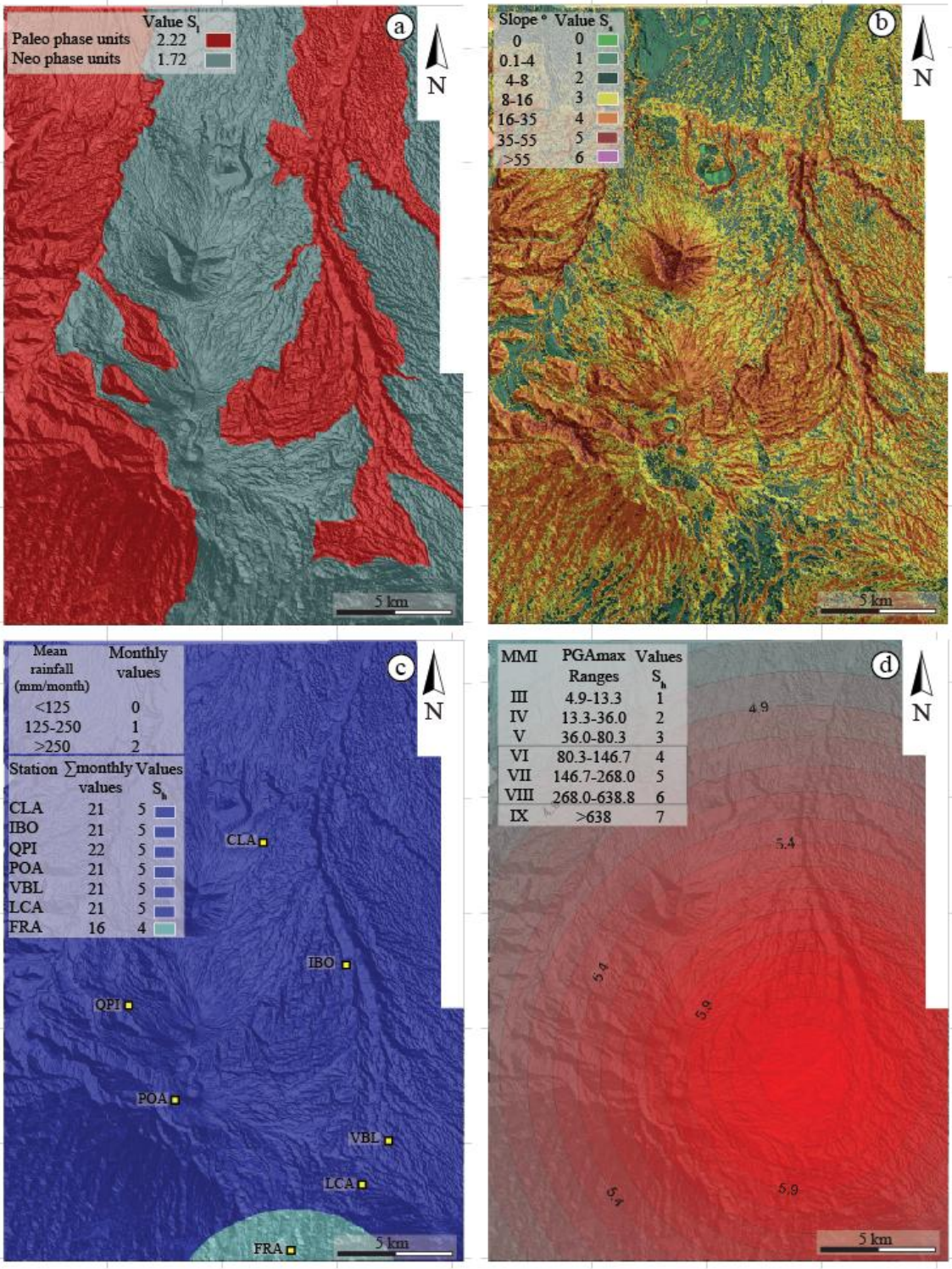
a
Value S_i
Paleo phase units 2.22
Neo phase units 1.72
N
5 km
b
Slope ° Value S_s
0 0
0.1-4 1
4-8 2
8-16 3
16-35 4
35-55 5
>55 6
N
5 km
c
Mean rainfall (mm/month) Monthly values
<125 0
125-250 1
>250 2
Station ∑monthly values Values S_h
CLA 21 5
IBO 21 5
QPI 22 5
POA 21 5
VBL 21 5
LCA 21 5
FRA 16 4
CLA
IBO
QPI
POA
VBL
LCA
FRA
N
5 km
d
MMI PGAmax Ranges Values S_h
III 4.9-13.3 1
IV 13.3-36.0 2
V 36.0-80.3 3
VI 80.3-146.7 4
VII 146.7-268.0 5
VIII 268.0-638.8 6
IX >638 7
4.9
5.4
5.4
5.9
5.4
5.9
N
5 km

Figure 10

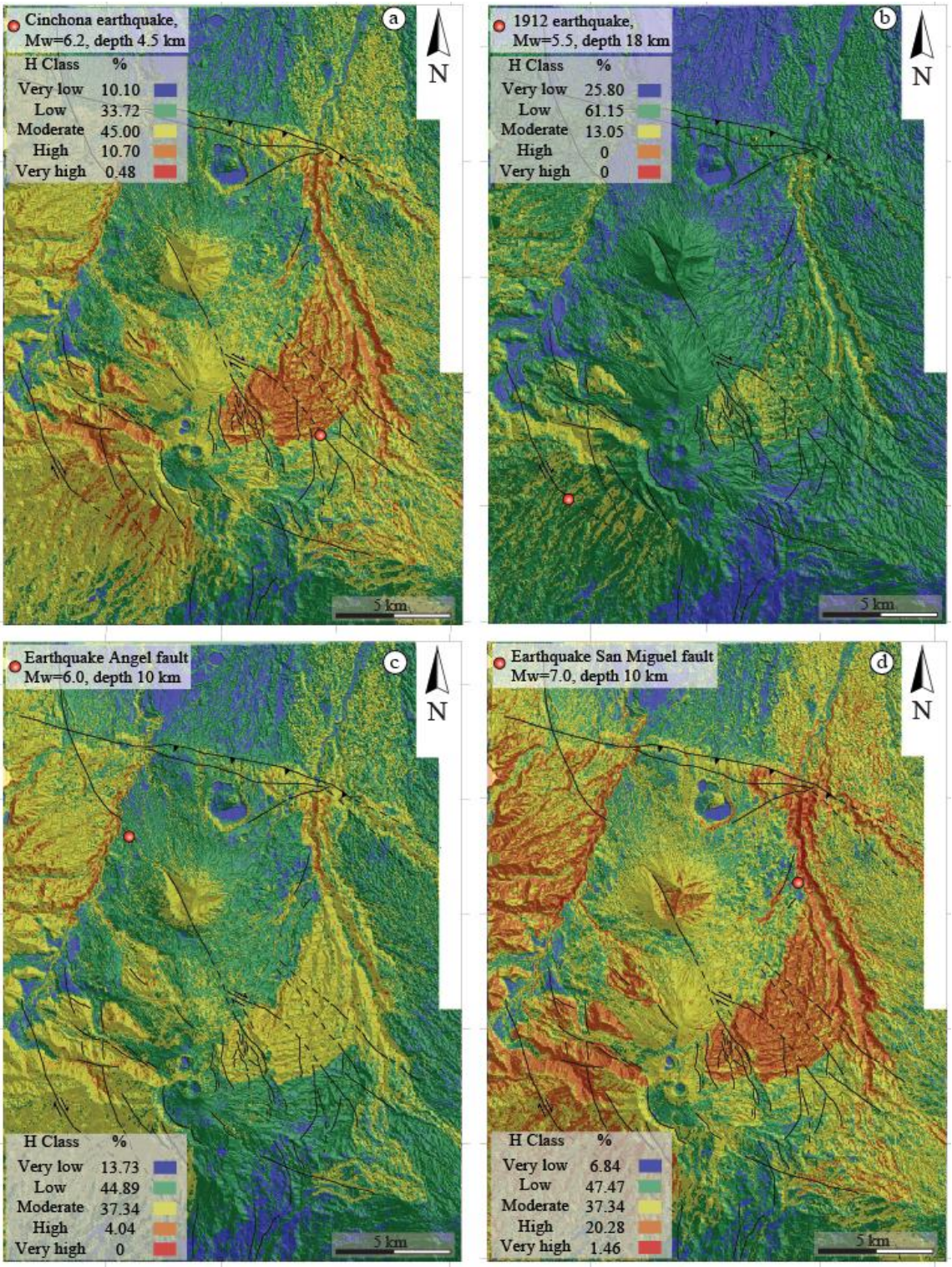
a
Cinchona earthquake,
Mw=6.2, depth 4.5 km
H Class %
Very low 10.10
Low 33.72
Moderate 45.00
High 10.70
Very high 0.48
N
5 km
b
1912 earthquake,
Mw=5.5, depth 18 km
H Class %
Very low 25.80
Low 61.15
Moderate 13.05
High 0
Very high 0
N
5 km
c
Earthquake Angel fault
Mw=6.0, depth 10 km
H Class %
Very low 13.73
Low 44.89
Moderate 37.34
High 4.04
Very high 0
N
5 km
d
Earthquake San Miguel fault
Mw=7.0, depth 10 km
H Class %
Very low 6.84
Low 47.47
Moderate 37.34
High 20.28
Very high 1.46
N
5 km

Table 1. Summary of the main features of tectonic faults and their historical activity around the Poás volcano.

Fault code (*)	Fault name	Location	Fault type	Strike angle	Length (km)	Geomorphology expression	Historical and recent seismic activity	References
A	Alajuela	S flank of Poás volcano, from Grecia to Santa Bárbara	Thrust propagation fault bend fold	E-W and WNW	~20	Anticline and synclinal folds in the front scarp, tectonic valleys	1772 earthquake?	(b and e)
B	Ángel	E and NE flanks of Poás volcano, W flank of Barva volcano	Dextral-small normal component	N25W, N70W, N30W, N-S, N50W	> 20	Right lateral displacement of drainage divide (Angel River), slopes changes, linear valleys, sag ponds, drainage offset.	Fraijanes Earthquake 1888, Cinchona Earthquake 2009	(a, c and e)
C	Sabanilla	W and SW flanks of Poás volcano, from NW of Bajos de Toro to N of Alajuela	Strike-slip fault (Dextral)	NW	> 25	Right lateral displacement of drainage systems, linear valleys, fault berms	Toro Amarillo Earthquake 1911, Sarchí Earthquake 1912	(e)
D	Carbonera	W flank of Poás volcano	Strike-slip fault (Dextral)	NNW	> 6.5	Fault scarps, right lateral displacement of streams	Seismic swarm, March 1990, January 1997	(a and e)
E	Volcán Viejo-Aguas Zarcas	NE flank of Platanar-Viejo volcano	Strike-slip fault (Dextral)	N10W	> 25	Linear valley in the Aguas Zarcas river	Bajos del Toro Earthquake 1955, seismic swarm April-May 1998	(a and e)
F	San Miguel	N flank of Poás volcano	Bifurcated reverse propagation fault bend fold	N70W	~15	Straight fault scarp related with an anticline fold in the front and a synclinal fold in the back	Potentially active (CO_2 & CH_4 emissions and Sarapiqui and Toro river displacements	(b, c and e)
G	Venecia	SW of Platanar-Viejo volcano	Strike-slip fault (Dextral)	N20W	~8	Alignment NW	Seismic swarm September 1989?	(a)
H	Poás summit faults system	E and W side of Main and Botos craters on Poás volcano	Normal arched	N-S, NNW-SSE	~2 - 3	Faceted scarps, seudo-caldera, volcanic graven, rivers and streams are parallel to these faults	Seismic activity after Cinchona earthquake?	(a, c and e)
I	Volcano tectonic fracture of Poás	S flank of Poás volcano, near Sabana Redonda	Normal	N-S	~5	Depression (graben) N-S limited in the E and W by linear scarps	Seismic activity after Cinchona earthquake?	(d and e)

(*) Fault code corresponds to letter code used in figures 1c and 3a. References: a (Alvarado et al., 1988), b (Borgia et al., 1990), c (Soto 1999), d (Gazel and Ruiz 2005) and e (Montero et al 2010)

Table 2. Earthquakes in Costa Rica resulting in coseismic landslides in the last 250 yr, numbers 1-19 correspond to event code from figure 1.

Event code (*)	Earthquake Name/ Location	Date	Epicenter		Depth (km)	Magnitude Mw	I_o	Death toll	References
			Lat N	Lon W					
1(^{Po})	Barva	15-Feb-1772	10.12	-84.20	10	6	VIII	-	f, h, j, k
2(^{Po})	Fraijanes	30-Dic-1888	10.15	-84.18	15	6	VIII	5	a, j, k
3(^{Po})	Bajos del Toro	29-Aug-1911	10.20	-84.30	10	6	VIII	3	a, i, j, k
4	Guatuso	10-Oct-1911	10.60	-84.92	10	6.5	VIII	6	i, j
5(^{Po})	Sarchí	12-Jun-1912	10.17	-84.28	18	5.5	VII	-	a, i, j, k
6(S)	Papagayo	27-Feb-1916	10.70	-85.99	50	7.3	IX	-	i, j
7(^{Po})	Orotina	4-Mar-1924	9.83	-84.56	15	7	IX	-	h, i, j
8(S)	Golfito	5-Dec-1941	8.70	-83.20	28	7.4	IX	-	j, k
9(S)	Samara	5-Oct-1950	10.10	-85.30	55	7.8	VIII	-	j, k
10	Patillos	30-Dec-1952	10.05	-83.92	10	6.2	VIII	21	g, j, k
11(^{Po})	Bajos del Toro	01-Set-1955	10.23	-84.32	3	6.1	VIII	10	a, j, k, l
12	Tilaran	14-Apr-1973	10.45	-84.90	10	6.5	IX	23	f, j, k
13(S)	Golfito	3-Apr-1983	8.50	-83.50	34	7.3	VIII	-	h, j, k
14	División-Buvis	3-Jul-1983	9.49	-83.67	14	6.2	VIII	-	b, j, k
15	Piedras Negras	May-Dec 1990	9.91	-84.31	4	6	VIII	-	c, j, k
16	Limón	22-Apr-1991	9.63	-83.15	23	7.7	X	-	e, j, k
17	Pejibaye swarm	10-13 Jul-1993	9.75	-83.67	14	6	VIII	-	d, j, k
18(^{Po})	Cinchona	8-Jan-09	10.19	-84.18	4.6	6.2	IX	30	h, k, l
19	Upala	July- 2011	10.79	-85.11	10	5.5	VI	-	This study

(*) Event code corresponds to letter code used in figure 1b and 1c, (S): subduction event, (^{Po}): Event that produced coseismic landslides near or on the Poás volcano. I_0 Epicentral Modifeid Mercalli Intensity. References: a(Alvarado et al., 1988), b(Boschini et al., 1988), c(Montero et al., 1991) d(Barquero and Peraldo 1993), e(Mora and Mora 1994), f(Peraldo and Montero 1994), g(Montero and Alvarado 1995), h(Montero 1999) i(Peraldo and Montero 1999) (1, 7), j(Bommer and Rodríguez., 2002), k(Climent et al 2009) and l(Montero et al 2010).

Table 3. Geology summary of the volcanic units that were affected by the induced landslides from the Cinchona earthquake

Volcano	Unit	Age and temporal phase(Paleo or Neo)	Lithology	Slope angle	Geomorphology	Weathering	Drainage system	Soil type and thickness
Platanar V.	Viejo	~ 1 Ma (Paleo-Platanar)	Lavas, volcanic breccias and pyroclastic flows	30°-60°	Uneven slopes, deeply eroded river valleys truncated by faults	Very badly weathered	Sub-parallel	Residual volcanic (~5m)
Barva	Paleo-Barva	0.8-0.2 Ma (Paleo-Barva)	Porphyritic lava flows, breccias and subordinated tuffs	30°-60°	Uneven slopes, deeply eroded river valleys truncated by strike-slip faults	Very badly weathered	Sub-parallel	Tuff and weather lapilli (5-25m)
Barva	Neo-Barva	<0.2 Ma (Neo-Barva)	Lava flows, tuffs and epiclasts	10°-30°	Smooth surface given by a pumiceous flow 10 m thick	Slightly to moderately weathered	Parallel to sub-parallel	Pumiceous flow and residual soil (~5 m)
Barva	Pozo Azul	<0.2 Ma (Neo-Barva)	Lava flows	10°-30°	Shield morphology given by the lava flow and smoothed by pumice flow	Moderately weathered	Semi radial	Residual volcanic (~2m)
Póas	Río Sarapiquí	0.6 - 0.7? Ma (Paleo-Póas)	Breccias and ash-flow tuffs, with epiclastic lenses and subordinate lavas	> 50°	Sarapiquí river canyon	Moderately to badly weathered	Parallel	Residual volcanic <2m
Póas	La Paz Andesites	0.6-0.5 Ma (Paleo-Póas)	Several (at least 7) andesitic lava flows with a characteristic porphyritic texture with megaphenocrysts of plagioclase (2-3cm)	30°-60°	Uneven slopes, deeply eroded river valleys truncated by right lateral faults	Very badly weathered	Sub-parallel	Tuffs and weathered lapilli tuffs with thickness between 5-40 m
Póas	Achiote	0.5-0.2 Ma (Paleo-Póas)	Lava flows	30°-60°	Uneven slopes with river valleys are less truncated than La Paz Andesites U.	Moderately weathered	Parallel to sub-parallel	Material from the Lapilli Tuff Unit (see below) and/or residual soils > 2m
Póas	Río Cuarto Lavas	0.2 Ma (Paleo-Póas)	Lavas	3°-5°	Relatively flat lava field with a slight downward slope to the north	Unweathered to slightly weathered	Parallel	Residual soil and material from Laguna Río Cuarto Maar (see below) < 8m
Póas	Von Frantzious	0.04-0.01 Ma (Neo-Póas)	Lava flows with breccias, epiclasts and pyroclasts on the top	30°-60°	Volcanic cone with smoth slopes	Unweathered to slightly weathered	Semi radial	Residual soils rarely surpass 5 m

Table 3. (continued)

Volcano	Unit	Age and temporal phase(Paleo or Neo)	Lithology	Slope angle	Geomorphology	Weathering	Drainage system	Soil type and thickness
Póas	Congo volcano	0.04-0.01 Ma (Neo-Póas)	Lavas, epiclasts and pyroclastic flows	30°-80°	Volcanic cone which does not have a well defined crater; instead it is open in two main previous landslide scarps to the NNW and NNE	Slightly to moderately weathered	Semi radial	Residual volcanic soils ~ 5 m
Póas	Póas Summit	0.056-present (Neo-Póas)	Lavas and pyroclasts	15°-60°	Main Crater and Botos Crater	Slightly to moderately weathered	Radial to semi radial	Residual soil and thick set (~10 m) of pyroclasts in the Pulga stream valley
Póas	Poasito	0.04-0.025 Ma (Neo-Póas)	Massive lava flows	10°-30°	Smooth surface	Unweathered to slightly weathered	Parallel to sub-parallel	Residual volcanic soils and material from the Póas Lapilli tuff unit > 7 m
Póas	Bosque Alegre	0.0062-0.0028 Ma (Neo-Póas)	Lavas (inner cones)but mostly pyroclasts	40°-60°	Explosion crater	Moderately to badly weathered	Radial into the maar	Residual volcanic soils and pyroclasts ~ 20 m
Póas	Laguna Kopper	0.0003-0.0004 Ma (Neo-Póas)	Pyroclastic material	~60°	Explosion crater	Moderately to badly weathered	Radial into the maar	Residual soils and pyroclastic material<15 m
Póas	Póas Lapilli tuff	< 0.04 Ma (Neo-Póas)	Lapilli tuff	10°-30°	Smooth topography	Moderately to badly weathered	Parallel to sub-parallel	Residual soils and pyroclastic material < 7 m

Table 4. Distribution of landslides and their area based on the orographic regions of the study area approach and precipitation data from meteorological stations near Poás volcano.

Orographic regions	Pacific Region		Caribbean Region	
Region area (km^2), (%)	181.65	35	337.25	65
Landslides frequency (No), (%)	251	5	4595	95
Landslides area (km^2), (%)	0.6	2.7	21.38	97.3
(landslides frequency No / region area km^2)	1.38		13.62	
(landslides area km^2 / region area km^2)	0.003		0.06	
Precipitation one year previous the earthquake (mm)	4796[a], 5042[b]		3994[c]	
Precipitation one month previous the earthquake (mm)	13[a], 93[b]		435[c], 233[d]	
Precipitation one day previous the earthquake (mm)	0[a], 0.9[b]		6.4[c] 1.5[d]	

[a] San Rafael meteorological station (15 km southern from epicenter), [b] Fraijanes meteorological station (10 km from epicenter), [c] La Selva de Sarapiquí meteorological station (25 km northern from epicenter) and [d] Poás meteorological station (located near the summit of the volcano and 6 km western of the epicenter, this station does not have complete the data of mm of rain one year before the earthquake).

Table 5. Distribution of landslides and their areas based on land use approach

Land use	Land use area		Landslides frequency		Landslides area		Density (landslides frequency No /Land use area km^2)	(landslides area km^2/ Land use area km^2)
	(km^2)	(%)	(No)	(%)	(km^2)	(%)		
Primary tropical rain forest	197.2	38	2381	49.00	14.84	67.50	12.07	0.075
Secondary tropical rain and/or gallery forest	103.8	20.0	1494	31.00	5.72	26.00	14.39	0.055
Crops and/or farming areas	207.6	40.0	892	892.00	1.23	5.70	4.30	0.006
No vegetation	9.6	1.9	79	18.00	0.17	0.80	8.23	0.018
Water	0.8	0.2	NA	NA	NA	NA	NA	NA

Table 6: Distribution of landslides and their areas based on volcanic edifice approach

Volcano	Volcano area		Landslides frequency		Landslides area		Density (landslides frequency No /Volcano area km^2)	(landslides area km^2/Volcano area km^2)
	(km^2)	(%)	(No)	(%)	(km^2)	(%)		
Platanar V.	83.04	16	306	6	0.38	1.8	3.68	0.005
Poás V.	285.45	55	3322	69	18	82	11.64	0.063
Barba V.	150.51	29	1218	25	3.6	16.2	8.09	0.024

Table 7: Landslides distribution and their areas based on volcanic units approach

Unit	Volcanic units area		Landslides frequency		Landslides area		Density (landslides frequency No/Volcanic unit area km^2)	(landslides area km^2/Volcanic unit area km^2)
	(km^2)	(%)	(No)	(%)	(km^2)	(%)		
Platanar	74.84	14.42	306	6.00	0.38	1.73	4.09	0.005
Río Sarapiquí	2.85	0.55	129	3.00	0.95	4.32	45.19	0.333
La Paz Andesites	53.04	10.22	1756	35.80	7.98	36.30	33.11	0.150
Achiote	64.36	12.40	93	2.00	0.26	1.18	1.45	0.004
Río Cuarto Lavas	29.58	5.70	22	0.10	0.02	0.08	0.74	0.001
Von Frantzious	56.21	10.83	448	9.00	3.53	16.06	7.97	0.063
Congo volcano	38.41	7.40	288	6.00	3.82	17.37	7.50	0.099
Poás Summit	38.20	7.36	517	11.00	1.25	5.69	13.53	0.033
Poasito	19.46	3.75	14	0.10	0.01	0.05	0.72	0.001
Maar units	5.71	1.10	55	1.00	0.20	0.90	9.63	0.035
Sabana Redonda	0.67	0.13	NA	NA	NA	NA	NA	NA
Paleo-Barva	61.03	11.76	851	18.00	3.03	13.78	13.94	0.050
Neo-Barva	64.36	12.40	343	7.00	0.54	2.45	5.33	0.008
Pozo Azul	8.30	1.60	24	1.00	0.02	0.09	2.89	0.002
Recent deposits	1.97	0.38	NA	NA	NA	NA	NA	NA

Table 8. Landslides distribution and their areas based on volcanic temporal phases units (Paleo and/or Neo)

Temporal volcanic phase unit	Temporal volcanic phase unit area		Landslides frequency		Landslides area		Density (landslides frequency No / Temporal volcanic phase unit area km^2)	(landslides area km^2/Temporal volcanic phase unit area km^2)
	(km^2)	(%)	(No)	(%)	(km^2)	(%)		
Platanar	74.84	14.42	306	6.30	0.38	1.73	4.09	0.005
Paleo-Poás	149.73	28.85	1997	41.20	9.21	41.88	13.34	0.061
Paleo-Barva	60.98	11.75	851	17.56	3.03	13.77	13.95	0.050
Neo-Barva	160.58	30.94	1325	27.34	8.81	40.08	8.25	0.055
Neo-Poás	72.87	14.04	367	7.58	0.56	2.54	5.04	0.008
Paleo-Unit (Platanar, Poás and Barva)	285.55	55.02	3154	65.08	12.61	57.38	11.05	0.044
Neo-Units(Poás and Barva)	233.45	44.98	1692	34.92	9.37	42.62	7.25	0.040

Table 9. Landslides distribution based on slope.

Slope angle range (°)	Slope angle range area		Landslides frequency		Landslides area		Density (landslides frequency No /slope range area km^2)	(landslides area km^2/slope range area km^2)
	(km^2)	(%)	(No)	(%)	(km^2)	(%)		
1 - 14	196.55	37.87	42	0.87	0.04	0.17	0.21	0.0002
15 - 29	166.70	32.12	373	7.70	2.84	12.92	2.24	0.017
30 - 44	110.72	21.33	1956	40.36	6.42	29.21	17.67	0.058
45 - 59	36.08	6.95	2058	42.47	10.62	48.32	57.05	0.294
60 -74	7.46	1.44	390	8.05	1.93	8.78	52.25	0.259
75- 89	1.49	0.29	27	0.56	0.13	0.60	18.09	0.088

Table 10.Landslides distribution base on event type

Landslide Type	Number of event by type	Area of events by type (km^2)	Area/No
Rock fall	17	0.03	0.0017
Slide	2555	8.22	0.0032
Slump	1725	5.38	0.0031
Debris Flow	486	7.93	0.0163
Unknown	63	0.43	0.0069

Table 11. Monthly rainfall data from seven meteorological stations within the study area used in to obtain the ground moisture susceptibility factor (S_h)

Station (Code)	Period	Jan	Feb	Mar	Apr	May	Jun	Jul	Aug	Sep	Oct	Nov	Dec	Annual
Fraijanes (FRA)	1976-2008	11.7	67.8	60.6	124.4	401.3	408.7	336.0	380.6	506.6	510.1	323.4	170.6	3301.8
Vara Blanca (VBL)	1959-2006	252.7	135.0	101.2	137.8	324.9	356.9	370.0	354.8	366.7	408.6	439.8	411.0	3659.4
Poás (POA)	1972-1979	255.0	150.0	100.0	117.0	400.0	390.0	385.0	345.0	365.0	400.0	415.0	398.0	3720.0
Colonia Los Angeles (CLA)	1982-2001	448.7	245.2	222.2	198.7	541.5	607.5	606.7	601.7	595.1	628.8	605.5	560.1	5861.7
Quebrada Pilas (QPI)	1986-2001	502.8	277.7	216.6	204.3	392.0	444.0	485.5	478.3	470.1	498.5	524.1	615.7	5109.6
Isla Bonita (IBO)	1981-1983	385.2	222.5	180.1	193.4	429.6	473.2	468.0	469.0	443.4	515.6	563.3	502.1	4845.4
Los Cartagos (LCA)	1968-1984	250.0	130.0	105.0	140.0	420.0	410.0	379.0	360.0	370.0	410.0	450.0	415.0	3839.0

Chapter 3

Reconstruction of Turrialba volcano

This chapter resulted in one submitted paper:

Ruiz P., Turrin B., del Potro R., Gagnevin D., Gazel E., Soto G. J., Carr M.J., Mora M. & Swisher III C. $^{40}Ar/^{39}Ar$ ages of Late Pleistocene-Holocene lavas from Turrialba volcano Costa Rica, some of the youngest lavas reported in Central America by this method. (G3), in revision.

Abstract

$^{40}Ar/^{39}Ar$ dating of eight lava flow units from Turrialba volcano, yield ages that range from 251 to 3 ka. These ages are in agreement with the local stratigraphy and with prior ^{14}C age determinations. Three of these units, with K_2O between 1.57 - 3.56 wt.% of K_2O, gave remarkably young $^{40}Ar/^{39}Ar$ ages (25 ka or less), among the youngest lavas dated in Central America by this method. Prior geologic mapping indicated two temporal stages of volcanic growth, the Paleo Turrialba stage and Neo Turrialba stage. Our sampling included one of the youngest flows from Paleo Turrialba (251 ± 4ka) and most of the youngest flows from Neo-Turrialba. The Neo-Turrialba flows consist of a low silica group and a high silica group, separated by a gap between 54 and 59 wt.% SiO_2. Because we were able to date most of the recent flows we suggest that the Neo-Turrialba stage includes at least 4 episodes: 99-90, 61-60, 25 and 10-3 ka. Three of these episodes

include lavas from both the high silica group and the low silica group, consistent with the presence of a zoned magma chamber with a silicic top and mafic base. The current unrest at Turrialba started in 2007 and in 2010 produced a fumarolic-phreatic eruption of lithic ash. This paper contributes to the evaluation of future hazards by demonstrating that the volcano has recently produced lavas from both a mafic group of similar basaltic andesites and a silicic group of andesites to dacites.

1.Introduction

Turrialba is the easternmost volcano of the Costa Rican Central Volcanic Range (CVR). It is located 35 km northeast of the capital, San José, and the other major cities of the Central Valley which host ~2.1 million inhabitants, (Figure 1). Since the prevailing winds blow from the Caribbean into the mainland (E-W), and the Central Valley is downwind from Turrialba, ash eruptions from Turrialba pose a major threat to cities there. Understanding Turrialba geologic evolution and periods of activity is important for hazard mitigation.

The main vent of Turrialba volcano is located about 10 km to the northeast of Irazú volcano, and behind the main N60W alignment of the CVR (Figure 1b). It is possible its location is a consequence of deep crustal fractures that allowed the rise of magma along different pathways [*Stoiber & Carr* 1973*; Soto* 1988a]. Turrialba is a complex composite volcano with a maximum elevation of 3340 m (a.s.l.).The newest volcanic center (defined as Neo-Turrialba) consists of a pile of approximately 112 km^3 of lava flows and associated pyroclastic deposits, which crown the whole ~ 400 km^3 edifice and covers an area of ~500 km^2 [*Carr et al.,* 2007*; Alvarado* 2009].

Turrialba has had summit fumaroles since at least 1723 CE. The last historical eruption was between 1864 and 1886 CE. It consisted of strombolian and vulcanian activity in which ash-fall affected the Central Valley and even reached the Pacific Coast and the Gulf of Nicoya ~130 km away (Figure 1b). After this eruptive period, the activity at Turrialba consisted only of low temperature (<95^{o}C) fumaroles [*Soto,* 1988a*; Tassi et al.,* 2004*; Vaselli et al.,* 2010]. In 2007 the gas flux (e.g CO_2, SO_2 and H_2S) and temperature of the fumaroles increased, as did the seismicity [*Martini et al.,* 2010]. This increase in activity culminated in a fumarolic-phreatic eruption that opened a new small (65 m × 20 m) vent in the summit region on the 5 and 6 January 2010 [*GVN,* 2007; *GVN* 2008; *GVN* 2010*; Soto el al.,* 2010]. Lithic ash from this explosion traveled southwest, reaching the cities of the metropolitan area of Cartago, Tres Ríos and San José, ~35 km away (Figure 1c). Today, high temperature (>500^{o}C) gases continue to escape from the volcano and the possibility of more phreatic and phreato-magmatic eruptions persists.

This recent increase in volcanic activity has prompted a reevaluation of the volcanic risks associated with Turrialba volcano. Previously, the only dating of Turrialba units was done via ^{14}C by *Reagan et al.* [2006] and was restricted to the summit units. As result, a lack of age control from the volcanic deposits on the flanks of the volcano has hindered the reconstruction of the volcanic stratigraphy and the volume calculations required to determine the lava/magma production potential of the Turrialba volcanic system. The data presented here are aimed to better characterize the main periods of activity of the Turrialba volcano.

Herein, we present eight new ^{40}Ar/^{39}Ar age results with geochemical and petrographic data from lava flow units mapped by *Soto* [1988a] and revised for this

study, from the upper and lower flanks of the newest volcanic center of Turrialba. Anticipating young ages for some of the lava flows, based on aerial photos, geomorphology studies, their proximity to the summit and stratigraphic correlation, we followed the measurement protocol recently described in *Turrin et al*. [2008] and *Turrin et al*. [2010] that facilitates the accurate determination of very young $^{40}Ar/^{39}Ar$ ages.

2. Geology of Turrialba volcano

On its southeastern and eastern flanks, the Turrialba volcanic massif overlies the sedimentary sequence of the Limón Basin, an alkaline volcanic sequence dated at 4.51 ± 0.37 – 4.33 ± 0.07 Ma [*Gazel et al.,* 2011] and a calk-alkaline andesitic sequence dated at 2.15 ± 0.30 Ma [*Tournon,* 1984]. Based on *Gans et al.* [2003], the oldest rocks of the CVR are about 1 Ma. This age is in agreement with the age of the Intracañon Formation lavas (758 ± 16 ka) [*Marshall et al,* 2003] from the southwestern limits of the CVR and the oldest age from the Irazú massif around 0.85 Ma [*Alvarado et al.,* 2006]. Thus we speculate a similar age range for the volcanics immediately beneath Turrialba volcano.

Only two previous surveys have focused on the geology of Turrialba. *Soto* [1988a] established the first stratigraphic sequence and geologic map of the crowning cone, identifying 15 major units, with the older flows of the sequence located mainly in the southern and eastern flanks of the volcano. The Turrialba volcano evolved in three main stages (Proto-, Paleo- and Neo-Turrialba) with different volcanic foci, piling up into a voluminous massif [*Soto1988a*]. It has been possible through $^{40}Ar/^{39}Ar$ data to date similar volcanic pulses in other main volcanoes of the CVR, namely Barva, Irazú and Poás [*Pérez et al.,* 2006; *Alvarado et al.,* 2006, *Carr et al.,* 2007 and *Ruiz et al.,* 2010]. The second survey to focus on Turrialba was carried out by *Reagan et al.* [2006] who

studied the most recent activity (last 10 ka) from Turrialba identifying deposits from at least 20 eruptions in the summit region.

The youngest unit of Paleo-Turrialba is Finca Liebres volcano and Neo-Turrialba grew to the east of its position (Figure 2). The current edifice has a flat summit region, elongated SW-NE. It is comprised of three craters (Southwest, Central and Northeast) as well as a fourth unnamed and eroded crater close to Cerro San Juan in the southwest region of the edifice (Figure 2). The origin of an amphitheater-like feature to the northeast of the summit is still unclear and has been attributed to erosional phases that occurred sometime between 9 and 50 ka [*Reagan et al.,* 2006]. Two small pyroclastic cones (Tiendilla and El Armado, 70 m high and 3.6×10^6 m^3, 120 m high and 1.8×10^7 m^3, respectively) lie on the southwestern flank, which is cut by scarps and faults mainly trending NE, then forming a summit graben [*Soto,* 1988b]. Other faults have cut the newest edifice, making it a structurally complex stratovolcano [*Linkimer,* 2003] (Figure. 2). Lavas and pyroclastic products of Turrialba range in composition from basalts to dacites [*Reagan et al.,* 2006 and this work].

Six major eruptions have taken place in Turrialba during the last 3400 years. The most significant eruption was considered as a Volcanic Explosivity Index (VEI) ~4 event and occurred about 1910 BP, producing pyroclastic flows and surges. The total erupted volume was approximately 0.2 km^3 and the tephra covered 5000 km^2 [*Reagan et al.,* 2006]. The products of the other five recent eruptions have variable thicknesses around Turrialba's summit and are not recognizable in soils downwind, suggesting that their volumes were less than 0.05 km^3 (VEI between 2-3) [*Reagan et al.,* 2006].

3. 40Ar/39Ar methods and data handling

Based on the inferred stratigraphy [*Soto,* 1988a] revised by recent mapping (Fig. 2), eight volcanic units were selected for radiometric dating. The eight samples were selected to span the oldest unit (Upper Finca Liebres), intermediate units, and the youngest units that comprise the cone, bracketing the age of the main construction phase of the Neo-Turrialba edifice.

The $^{40}Ar/^{39}Ar$ measurements were done at the Noble Gas Laboratory at Rutgers University using methods similar to those of *Turrin et al.* [1994; 1998; 2008] and *Carr et al.* [2007]. Argon isotopic ratios were measured on a MAP-215-50 mass spectrometer. The mass spectrometer detector system has been upgraded to digital ion-counting as described in *Turrin et al.* [2010]. Data collection and data reduction were performed using the software "MassSpec" written by Alan Deino.

The rock samples were crushed, sieved to 600 μm to 300 μm, washed in distilled water, and then dried in an oven at 60^{o} C. The magnetic fraction was removed using a hand magnet and the plagioclase phenocrysts were removed using a Frantz Isodynamic Separator. The remaining plagioclase and pyroxene phenocrysts were hand-picked from the matrix fraction under a binocular microscope.

Approximately 100 mg of the cleaned matrix separates were then loaded into individual sample wells of an Al-irradiation disk. The neutron fluence was determined using the Alder Creek Sanidine with a reference age of 1.194 ± 0.006 Ma [*Nomade,* 2005]. The loaded sample disks were wrapped in Al foil, sealed in quartz glass tubes, and

then irradiated for 10 minutes in Cd foil shielding with a neutron irradiation in the central thimble of the USGS TRIGA reactor.

Samples were incrementally heated by step-wise increases in laser wattage output, from approximately 400^{o} C to 1400^{o} C, until the samples fused. The reported $^{40}Ar/^{39}Ar$ plateau age results meet the criteria presented by *Dalrymple and Lanphere* [1969], *Fleck et al.* [1977] and *Carr et al.* [2007] and summarized by *Turrin et al.* [2008]. Here we recap the main points that processed data should meet to be considered acceptable and then reported.

1. An incremental-heating plateau with at least three contiguous increments that together represent at least 50 % of the total $^{39}Ar_k$ released from the sample, any two adjacent fractions must be analytically indistinguishable at the 95% confidence level.

2. The data in the isochrones, should form a linear array that yields a mean square of weighted deviates (MSWD) of approximately two or less [*York, 1969*]. A value of 1.0 indicates that the scatter about the regression line is accounted for by the measurements errors. If the value is less than unity, then the analytical errors are likely overestimated. Ages whose isochron plots results in MSWSs close to 1.0 are considered most reliable.

3. The isochron age should be analytically indistinguishable from the plateau age at 95 % confidence level.

4. The initial $^{40}Ar/^{39}Ar$ ratio should be analytically indistinguishable at 95% confidence level from the accepted atmospheric ratio of 295.5 ± 2.

5. The integrated (total-fusion) age should be analytically indistinguishable from the plateau and isochron ages at 95% confidence level.

If the data meet these criteria above, the first age to be considered to report is the plateau age, the isochron age is the second age to be considered (for our samples it was obtained with the plateau data only), finally the integrated (total-fusion) age is the last to be considered to report.

One of the difficulties of obtaining precise radiometric ages on young, low-potassium volcanic rocks by the $^{40}Ar/^{39}Ar$ method is the large correction caused by the subtraction of atmospheric Ar from the total Ar concentration measured in the sample. Therefore, to obtain accurate and precise $^{40}Ar/^{39}Ar$ ages on young volcanic rocks, an accurate "mass discrimination correction" must be applied to all of the measured isotopic ratios used to calculate the ages. This correction was applied to the Turrialba samples using the method presented in *Turrin et al.* [2008] and *Turrin et al* [2010]. During the analysis of the samples and AC-1 standard, the mass discrimination was monitored by measurement of an air aliquot of approximately $1x10^{-13}$ moles of ^{40}Ar, delivered via an online automated air pipette system, after every seventh isotope measurement.

These mass discrimination data, determined from the measured apparent $^{40}Ar/^{36}Ar$ ratio of the air aliquots, was then plotted through time, tracking any temporal drift in the mass discrimination and modeled with a best-fit regression through the time series data. The resultant curve was then applied to the standards and unknown sample measurements. Modeling the mass discrimination data throughout the run period

significantly improved the accuracy of the analytical data for both the standard and unknowns.

The methodology employed here and the relatively high K_2O of Turrialba lavas (1.54 to 3.56 wt.%), resulted 10 times the percent radiogenic ^{40}Ar yields typically obtained on geologically young, low potassium (0.3 to 1 wt.% K_2O) bearing samples. Relative high potassium content is common in magmatic rocks from Central Costa Rica and is thought to be related to mantle metasomatism [*Gazel et al.*, 2009].

Major elements analyses were carried out at Michigan State University, following the procedure described in *Hannah et al.* [2002]. These data were collected by XRF using Bruker S4 Pionner equipment giving errors that are proportional to each element and should not be greater than 2%. Geochemical data for sample T-68 are from *Reagan et al.* [2006], and were obtained with techniques described in *Reagan* [1987] and *Reagan and Gill* [1989].

4. Data and Results

The results of eight $^{40}Ar/^{39}Ar$ measurements on rock matrix from key lava flow units from Turrialba volcano are reported here. The sample locations and the best estimated ages are presented in Table 1. The data from the step heating measurements for each sample are summarized in Table 2. All uncertainties are expressed as standard deviations (1σ) unless otherwise specified. In addition, we report major element results and petrographic descriptions for the dated samples in Tables 3 and 4.

Rock samples belong to the High-K Calc-Alkaline Series and range from basaltic-andesites to dacites based on the SiO_2 vs. K_2O classification of *Peccerillo and Taylor*

[1976] (Figure 3). In the following paragraphs, we describe the location of the samples, and present the measurements and best age estimate from oldest to youngest, for the samples that meet the criteria described in the previous section.

Sample TUR-38 (Upper Finca Liebres Unit) was collected ~4 km southwest of the summit of Turrialba (Figure 2). This sample yielded a four step plateau age of 251 ± 4 ka, comprising 72.6 % of the total $^{39}Ar_K$ released (Figure 4a, Tables 1 and 2). The total fusion age (244 ± 4 ka) is concordant with the plateau age at the α-95% confidence level. The isotopic data from the plateau steps yield an isochron age of 260 ± 60 ka (MSWD = 0.091) and an initial $^{40}Ar/^{36}Ar$ ratio of 294.2 ± 7.6. We consider the best estimate age for this sample to be the plateau age of 251 ± 4 ka.

Sample TUR-30 (Lower Los Cabros Unit) was collected ~3 km northeast from the crater zone (Figure 2). The data for the step-heating experiment of this sample do not meet the criteria described above for defining a plateau (Figure 4b, Tables 1 and 2). When cast on an isotope correlation diagram, the isotopic data yield an isochron age of 100 ± 16 ka (MSWD =19) and an initial $^{40}Ar/^{36}Ar$ ratio of 295.6 ± 6.5. The high MSWD value indicates that the dispersion of the data about the regression line is greater than the analytical errors. This indicates that the distribution of ^{40}Ar (radiogenic) relative to K is heterogeneous likely due to weathering and/or alteration [*York, 1969*]. For this sample, the integrated date of 99 ± 3 ka may be a good approximation of the age.

Sample TUR-19 (Upper Los Cabros Unit) is located 5 km southeast from the summit of Turrialba (Figure 2) and is one of three samples with relatively low K_2O content (1.54 wt.%) (Figure 3). The sample yielded a five step plateau age of 90.0 ± 4 ka,

comprising 86.7% of the total $^{39}Ar_K$ released (Figure 4c, Tables 1 and 2). Combining all the step heating data, a total fusion age of 107 ± 6 ka is obtained. The isotopic data from the plateau step yield an isochron age of 82 ± 12 ka (MSWD = 0.61) and an initial $^{40}Ar/^{36}Ar$ ratio of 297.3 ± 2.1. All three of these ages are concordant at the α-95 % confidence level. Based on these results, the best estimate for this sample is the plateau age of 90.0 ± 4 ka.

Sample TUR-32 (Bajos 1 Unit) was collected ~3 km northeast from the summit crater region (Figure 2). The step-heating experiment for this sample produced a undisturbed spectra, consisting of 100 % of the total $^{39}Ar_K$ released, defining a six step plateau age of 62.0 ± 2 ka (Figure 4d, Tables 1 and 2). The total fusion age is concordant with the plateau age, indicating an age of 62.0 ± 3 ka. When the isotopic data are cast on an isotope correlation diagram, an isochron age of 62.0 ±5 ka (MSWD = 0.45) with an indicated initial $^{40}Ar/^{36}Ar$ ratio of 295.7 ± 4.3 is obtained. This sample meets all five criteria discussed above. Moreover, the three ages of this sample are concordant at the α-95 % confidence level. The best age estimate for this sample is the plateau age 62.0 ± 2 ka.

Sample TUR-33 (El Armado Flow Unit) was collected ~4 km south from El Armado pyroclastic cone (Figure 2). This is one of the three samples with low K_2O (1.57 wt.%) concentrations (Figure 3). A three step plateau age of 61.0 ± 6 ka consisting of 76% of the total $^{39}Ar_K$ released was obtained for this sample. The total fusion age is 59 ± 7 ka, concordant with the plateau age at the α-95 % confidence level (Figure 4e, Tables 1 and 2). The isotopic data from the plateau step yield an isochron age of 30 ± 40 ka

(MSWD = 2.2) and an initial $^{40}Ar/^{36}Ar$ ratio of 299.1 ± 8.9. The best age estimate for this sample is the plateau 61.0 ± 6 ka.

Sample TUR-12 (Lower Turrialba Unit) is located ~5 km southeast of the summit, and presents the highest K_2O content (3.56 wt.%.) of the eight samples (Figures 2 and 3). The incremental heating experiment for this sample produced a five step plateau age of 25.6 ± 1.9 ka comprising 85 % of the total $^{39}Ar_K$ released (Figure 4f, Tables 1 and 2). The total fusion age (42 ± 2 ka) is older than the plateau age. The total fusion age and the plateau age are discordant at the at the α-95 % confidence level. The discrepancy between the total fusion age and the plateau age is due to the anomalously old ages for the first three low temperature steps. However these old ages only represent the 15 % of the total $^{39}Ar_K$ released. When the isotopic data from the plateau steps are cast on an isotope correlation diagram, an isochron age of 24 ± 10 ka (MSWD = 0.54) with an initial $^{40}Ar/^{36}Ar$ ratio of 297 ± 13.2 is obtained. Given that the isochron age is concordant with the plateau age at α-95 % confidence level, the plateau age of 25.6 ± 1.9 ka is the best age estimate for this sample.

Sample TUR-36 (La Silvia Unit), collected ~3 km south from the summit crater region, is one of the three samples with relatively low K_2O (1.57 wt.%) content (Figures 2 and 3). This sample produced an undisturbed release spectra, defining a seven step plateau age of 10.0 ± 3 ka consisting of 99.9 % of the total $^{39}Ar_K$ released (Figure 4g, Tables 1 and 2). The total fusion age (14 ± 4 ka) for this sample is concordant at α-95 % confidence level with the plateau age. The isotopic data from the plateau step yields an isochron age of 19 ± 14 ka (MSWD = 0.54) and an initial $^{40}Ar/^{36}Ar$ ratio of 292.9 ± 5. The best age estimate for this sample is the plateau age 10.0 ± 3 ka.

Sample TUR-08 (La Picada Unit), is from a dacite lava flow located high on the flank of the main vent complex, 2 km west of the summit area, (Figure 2). This sample is one of two samples with the highest K_2O content (3.27 wt.%; Figure 3). This sample yielded an undisturbed release spectra, defining a seven-step plateau age of 3 ± 3 ka that is comprised of 98 % of total $^{39}Ar_K$ released (Figure 4h, Tables 1 and 2). The integrated age obtained is 4 ± 4 ka. When cast on a isotope correlation diagram, the isotopic data yield an isochron age of 7 ± 6 ka and an initial $^{40}Ar/^{36}Ar$ ratio of 294.2 ± 3 (MSWD = 0.93). All the ages are concordant at α-95 % confidence level. The best age estimate for this sample is the plateau age 3 ± 3 ka.

5. Discussion

5.1. Stratigraphic constraints

Based on geological mapping [*Soto,* 1988a] previous works in the CVR [*Gans et al.* 2003, *Alvarado et al.,* 2006 and] and the new $^{40}Ar/^{39}Ar$ ages we maintain the hypothesis that, similar to other volcanoes from the CVR, Turrialba volcano has evolved in three main stages: The initial stage, Proto-Turrialba 1000?-600? ka, stage that is not represented in this study. However, Turrialba volcano shares part of the southwestern flank basement with Irazú volcano and units from this sector have been dated as old as 0.85 Ma [*Alvarado et al.,* 2006]. This age is our best estimate of the start of activity at Turrialba. The second stage, Paleo-Turrialba 600?-250 ka is estimated to begin at about 600 ka. This age is based on work by *Gans et al.* [2003], and *Carr et al*. [2007] that found a well-defined pulse of volcanic activity in Costa Rica beginning at 600 ka. The minimum age for Paleo-Turrialba stage corresponds to the Upper Finca Liebres Unit (TUR-38) dated here at 251 ± 4 ka). Finally, the Neo-Turrialba stage includes all the eruptives after 250 ka.

The stratigraphic relationships for five of the eight dated units in this study are shown in the cross sectional sketch of the southern flank of Turrialba volcano (Figure 5a). The two oldest dated units on this side of the volcano, the Upper Finca Liebres Unit (TUR-38, 251 ± 4 ka) and Lower Los Cabros Unit (TUR-19, 90 ± 4 ka), are located to the west and east respectively of the main crater and appear to constrain the spatial extent of younger units. The El Armado Flow Unit (TUR-33, 61 ± 2 ka) unconformably overlies the Upper Finca Liebres Unit (TUR-38, 251 ± 4 ka). This lava flow appears from geomorphology to be contemporary to the cone, we speculate that this sample (TUR-33,

61 ± 2 ka) dates the cone formation as well as the lava flow. The El Armado Flow Unit underlies an undated unit (TU-4) that, based on stratigraphic constraints, we estimate to be between 10 ka and 25 ka. Specifically, this unit is capped by the La Silvia flow Unit (TUR-36, 10 ± 3 ka) and is lateral to the Lower Turrialba Unit (TUR-12, 25 ± 1.9 ka). The Lower Turrialba Unit (TUR-12, 25 ± 1.9 ka) unconformably overlies the Lower Los Cabros Unit (TUR-19, 90 ± 4 ka) on the east side of Turrialba volcano (Figure 5a). The radiometric data presented here is in good agreement with the stratigraphy suggested by Soto 1988a for this flank of the volcano.

For the units located in the northeastern flank of the volcano (Figure 5b), the stratigraphic correlation is more complex because this area has been affected by faulting and is inferred to have been affected by massive erosion either a large flank collapse or several episodes of mass wasting events: cf. *Reagan et al.*[2006] that has generated a horseshoe-shaped depression. The Upper Los Cabros Unit, dated at 99 ± 3 ka (TUR-30), is exposed on the scarp of the horseshoe and is almost indistinguishable from the overlying Lower Los Cabros Unit exposed on the western flank (TUR-19, 90 ± 4 ka). The TUR-30 age predates the formation of the scarp, and the TUR-19 probably does as well. Moreover, Bajos 1 Unit 62 ± 2 (TUR-32) is a lava flow infilling the depression and hence provides a minimum age limit for the formation of the scarp, the stratigraphic relationship between the Upper Los Cabros Unit (99 ± 3 ka; TUR-30) and (Bajos 1 Unit 62 ± 2; TUR-32) is not clear in this sector. The stratigraphic position of the units from Volcán Dos Novillos is still unclear, but we speculate that at least part of this volcano belongs to the Neo-Turrialba Stage (~ 200?-100 ka) and its materials contributed to the construction of the most recent massif.

The western flank of the volcano (Figure 2) is mostly occupied by the La Picada Unit dated at 3 ± 3 ka (TUR-08), which overlies the surrounding lavas including the La Silvia Unit (TUR-36, 10 ± 3 ka). The lava from La Picada Unit erupted from the summit area of Turrialba and, based on petrographical and geochemical analyses, we interpret it as being equivalent to the unit exposed in the summit crater walls, named by *Reagan et al.* [2006] as Unit 12, and sampled as T-68.

Samples TUR-8 and T-68 are very similar. Both samples have a porphyritic texture with a phenocryst mineralogy of: plag + cpx + opx with a hypocrystalline groundmass, which is representing ~50% of the sample section. These two samples also have a glomeroporphyritic texture, with the dominant presence of (cpx + ol + opx) glomerocrysts (Figure 6a).

Both samples are dacites based on the classification scheme of SiO_2 vs. K_2O of *Peccerillo and Taylor* [1976] (Figure 3). TUR-08 shows 63 wt. % of SiO_2, and 3.27 wt. % of K_2O; almost identical, within the error to those of T-68 (Figure 3). The major oxides (e.g., TiO_2, Al_2O_3, Fe_2O_3, CaO, Na_2O, MgO among others oxides) between samples TUR-8 and T-68, are indistinguishable within error (Figure 6b).

Reagan et al. [2006] carried out ^{14}C dating on two pyroclastic units (Unit 3 and 4 of *Reagan et al.* [2006]) exposed inside the Central and Southwest Craters of Turrialba. They obtained dates of 1975 ± 45 yr B.P and 2330 ± 90 yr B.P respectively. The outcrops in the summit craters show that these two units are overlying Unit-12 represented by sample T-68 (Figure 7). This indicates that La Picada Unit is surely older than 2.3 ka, which is within the error for the $^{40}Ar/^{39}Ar$ age (TUR-08, 3 ± 3 ka) presented here. Since

La Silvia Unit (TUR-36, 10 ± 3 ka) is stratigraphically underlying La Picada Unit, the ^{14}C ages from the summit are also, providing more support to our young $^{40}Ar/^{39}Ar$ ages.

5.2 Parallel evolution of high and low silica magmas at Turrialba volcano

Variations in the bulk composition, such as those found here in the lavas from Turrialba commonly reflect two processes that the magma may be subjected to during its storage and ascent to the surface: fractional crystallization and/or magma mixing. The variation diagrams for major oxides (TiO_2, Fe_2O_3, MnO, CaO, Na_2O and K_2O) (Figure 6b), and trace elements (Figure 8) reveal roughly linear trends that are consistent with both mixing between different batches of magma and fractional crystallization. With decreasing MgO, the increase in Al_2O_3 to a peak at about 18 wt % Al_2O_3 (Figure 6b) is characteristic of fractional crystallization in the absence of plagioclase. The MgO versus Al_2O_3 variation is consistent with fractional crystallization but the data set is too sparse to be certain. Petrographic observations (Table 4), such as the common occurrence of sieved texture in plagioclase argue for magma mixing as a fundamental process occurring throughout the evolution of the volcano [*Sakuyama*, 1984]. The sample with the highest MgO (TUR-33, 61 ± 6 ka) is not collinear with the rest of the data (Figures 6b and 8) the high MgO, Ni and Cr contents (Table 3, Figure 8) of this lava make it the most primitive magma found in our data set. These characteristics suggest that this sample comes from a slightly different magma than the other sampled lavas. Several magma chamber processes are likely to have occurred at Turrialba, similar to the complexity *Alvarado et al*. [2006] described for Irazú volcano.

Our new geochronological and geochemical data identified three pairs of co-erupting lavas (TUR-30, 99 ± 3 ka and TUR-19, 90 ± 4), (TUR-32, 62 ± 2 ka and TUR-

33, 61 ± 6 ka) and (TUR-08, 3 ± 3 ka and TUR-36, 10 ± 3 ka). Each corresponding pair presents significant differences in the silica content (Figure 9), other major elements, and trace elements (Figures 6b and 8). The youngest pair of samples has the widest variation of silica, thus the rock type from this pair includes a basaltic-andesite and a dacite, while the rocks from the other two pairs only range from basaltic-andesite to andesite (Figure 3).

There appears to be a characteristic eruptive behavior during the last 100 ka with near simultaneous eruption of mafic and silicic lavas. We define two geochemical groups: high silica group (SiO_2 60-67 wt. %) and low silica group (SiO_2 53-55 wt. %) (Figure 9). The lavas of the high silica group are also enriched in K_2O, Zr and Rb, and depleted in oxides like, MnO, Fe_2O_3 TiO_2 and CaO. Without the new $^{40}Ar/^{39}Ar$ data the contemporaneous eruptive behavior of the high and low silica groups would not be recognized, because their co-evolution results in an overall even distribution of SiO_2 values located in the High-K Calc-Alkaline Series (Figure 3).

The presence of lavas with high and low silica contents erupting nearly at the same time is a common complexity in stratovolcanoes (e.g., Santa Ana in El Salvador, Irazú in Costa Rica, Cotopaxi in Ecuador, among others) [*Carr and Pontier*, 1981; *Alvarado et al.*, 2006; *Hall and Mothes*, 2007]; however, this complexity is compounded at Turrialba because in the high silica group, the content of silica and several incompatible elements (K, Zr and Rb) (Figure 8) increases over time, suggesting an enrichment of these elements for most of the episodes of activity. This could be evidence of a long-lived magma chamber with an evolving silicic top above a mafic base that is fed from the mantle [*McBirney,* 1980 and *McBirney et al.* 1985].

Other cases of co-erupting high and low SiO_2 lavas have been explained by the presence of more evolved magma near the top of the chamber that is erupted at the onset of a new eruptive phase, while the discharge of less evolved magma comes in the final stages of the eruption [*McBirney et al.* 1985]. With the available information, we cannot demonstrate this hypothesis for the case of Turrialba, since the lava pairs with similar ages are within the error in age dating and sufficiently spatially separated to not allow determination of superposition, so we cannot tell whether the high or low silica magma erupted first.

The vent locations for Turrialba's recent flows provide weak evidence in support of a zoned magma chamber as envisioned by *McBirney et al.* [1985]. The only flow that clearly erupted on the flank is a basaltic andesite (TUR-33, 61 ± 2ka), consistent with eruption of a lower part of a magma chamber. This flow came from El Armado cone, which is located over a fissure that cuts this basaltic cinder cone, and currently has seismicity and active fumaroles. The silicic units would logically erupt from the central vent and two of the four clearly do. The vent locations of the four remaining flows dated from Neo-Turrialba can no longer be determined.

6. Summary and conclusions

Three of the ages obtained in this study (TUR-12, 25 ± 1.9 ka; TUR-36, 10 ± 3; and TUR-08, 3 ± 3 ka) are among the youngest lavas dated by $^{40}Ar/^{39}Ar$ method in Costa Rica and Central America. The Cervantes flow at Irazú volcano dated at 20 ± 12 ka [*Alvarado et al.,* 2006] is another example of young lavas dated by $^{40}Ar/^{39}Ar$. Stratigraphic studies and correlations to previous ^{14}C ages from the summit of Turrialba supported our young $^{40}Ar/^{39}Ar$ results. Geochemical and petrographical data enable us to

correlate a sample from the La Picada Unit (TUR-08, 3 ± 3 ka) found in the west flank of the volcano, and a flow located in summit crater walls described by *Reagan et al.* [2006]. Since the equivalent flow of La Picada Unit in the crater walls is capped by two pyroclastic units (Units 3-4) younger than 2.3 ka, this allowed us to give a minimum age to La Picada Unit of ~2.4 ka. This means that La Picada Unit was emplaced in period of time approximately between 2.4 and 6 kyr ago, since La Silvia Unit (TUR-36, 10 ± 3 ka) is underlying it.

New geochronological and geochemical data reveal a range of lava compositions from 52 to 64 wt% SiO_2 during just the last 100 kyr. The lavas occur in four different eruptive episodes one around (99-90 ka, another around 61-60 ka, one about 25 and the last 10-3 ka). In three of these episodes there were contemporaneous eruptions of both high and low silica magmas. The common co-eruption of mafic and silicic magmas is consistent with a magma chamber model proposed by [*McBirney et al.* 1985]. In this model, a zoned silicic magma is above a convecting, rather uniform mafic magma. At least one of the low silica magmas at Turrialba came from a satellite cone, El Armado cinder cone, along a fissure that radiates from the central crater and may connect at depth to zones in the magma chamber where the less evolved magmas are located [*McBirney et al.* 1985].

The variations in the SiO_2 and other elements can be explained by fractional crystallization and/or magma mixing. It is likely that crystal fractionation is occurring, but petrography indicates that magma mixing is clearly present.

Regardless the origin of the silica-rich lavas described here and also by Reagan et al. (2006), their presence makes possible a very explosive eruption style that should be accounted for in a volcanic hazard response plan.

7. References

Alvarado, G. E 2009. Los volcanes de Costa Rica: Geología, historia, riqueza natural y su gente. 3ª edición, XXXII + 16 laminas + 330 pp. Editorial Universidad Estatal a Distancia, Costa Rica.

Alvarado, G. E., M.J. Carr, B.D. Turrin, C. C. Swisher, H. U. Schmincke, and K. W. Hudnut 2006. Recent volcanic history of Irazú volcano, Costa Rica: Alteration and mixing of two magma batches, and pervasive mixing, in Volcanic Hazards in Central America, edited by W. I. rose et al., Spec Pap. Geol. Soc. Am., 412, 259-276, doi: 10.1130/2006.2412(14).

Carr, M. J., and Pontier N. K., 1981. Evolution of a young parasitic cone towards a mature central vent; Izalco and Santa Ana volcanoes in El Salvador, Central America. Journal of Volcanology and Geothermal Research. doi:10.1016/j.physletb.2003.10.071.

Carr, M. J., G. E Alvarado, L. Bolge, F. Linsay, K. Milidakis, B. Turrin, M. Feigenson, C.C. Swisher III 2007. Element fluxes from the volcanic front of Costa Rica and Nicaragua. Geochem Geophys Geosyst.,8Q06001. doi:10.1029/2006GC001396.

Dalrymple, G.B. and M.A. Lanphere 1969. Potassium-Argon Dating: Principles, Techniques, and Applications to Geochronology, Freeman and Company, San Francisco.

Fleck, R.J., J.F. Sutter and D.H. Elliot 1977. Interpretation of discordant $^{40}Ar/^{39}Ar$ age-spectra of Mesozoic tholeites from Antarctica, Geochim. Cosmochim. Acta, 41, 15-32.

Gans P, G.E Alvarado., W. Pérez, I. MacMillan, A. Calvert 2003., Neogene evolution of the Costa Rican arc and development of the Cordillera Central. Geol Soc Amer Abstr Progr 31: A479.

Gazel, E., M.J. Carr, K. Hoernle, M.D. Feigenson, F Hauff, D. Szymanski, and P. van den Bogaard 2009. The Galapagos-OIB signature in southern Central America: Mantle refertilization by arc-hotspot interaction. Geochemestry, Geophysics, Geosystems (G^3), Q02S11, doi: 10.1029/2008GC002246.

Gazel, E., K. Hoernle, M.J. Carr, C Herberg, I Saginor, P. van den Bogaard, F Hauff, M. Feigenson and C.C. Swisher III 2011. Plume-subduction interaction in southern Central America: Mantle upwelling and slab melting. Lithos, doi: 10.1016/j.lithos.2010.10.008.

González Víquez, C. 1910. Temblores, terremotos, inundaciones y erupciones volcánicas en Costa Rica 1608-1910: Tipografía de Avelino Alsina, San José de Costa Rica, p. 35-41.

GVN, 2007. Report of the Turrialba Volcanic Activity. Smithsonian Institution

GVN, 2008. Report of the Turrialba Volcanic Activity. Smithsonian Institution

GVN, 2010. Report of the Turrialba Volcanic Activity. Smithsonian Institution

Hannah, R.S., T.A. Vogel, L.C. Patino, G.E. Alvarado, W. Pérez and D.R.Smith, 2002. Origin of silicic volcanic rocks in Central Costa Rica: a study of chemically variable ash-flow sheet in Tiribi Tuff.- Bull. Volcanol. 64:117-133 doi: 10.1007/s00445-001-0188-8.

Hall, M., P. Mothes 2007. The rhyolithic-andesitic eruptive history of Cotopaxi volcano, Ecuador. Bull Volcanol. 70:6675-702, doi: 10.1007/s00445-007-0161-2.

Linkimer, L., 2003. Neotectónica del extremo oriental del Cinturón Deformado del Centro de Costa Rica. Lic thesis,. Central America School of Geology, Univ of Costa Rica, San José, Costa Rica.

Marshall, J. S., B.D. Idleman, T.W. Gardner, D.M. Fisher 2003. Landscape evolution within a retreating volcani arc, Costa Rica, Central America. Geology, v. 31 (5): 419-422. doi: 10.1130/0091-7613(2003)031<0419:LEWARV>2.0.CO;2.

Martini, F., F.Tass, O.Vaselli, R.Del Potro, M.Martinez, R.Van del Latt, E.Fernandez 2010. Geophysical, geochemical and geodetical signals of reawakeing at turrialba volcano (costa rica) after 150 years of quiescence. Journal of volcanology and Geothermal research 198: 416-432. doi: 10.1016/jvolgeores.2010.09021.

McBirney, A.R., 1980.. Mixing and unmixing of magmas. J. Volcanol. Geotherm. Res., 7: 357-371, doi: 10.1016/0377-0273(80)90038-4.

McBirney, A.R., B. H. Baker and R. H. Nilson 1985. Liquid fractionation. Part I: Basic principles and experimental simulations. Journal of Volcanology and Geothermal Research, Volume 24 doi: 10.1016/0377-0273(85)90026-5.

Nomade, S., P.R. Renne, N.Vogel, A.L. Deino, W.D. Sharp, T.A. Becker, A.R. Jaouni, and R. Mundil 2005. Alder Creek Sanidine (ACs-2): A Quaternary $^{40}Ar/^{39}Ar$ dating standard tied to the Cobb Mountain geomagnetic event. *Chemical Geology* 218, 319-342

Peccerillo, A. and S.R. Taylor 1976. Geochemistry of Eocene calc-alkaline volcani rocks from the Kastamonu area, northen Turkey: Contributions to Mineralogy and Petrology, v.58, p.63-81, doi: 10.1007/BF00384745.

Pérez, W., G.E. Alvarado, P Gans 2006. The Tiribí Tuff: stratigraphy, geochronology and mechanisms of deposition of the largest and most recent ignimbrite in the Central Valley, Costa Rica. –Bull. Volcanol. 69:25-40, doi: 10.1007/s00445-006-0053-x.

Reagan, M.K. 1987. Turrialba Volcano, Costa Rica: Magmatism at the southeast terminus of the Central American arc [Ph.D. dissertation]: Santa Cruz, University of California, 216 p.

Reagan, M.K., and J.B. Gill, 1989. Coexisting calcalkaline and high-niobium basalts from Turrialba Volcano, Costa Rica: Implications for residual titanates in arc magma sources: Journal of Geophysical Research, v.B94, p.4619-4633, doi 10.1029/JB094iB04p04619.

Reagan, M.K., E. Duarte, G.J. Soto, and E. Fernandez 2006. The eruptive history of Turrialba volcano, Costa Rica, and potential implication hazard from future eruptions. Geological Society of America, Special Paper 412: 237-257.

Ruiz, P., E. Gazel, G.E. Alvarado, M. Carr, G.J. Soto, 2010. Caracterización geoquímica y petrográfica de las unidades geológicas del macizo del volcán Poás, Costa Rica. Rev.Geol. Am.Centr. 43,37-66.

Sakuyama, M., 1984. Magma mixing and magma plumbing systems in Island Arcs. Bulletion Volcanologique, v. 47, no 4, p 685-703, doi: 10.1007/BF01952339.

Soto, G.J., 1988a., Geología y vulcanología del Volcán Turrialba, Costa Rica. – Costa Rican Volcanism Workshop, 14-18 de noviembre de 1988, Washington, D.C. y Shenandoah National Park, 18 pp.

Soto, G.J. 1988b. Estructuras volcano-tectónicas del Volcán Turrialba, Costa Rica, América Central. V Congreso Geol. Chileno, 8-12 de agosto de 1988, Santiago, Actas, III (I): 163-175.

Soto, G.J., R. Mora, M. Mora, R. Barquero, W Taylor, A.Vargas, G.E. Alvarado, C. Ramírez, G. González, R. Mora, C. Paniagua, and J.F. Fernández 2010. Turrialba volcano's threat to the cities of the Central Valley of Costa Rica. - Tenerife 2010 Cities on Volcanoes 6th, Puerto de la Cruz, Abstracts Volume, p. 138.

Stoiber, R. E & M. J. Carr, 1973. Quaternary volcanic and tectonic segmentation of Central America. Bull. Volcanol., 37: 304-325, doi: 10.1007/BF02597631.

Tassi, F., O. Vaselli, , V. Barboza, E. Fernandez, E. Duarte 2004., Fluid geochemistry and seismic activity in the period 1998-2002 at Turrialba volcano (Costa Rica). Annals of Geophysics 47 (4), 1501-1511.

Tournon, J. 1984. Magmatismes du Mesozoique a l'actuel en Amerique Centrale: L' example de Costa Rica, des phiolites aux andesites [Ph.D Dissertation]: Paris, Université Pierre and Marie Curie, IIX + 335 p.

Turrin, B.D., J.M. Donnelly-Nolan, B.C. Hearn Jr. 1994. $^{40}Ar/^{39}Ar$ ages from the rhyolite of Alder Creek, California; age of the Cobb Mountain normal-polarity subchron revisited, *Geology, 22-3*, 251-254, doi: 10.1130/0091-7613(1994)022<0251:AAAFTR>2.3.CO;2

Turrin, B.D., R.L. Christiansen, M.A. Clynne, D.E. Champion, W.J. Gerstel, L.J.P Muffler, D.A. Trimble, 1998., Age of Lassen Peak, California, and implications for the ages of late Pleistocene glaciations in the southern Cascade Range. Geol.Soc.Amer. Bull. 110, 931-945.

Turrin, B.D., J.T. Gutmann, C.C. Swisher III 2008. A 13 ± 3 ka age determination of a tholeiite, Pinacate volcanic field, Mexico, and improved methods for $^{40}Ar/^{39}Ar$ of young basaltic rocks. Journal of Volcanology and Geothermal Research 177 (4), 848-856, doi: 10.1016/j.jvolgeores.2008.01.049

Turrin, B.D., and C.C. Swisher III 2010. Mass discrimination monitoring and intercalibration of dual collectors in noble gas mass spectrometer systems. Geochem Geophys Geosyst., doi: 10.1029/2009GC003013.

Vaselli, O., F.Tassi, V. Barboza, E. Fernandez, R. Poreda, A. Delgado Huretas 2010. Evolution of fluid geochemistry at the Turrialba volcano (Costa Rica) from 1998 to 2008. Bullettin of Volcanology 72 (4), 397-410.

York, D., 1969. Least squares fitting of a straight line with correlated errors, Earth and Planet. Sci. Lett., 5, 320-324.

Figures Captions

Figure 1.

(a) Map of the Central American Volcanic Front and Middle-American Trench. (b) Digital elevation map of Costa Rica and distribution of ashes from 1864-1866 eruptive period, drawn by *Soto et al.* [2010], according to the accounts contained in *GonzálezViquez* [1910]. (c) Distribution of lithic ashes from fumarolic-phreatic activity of 5 and6 January 2010, the yellow rectangle denotes a close-up to the study area shown in Figure 2.

Figure 2.

Turrialba volcano lithologic units, geological features and main craters: A) unnamed old crater near Cerro San Juan, B) Southwest, C) Central and D) Northeast, over a digital elevation map of the study area. Geology, modified from *Soto* [1988a and 1988b].

Figure 3.

Rock classification diagram based in *Peccerillo and Taylor* [1976] for the lithologic units of Turrialba volcano that have been dated or correlated in this study. Major elements (oxides) in %.

Figure 4.(a-h)Experimental data plotted as age spectrum (plateau) and (isochron) diagrams for the eight Turrialba samples presented in this study. Step ages are shown as

horizontal rectangles in the plateau diagrams and as circles in the isochron diagrams. Isochrons diagrams were plot with plateau data only.

Figure 5.

(a) Cross section X-X^{1}sketch. (b) Cross section Y-Y^1. Units presenting bright colors and red dots have been dated with ^{40}Ar/^{39}Ar for this study, and blue dots are estimated ages based on stratigraphic correlation.

Figure 6.

(a) Pictures from thin sections of samples TUR-8 and TUR-68, both share similar general textures and both present glomerocryst made of clinopyroxene, olivine and orthopyroxene. (b) Variation diagram of major elements from dated samples from Turrialba volcano. Colors and symbols of the samples in the diagrams are the same as figure 3.

Figure 7.

Cross section sketch (Z-Z^1) of the of Turrialba volcano summit, its craters: A) unnamed old crater near Cerro San Juan, B) Southwest, C) Central, D) Northeast and new vent opened during the eruption in early January 2010. Units presented here are a synthesis from pictures and sketches of *Reagan et al.* [2006] of the places mapped and sampled. Yellow dots point the places where units have been dated with ^{14}C. Based on geochemical and petrographic correlations Unit 12 in the inner walls of the central and

southwest crater and the flow in the west flank of the summit are the same lava flow and belong to La Picada Unit.

Figure 8.

Binary plots of MgO and (Zr, Rb and Cr) Colors and symbols of the samples in the diagrams are the same as figure 3.

Figure 9.

Differences in silica content (wt.%), Rb and Zr (ppm) through time for Turrialba volcano lavas, they show two groups (low silica SiO_2 < 55 wt.% and high silica ≥ 60 wt.%) occurring contemporaneous to each other in the Neo-Turrialba stage. Dash line emphasizes the increment of these elements in the high silica group.

Figure 1

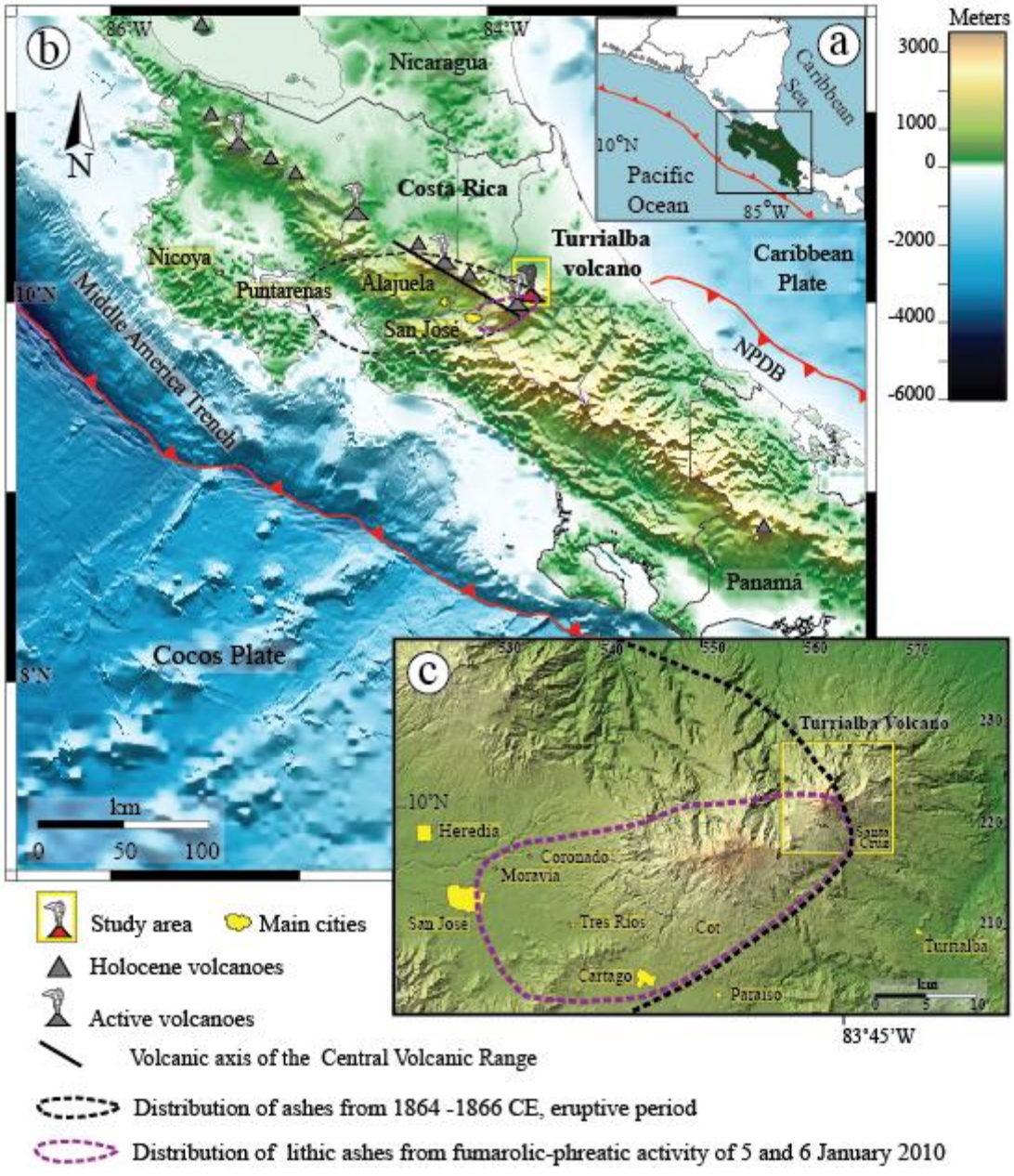
b
a
c
Meters
3000
1000
0
-2000
-4000
-6000
86°W
84°W
Nicaragua
Costa Rica
Caribbean Sea
Pacific Ocean
10°N
85°W
Nicoya
Puntarenas
Alajuela
San José
Turrialba volcano
Caribbean Plate
NPDB
Middle America Trench
Panamá
Cocos Plate
8°N
km
0 50 100
Turrialba Volcano
Heredia
Coronado
Moravia
San José
Tres Ríos
Cot
Cartago
Paraíso
Turrialba
Santa Cruz
83°45'W
Study area
Main cities
Holocene volcanoes
Active volcanoes
Volcanic axis of the Central Volcanic Range
Distribution of ashes from 1864 -1866 CE, eruptive period
Distribution of lithic ashes from fumarolic-phreatic activity of 5 and 6 January 2010

Figure 2

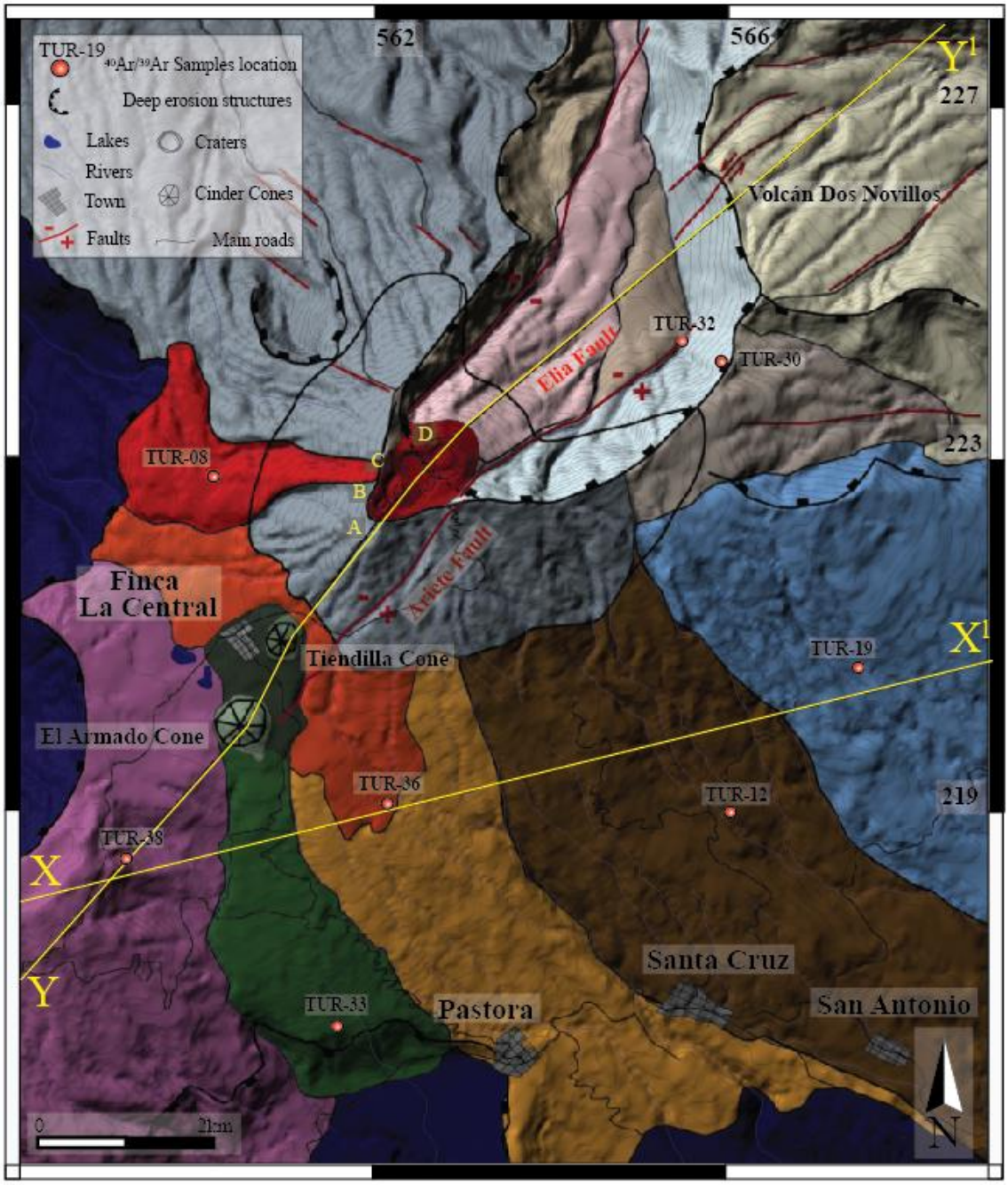

Lithologic units of Turrialba volcano

Turrialba Summit	TU-8 Unit (<10 ka) Estimated age	Bajos 1 Unit (TUR-32) (62 ± 2 ka) $^{40}Ar/^{39}Ar$ age	Volcán Dos Novillos (>200?-100? ka) Estimated age
Units without age	TU-4 Unit (10<X<25 ka) Estimated age		
La Picada Unit (TUR-08) (3 ± 3 ka) $^{40}Ar/^{39}Ar$ age	Lower Turrialba Unit (TUR-12) (25 ± 1.9 ka) $^{40}Ar/^{39}Ar$ age	Upper Los Cabros Unit (TUR-19) (90 ± 4 ka) $^{40}Ar/^{39}Ar$ age	Upper Finca Liebres Unit (TUR-38) (251 ± 4 ka) $^{40}Ar/^{39}Ar$ age
La Silvia Unit (TUR-36) (10 ± 3 ka) $^{40}Ar/^{39}Ar$ age	El Armado Flow Unit (TUR-33) (61 ± 2 ka) $^{40}Ar/^{39}Ar$ age	Lower Los Cabros Unit (TUR-30) (99 ± 3 ka) $^{40}Ar/^{39}Ar$ age	Pre Turrialba Unit (>250 ka) Estimated age

Figure 3

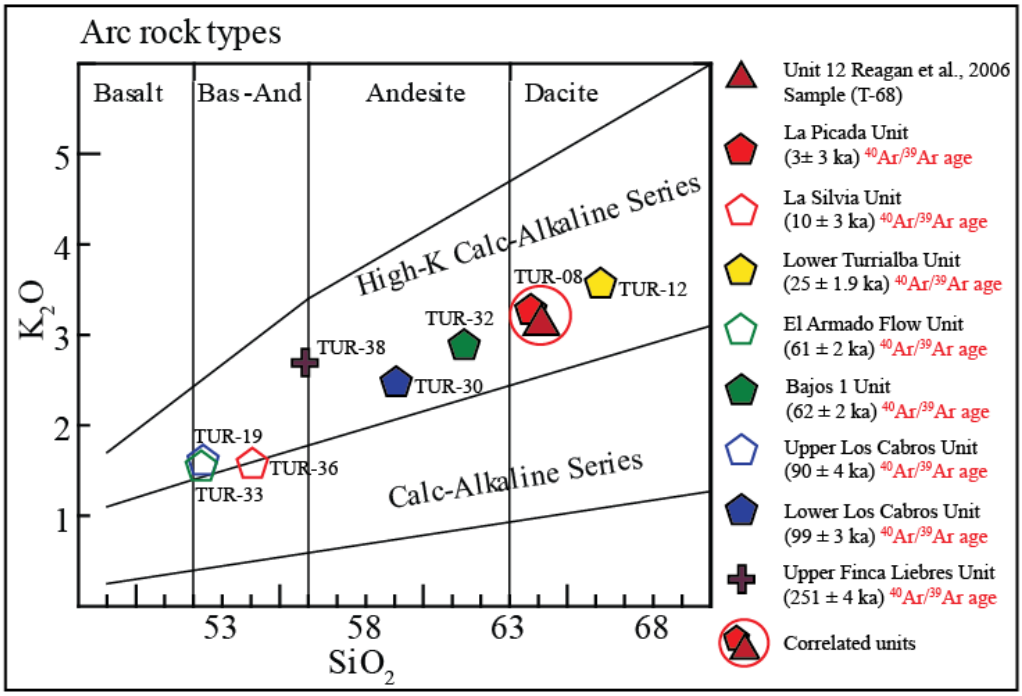
Arc rock types
Basalt
Bas -And
Andesite
Dacite
High-K Calc-Alkaline Series
Calc-Alkaline Series
TUR-08
TUR-12
TUR-32
TUR-38
TUR-30
TUR-19
TUR-36
TUR-33
K2O
SiO2
53
58
63
68
1
2
3
4
5
Unit 12 Reagan et al., 2006 Sample (T-68)
La Picada Unit (3± 3 ka) 40Ar/39Ar age
La Silvia Unit (10 ± 3 ka) 40Ar/39Ar age
Lower Turrialba Unit (25 ± 1.9 ka) 40Ar/39Ar age
El Armado Flow Unit (61 ± 2 ka) 40Ar/39Ar age
Bajos 1 Unit (62 ± 2 ka) 40Ar/39Ar age
Upper Los Cabros Unit (90 ± 4 ka) 40Ar/39Ar age
Lower Los Cabros Unit (99 ± 3 ka) 40Ar/39Ar age
Upper Finca Liebres Unit (251 ± 4 ka) 40Ar/39Ar age
Correlated units

Figure 4

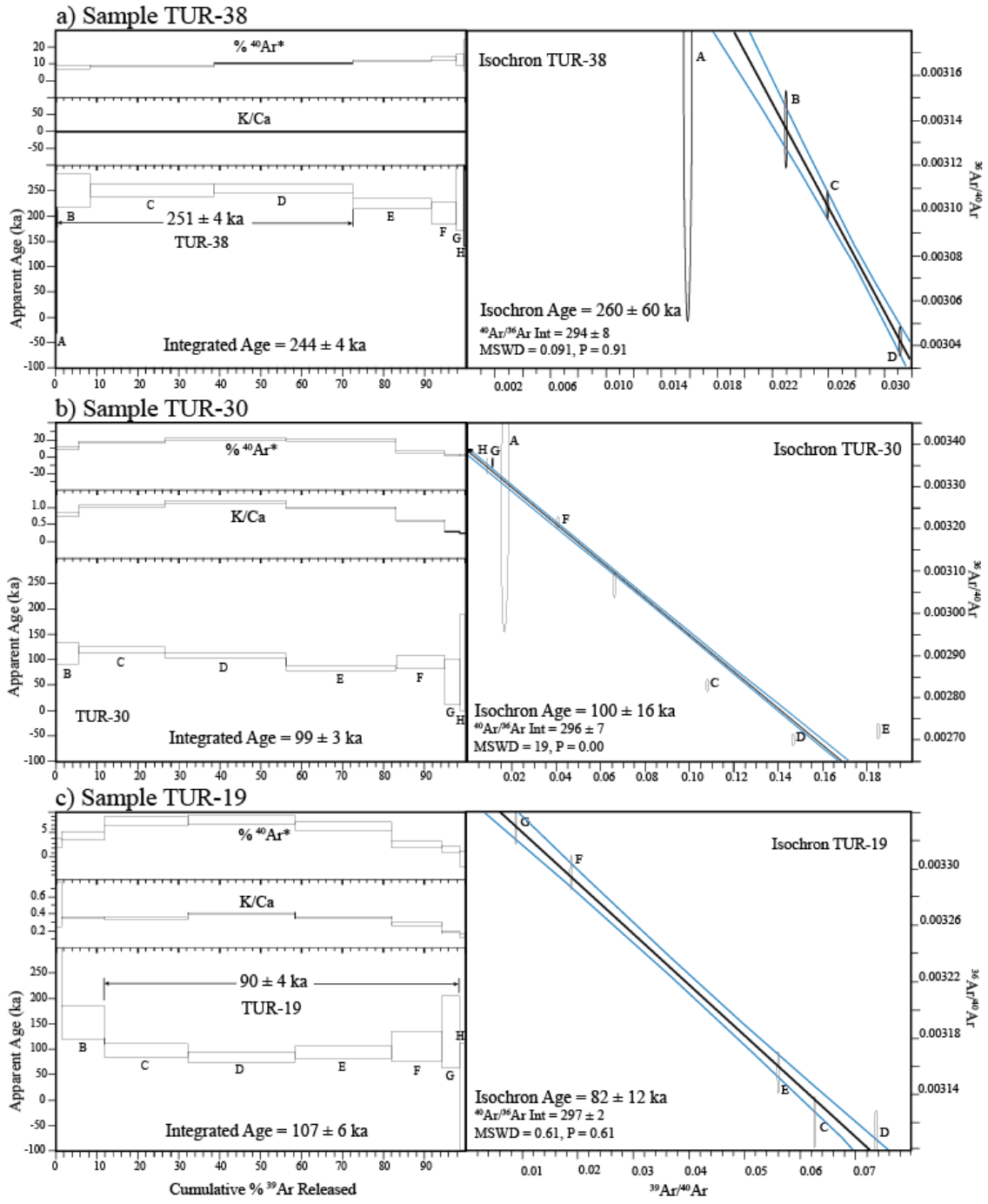
a) Sample TUR-38
% 40Ar*
K/Ca
Apparent Age (ka)
251 ± 4 ka
TUR-38
Integrated Age = 244 ± 4 ka
Isochron TUR-38
Isochron Age = 260 ± 60 ka
40Ar/36Ar Int = 294 ± 8
MSWD = 0.091, P = 0.91
36Ar/40Ar
b) Sample TUR-30
% 40Ar*
K/Ca
Apparent Age (ka)
TUR-30
Integrated Age = 99 ± 3 ka
Isochron TUR-30
Isochron Age = 100 ± 16 ka
40Ar/36Ar Int = 296 ± 7
MSWD = 19, P = 0.00
36Ar/40Ar
c) Sample TUR-19
% 40Ar*
K/Ca
Apparent Age (ka)
90 ± 4 ka
TUR-19
Integrated Age = 107 ± 6 ka
Isochron TUR-19
Isochron Age = 82 ± 12 ka
40Ar/36Ar Int = 297 ± 2
MSWD = 0.61, P = 0.61
36Ar/40Ar
Cumulative % 39Ar Released
39Ar/40Ar

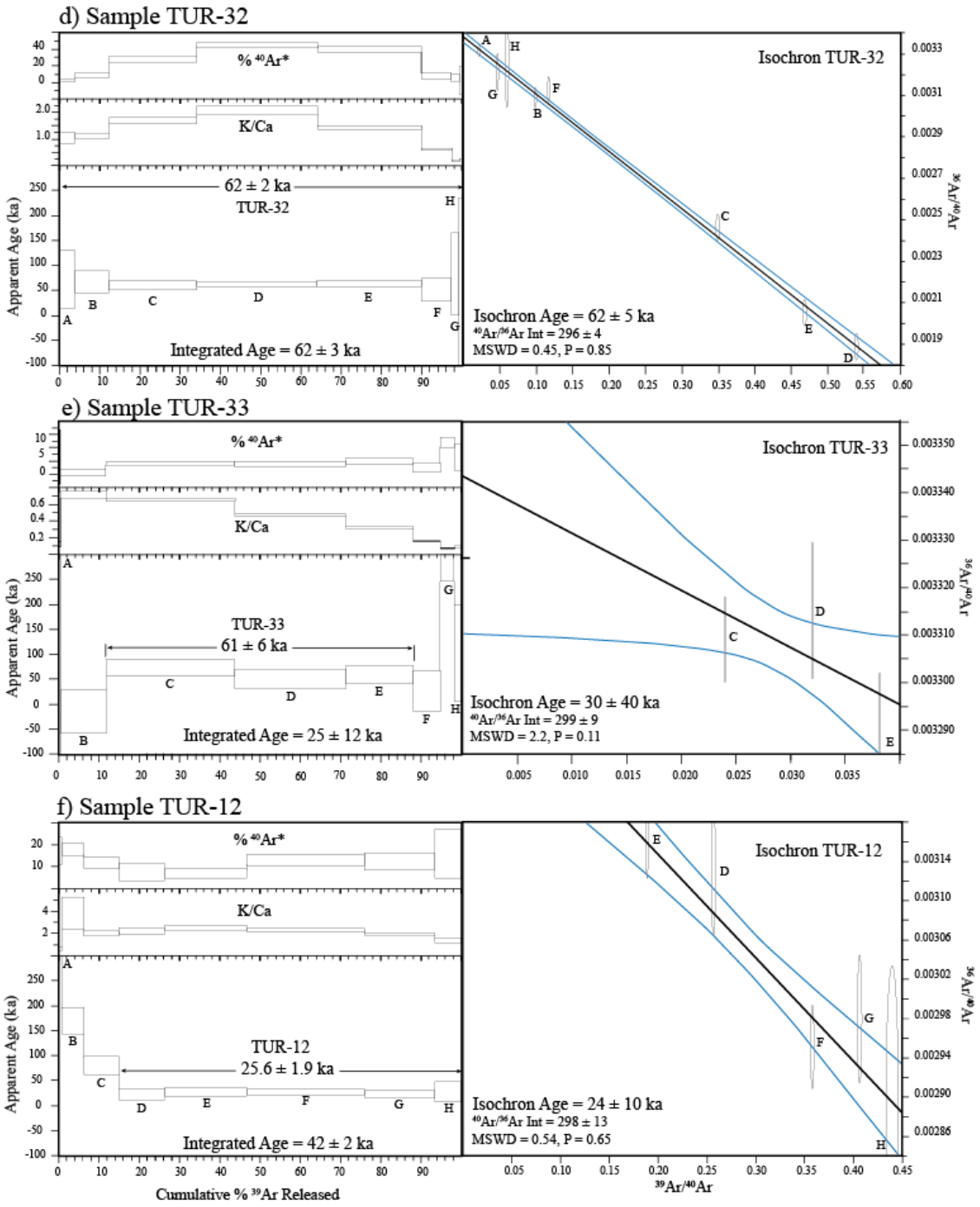
d) Sample TUR-32
% 40Ar*
K/Ca
62 ± 2 ka
TUR-32
Apparent Age (ka)
Integrated Age = 62 ± 3 ka
Isochron TUR-32
Isochron Age = 62 ± 5 ka
40Ar/36Ar Int = 296 ± 4
MSWD = 0.45, P = 0.85
36Ar/40Ar
e) Sample TUR-33
% 40Ar*
K/Ca
TUR-33
61 ± 6 ka
Apparent Age (ka)
Integrated Age = 25 ± 12 ka
Isochron TUR-33
Isochron Age = 30 ± 40 ka
40Ar/36Ar Int = 299 ± 9
MSWD = 2.2, P = 0.11
36Ar/40Ar
f) Sample TUR-12
% 40Ar*
K/Ca
TUR-12
25.6 ± 1.9 ka
Apparent Age (ka)
Integrated Age = 42 ± 2 ka
Isochron TUR-12
Isochron Age = 24 ± 10 ka
40Ar/36Ar Int = 298 ± 13
MSWD = 0.54, P = 0.65
36Ar/40Ar
Cumulative % 39Ar Released
39Ar/40Ar

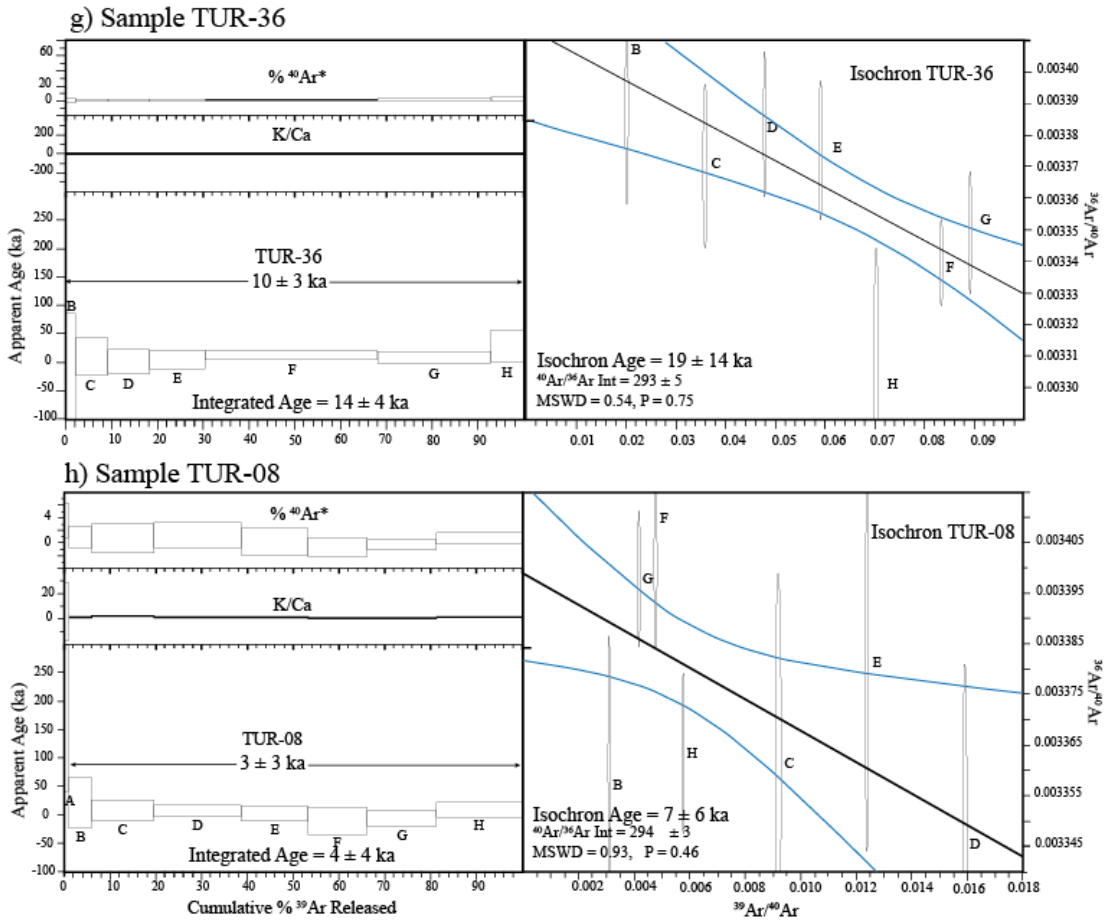
g) Sample TUR-36
% 40Ar*
K/Ca
Apparent Age (ka)
TUR-36
10 ± 3 ka
Integrated Age = 14 ± 4 ka
Isochron TUR-36
Isochron Age = 19 ± 14 ka
40Ar/36Ar Int = 293 ± 5
MSWD = 0.54, P = 0.75
36Ar/40Ar
h) Sample TUR-08
% 40Ar*
K/Ca
Apparent Age (ka)
TUR-08
3 ± 3 ka
Integrated Age = 4 ± 4 ka
Isochron TUR-08
Isochron Age = 7 ± 6 ka
40Ar/36Ar Int = 294 ± 3
MSWD = 0.93, P = 0.46
36Ar/40Ar
Cumulative % 39Ar Released
39Ar/40Ar

Figure 5

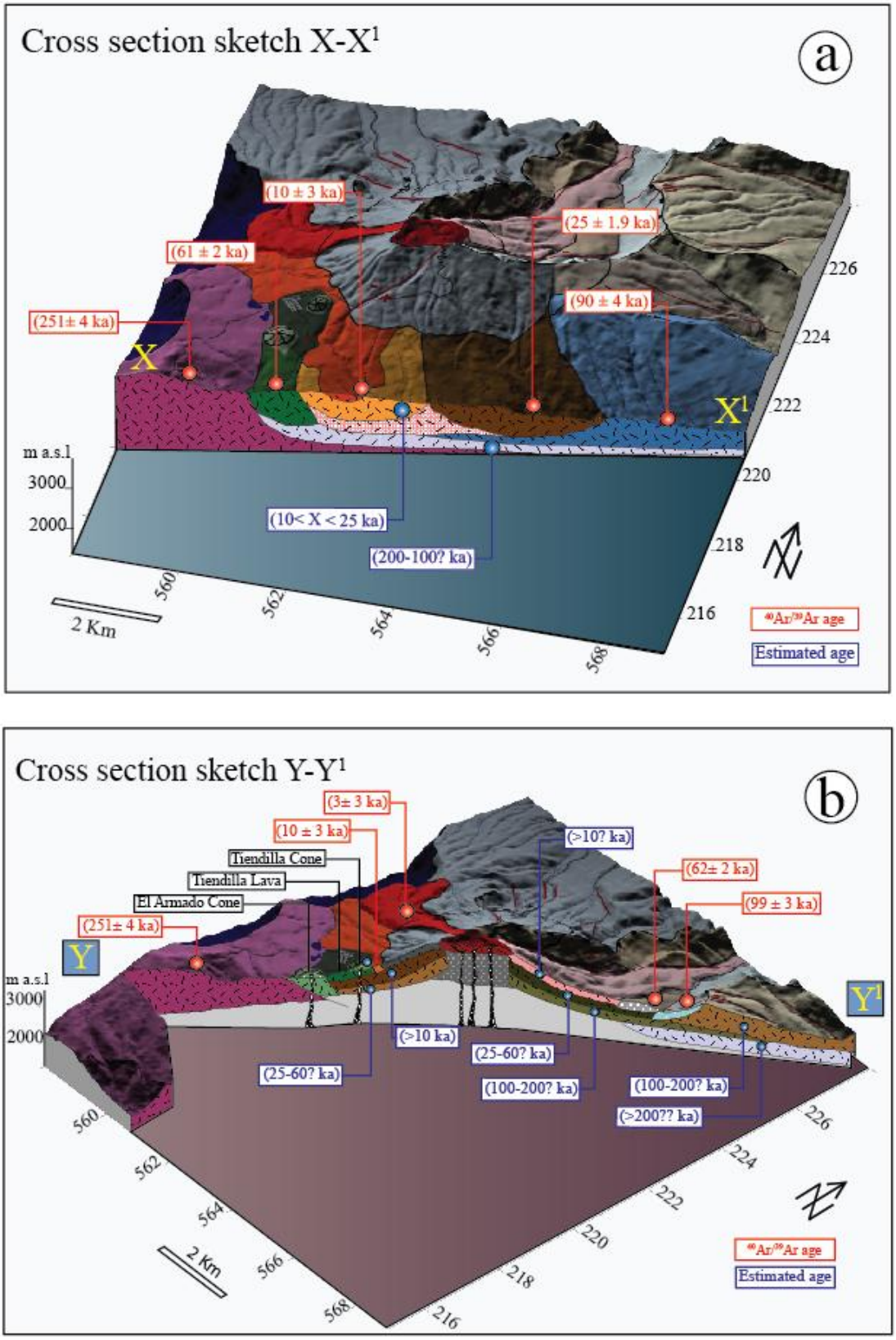
Cross section sketch X-X¹
a
(10 ± 3 ka)
(25 ± 1.9 ka)
(61 ± 2 ka)
(90 ± 4 ka)
(251± 4 ka)
X
X¹
226
224
222
220
218
216
m a.s.l
3000
2000
(10< X < 25 ka)
(200-100? ka)
560
562
564
566
568
2 Km
⁴⁰Ar/³⁹Ar age
Estimated age
Cross section sketch Y-Y¹
b
(3± 3 ka)
(10 ± 3 ka)
Tiendilla Cone
Tiendilla Lava
El Armado Cone
(251± 4 ka)
(>10? ka)
(62± 2 ka)
(99 ± 3 ka)
Y
Y¹
m a.s.l
3000
2000
(>10 ka)
(25-60? ka)
(25-60? ka)
(100-200? ka)
(100-200? ka)
(>200?? ka)
560
562
564
566
568
216
218
220
222
224
226
2 Km
⁴⁰Ar/³⁹Ar age
Estimated age

Figure 6

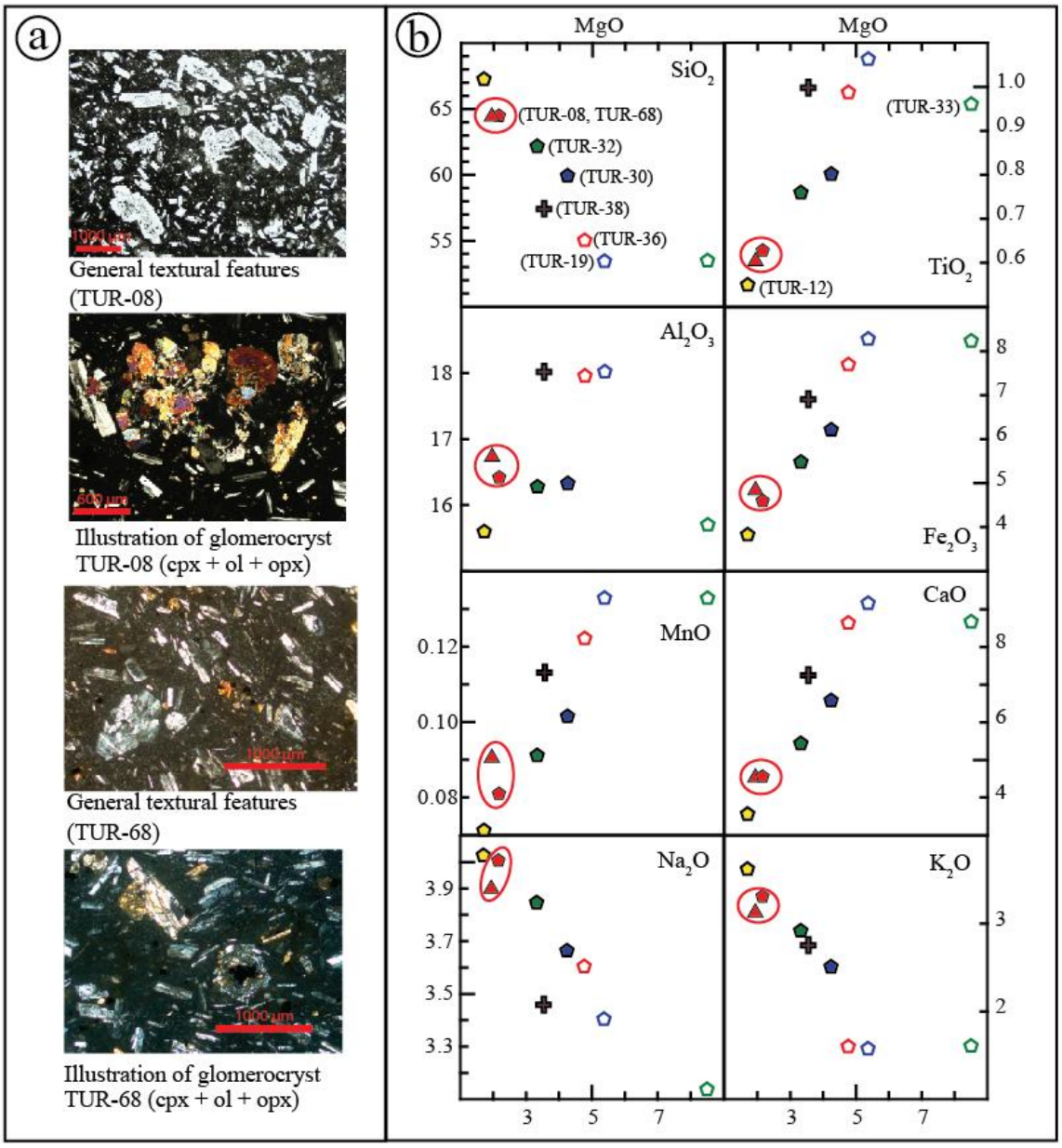
a
General textural features
(TUR-08)
Illustration of glomerocryst
TUR-08 (cpx + ol + opx)
General textural features
(TUR-68)
Illustration of glomerocryst
TUR-68 (cpx + ol + opx)
b
MgO
MgO
SiO2
TiO2
Al2O3
Fe2O3
MnO
CaO
Na2O
K2O
(TUR-08, TUR-68)
(TUR-32)
(TUR-30)
(TUR-38)
(TUR-36)
(TUR-19)
(TUR-33)
(TUR-12)

Figure 7

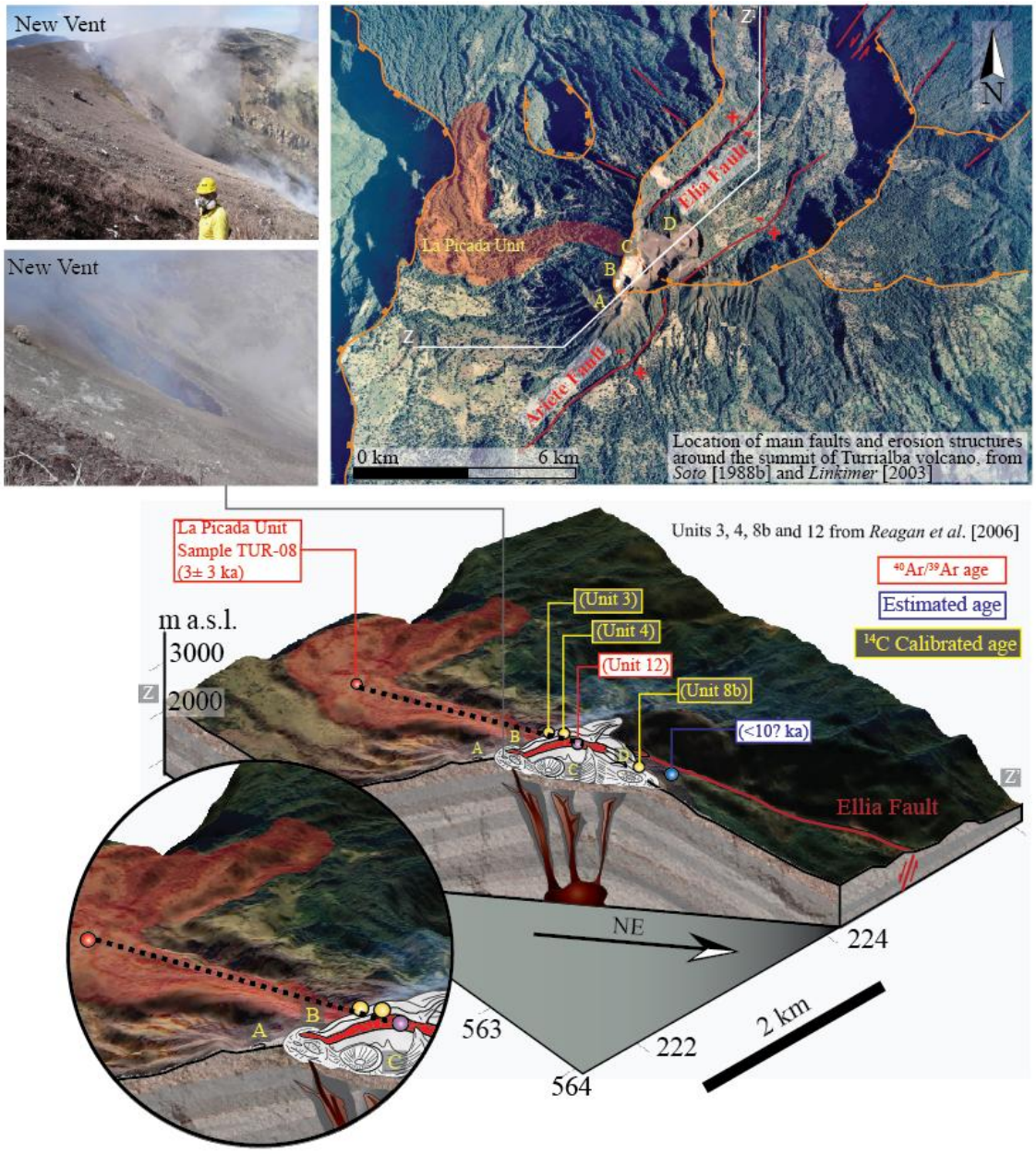
New Vent
New Vent
La Picada Unit
Ellia Fault
Arlete Fault
A
B
C
D
Z
Z'
N
0 km
6 km
Location of main faults and erosion structures around the summit of Turrialba volcano, from Soto [1988b] and Linkimer [2003]
La Picada Unit
Sample TUR-08
(3± 3 ka)
Units 3, 4, 8b and 12 from Reagan et al. [2006]
40Ar/39Ar age
Estimated age
14C Calibrated age
m a.s.l.
3000
2000
(Unit 3)
(Unit 4)
(Unit 12)
(Unit 8b)
(<10? ka)
Ellia Fault
NE
224
563
222
564
2 km

Figure 8

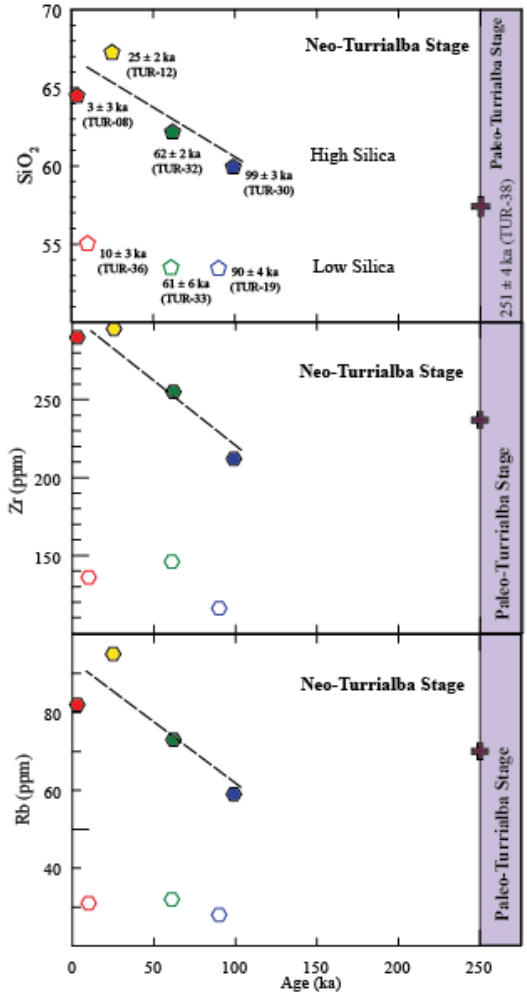
Neo-Turrialba Stage
25 ± 2 ka (TUR-12)
3 ± 3 ka (TUR-08)
62 ± 2 ka (TUR-32)
99 ± 3 ka (TUR-30)
High Silica
10 ± 3 ka (TUR-36)
61 ± 6 ka (TUR-33)
90 ± 4 ka (TUR-19)
Low Silica
Pako-Turrialba Stage
251 ± 4 ka (TUR-38)
SiO2
Neo-Turrialba Stage
Paleo-Turrialba Stage
Zr (ppm)
Neo-Turrialba Stage
Paleo-Turrialba Stage
Rb (ppm)
Age (ka)

Figure 9

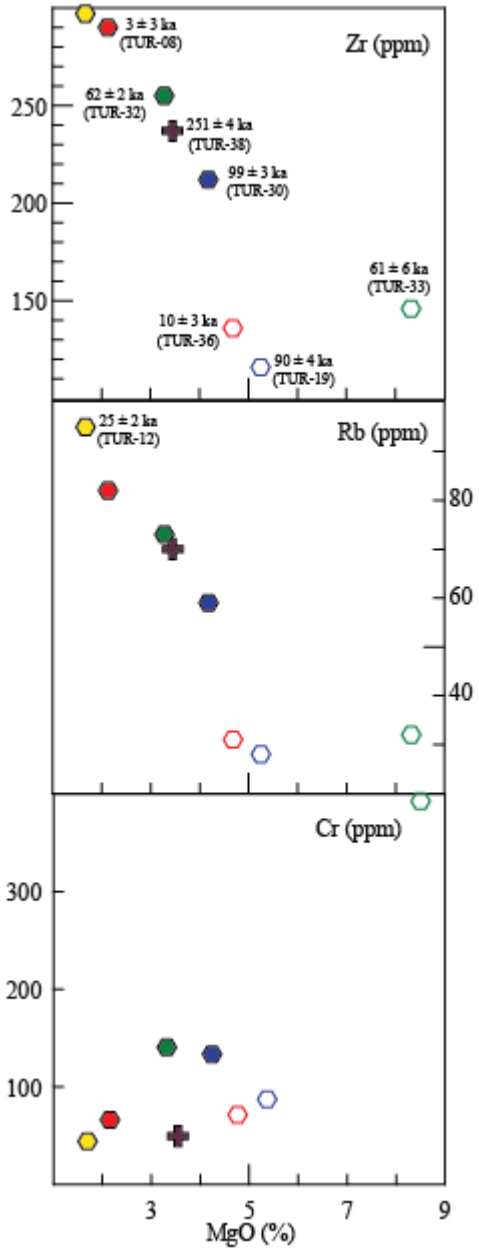
3 ± 3 ka
(TUR-08)
Zr (ppm)
62 ± 2 ka
(TUR-32)
251 ± 4 ka
(TUR-38)
99 ± 3 ka
(TUR-30)
61 ± 6 ka
(TUR-33)
10 ± 3 ka
(TUR-36)
90 ± 4 ka
(TUR-19)
250
200
150
25 ± 2 ka
(TUR-12)
Rb (ppm)
80
60
40
Cr (ppm)
300
200
100
3
5
7
9
MgO (%)

Tables

Table 1. Age Determination for Volcanic Rocks from Turrialba volcano. Radiometric ages in bold are the best estimates for each sample.

Sample ID	Location		Material	Plateau age, Ka	Isochron Age, Ka	Integrated Age, Ka	$^{40}Ar/^{36}Ar$ Intercept	MSWD	% ^{39} Ar on Plateau	K_2O*	Volcanic Unit name
	Lat N	Lon W									
TUR-38	9.984	83.794	matrix	**251 ± 4**	260 ± 60	244 ± 4	294.2 ± 7.6	0.091	72.6	2.68	Upper Finca Liebres
TUR-30	10.035	83.733	matrix	NP	100 ± 16	**99 ± 3 ka**	295.6 ± 6.5	19	NP	2.47	Lower Los Cabros
TUR-19	10.003	83.718	matrix	**90.0 ± 4**	80 ± 20	107 ± 6	297.3 ± 2.1	0.611	86.7	1.54	Upper Los Cabros
TUR-32	9.966	83.735	matrix	**62.0 ± 2**	62 ± 5	62 ± 3	295.7 ± 4.3	0.45	100	2.88	Bajos 1
TUR-33	9.966	83.772	matrix	**61.0 ± 6**	30 ± 40	59 ± 7	299.1 ± 8.9	2.22	76	1.57	El Armado flow
TUR-12	9.989	83.732	matrix	**25.6 ± 2**	24 ± 10	42 ±2	297 ± 13.2	0.54	85	3.56	Lower Turrialba
TUR-36	9.989	83.767	matrix	**10.0 ± 3**	19 ± 14	14 ± 4	292.9 ± 5	0.539	99.9	1.57	La Silvia
TUR-08	10.023	83.784	matrix	**3 ± 3**	7 ± 6	4 ± 4	294.2 ± 3	0.93	98	3.27	La Picada

NP= No plateaus, K_2O*=wt% from Geochemistry analyses

Table 2.

Sample	Run ID	Laser Power (watts)	Ca/K	Cl/K	$^{36}Ar/^{39}Ar$	$\%^{36}Ar(Ca)$	$^{40}*Ar/^{39}Ar$	Mol ^{39}Ar	%Step	% Cum	%Ar*	Age (ka)	±1s	J ± 1 × 10^{-5}
TUR-38	•20911-01A	1	0.17138	-0.00796	0.198319	0	4.01476	0.0036	0.3	0.3	6.4	312.86741	171.69664	4.32 ± 0.016
	•20911-01B	3	0.67612	0.00951	0.136728	0.1	3.1905	0.0887	8.3	8.6	7.3	248.63822	16.83866	
	•20911-01C	5	0.74569	0.00344	0.11942	0.1	3.20408	0.3245	30.2	38.8	8.3	249.69629	5.87577	
	•20911-01D	7	1.24277	0.00446	0.097691	0.2	3.24225	0.3631	33.8	72.6	10.1	252.67099	4.85535	
	20911-01E	10	2.1889	0.00157	0.074405	0.4	2.87676	0.205	19.1	91.6	11.6	224.18932	5.08694	
	20911-01F	15	4.00989	0.00404	0.060769	0.9	2.61939	0.0664	6.2	97.8	12.8	204.13338	10.69896	
	20911-01G	20	7.90399	0.00799	0.079672	1.3	3.20465	0.0183	1.7	99.5	12.1	249.74051	40.23888	
	20911-01H	25	11.37233	-0.00463	0.082957	1.8	4.29086	0.0051	0.5	100	15.1	334.38183	97.52768	
	Integ. Age											244	4	
	(•) **Plat. Age**								72.6			**251**	4	
TUR-30	20909-01A	1	9.04381	0.03099	0.197197	0.6	-0.32651	0.0009	0.1	0.1	-0.6	-25.44677	592.39474	4.32 ± 0.016
	20909-01B	3	1.29728	0.00005	0.046382	0.4	1.41844	0.0609	5.5	5.6	9.4	110.54417	10.33957	
	20909-01C	5	0.98234	-0.00173	0.026314	0.5	1.51555	0.2316	21.1	26.7	16.4	118.11257	3.02899	
	20909-01D	7	0.86709	-0.00291	0.01853	0.6	1.37154	0.3252	29.6	56.2	20.1	106.88942	2.17952	
	20909-01E	10	1.02394	-0.00163	0.014808	0.9	1.05968	0.2934	26.7	82.9	19.6	82.58521	2.24001	
	20909-01F	15	1.64456	-0.00011	0.078675	0.3	1.20506	0.1326	12.1	95	4.9	93.91503	6.67181	
	20909-01G	20	3.69338	-0.01059	0.290963	0.2	0.70092	0.0405	3.7	98.6	0.8	54.62634	22.76576	
	20909-01H	25	4.52423	-0.00587	0.377803	0.2	1.19678	0.0149	1.4	100	1.1	93.26992	47.34327	
	Integ. Age											**99**	3	

Table 2. (continued)

Sample	Run ID	Laser Power (watts)	Ca/K	Cl/K	$^{36}Ar/^{39}Ar$	$\%^{36}Ar(Ca)$	$^{40}*Ar/^{39}Ar$	Mol ^{39}Ar	%Step	% Cum	%Ar*	Age (ka)	±1s	J ± 1 × 10^{-5}
TUR-19	20899-01A	1	2.01633	-0.05166	1.123209	0	9.7958	0.0071	1.4	1.4	2.9	747.38676	127.44434	4.23 ± 0.091
	20899-01B	3	2.89217	0.00201	0.138244	0.3	1.97747	0.053	10.4	11.8	4.6	150.89923	15.85985	
	•20899-01C	5	2.97534	-0.00167	0.05016	0.8	1.24757	0.1035	20.4	32.2	7.8	95.20235	6.59576	
	•20899-01D	7	2.54583	-0.00298	0.042494	0.8	1.09198	0.1332	26.2	58.4	8.1	83.33008	5.10554	
	•20899-01E	10	2.86024	-0.00055	0.056474	0.7	1.20626	0.1199	23.6	82	6.8	92.05055	5.94554	
	•20899-01F	15	3.70599	-0.00362	0.174236	0.3	1.36191	0.0623	12.3	94.3	2.6	103.9275	14.57871	
	•20899-01G	20	5.6217	-0.00885	0.36913	0.2	1.7445	0.0217	4.3	98.5	1.6	133.12217	35.36099	
	20899-01H	25	7.27165	-0.00284	0.429035	0.2	-0.64134	0.0074	1.5	100	-0.5	-48.94306	79.26818	
	Integ. Age											107	6	
	(•) **Plat. Age**								86.7			**90**	4	
TUR-32	•20896-01A	1	0.96959	0.01496	0.151202	0.1	0.94161	0.0353	4	4	2.1	71.85551	28.98275	4.23 ± 0.091
	•20896-01B	3	0.92334	0.00391	0.031153	0.4	0.87352	0.0762	8.5	12.5	8.7	66.65885	10.85077	
	•20896-01C	5	0.59661	-0.00479	0.007107	1.1	0.78024	0.1935	21.6	34.1	27.3	59.54138	3.99385	
	•20896-01D	7	0.48833	-0.00467	0.003566	1.8	0.819	0.2682	30	64.1	44.2	62.49881	2.57719	
	•20896-01E	10	0.71292	-0.00272	0.004469	2.1	0.84029	0.2313	25.9	90	39.4	64.12313	3.1122	
	•20896-01F	15	1.68045	0.00038	0.026927	0.8	0.65149	0.0657	7.3	97.3	7.6	49.71648	11.28377	
	•20896-01G	20	5.89767	0.00537	0.068547	1.2	1.07761	0.0179	2	99.3	5.1	82.23328	41.19822	
	•20896-01H	25	4.81289	0.00511	0.056041	1.2	0.29374	0.0061	0.7	100	1.8	22.41553	105.68386	
	Integ. Age											62	3	
	(•)**Plat. Age**								100			**62**	2	

Table 2. (continued)

Sample	Run ID	Laser Power (watts)	Ca/K	Cl/K	$^{36}Ar/^{39}Ar$	$\%^{36}Ar(Ca)$	$^{40}*Ar/^{39}Ar$	Mol ^{39}Ar	%Step	% Cum	%Ar*	Age (ka)	±1s	J ± 1 × 10^{-5}
TUR-33	20908-01A	1	8.36393	0.00449	0.258619	0.4	3.29973	0.0023	0.4	0.4	4.1	257.15019	248.00665	4.32 ± 0.016
	20908-01B	3	1.39698	0.00178	0.175017	0.1	-0.1946	0.065	11.5	11.9	-0.4	-15.16634	21.73543	
	•20908-01C	5	1.53199	0.00437	0.137702	0.1	0.9206	0.1802	31.9	43.8	2.2	71.74658	8.3508	
	•20908-01D	7	2.1271	0.00048	0.103778	0.3	0.63902	0.1545	27.4	71.2	2	49.80226	10.03213	
	•20908-01E	10	3.12045	0.00262	0.086459	0.5	0.74921	0.0948	16.8	88	2.9	58.38995	8.79757	
	20908-01F	15	6.20162	0.00294	0.119557	0.7	0.32815	0.0385	6.8	94.8	0.9	25.57454	20.18956	
	20908-01G	20	12.77689	0.00293	0.143634	1.2	3.91247	0.0188	3.3	98.1	8.5	304.89709	29.86142	
	20908-01H	25	11.14607	0.00433	0.106662	1.4	1.29939	0.0107	1.9	100	4	101.2664	48.56423	
	Integ. Age											59	7	
	(•) Plat. Age								76			**61**	6	
TUR-12	20897-01A	1	1.86326	0.02605	0.103677	0.2	6.17931	0.0086	0.8	0.8	16.8	471.49644	87.23564	4.23 ± 0.091
	20897-01B	3	0.2654	0.00722	0.035352	0.1	2.21396	0.0608	5.6	6.4	17.5	168.94504	13.10662	
	20897-01C	5	0.50619	0.00555	0.027444	0.2	1.04397	0.0945	8.7	15	11.4	79.66653	8.85411	
	•20897-01D	7	0.45809	0.0055	0.012246	0.5	0.29295	0.1245	11.4	26.5	7.5	22.35576	5.69142	
	•20897-01E	10	0.40517	0.00628	0.016749	0.3	0.35735	0.2213	20.3	46.8	6.8	27.26989	4.1081	
	•20897-01F	15	0.43948	0.00691	0.008295	0.7	0.35806	0.3197	29.3	76.1	12.8	27.32459	2.66903	
	•20897-01G	20	0.53583	0.00615	0.007395	1	0.29358	0.1908	17.5	93.6	11.9	22.40393	3.57085	
	•20897-01H	25	0.7252	0.00543	0.006577	1.5	0.35767	0.07	6.4	100	15.7	27.29464	9.42763	
	Integ. Age											42	2	
	(•) Plat. Age								85			**25.6**	1.9	

Table 2. (continued)

Sample	Run ID	Laser Power (watts)	Ca/K	Cl/K	$^{36}Ar/^{39}Ar$	$\%^{36}Ar(Ca)$	$^{40}*Ar/^{39}Ar$	Mol ^{39}Ar	%Step	% Cum	%Ar*	Age (ka)	±1s	J ± 1 × 10^{-5}
TUR-36	20910-01A	1	-0.17472	-0.06988	0.453526	0	94.35572	0.0004	0.1	0.1	41.3	7338.77367	1489.66642	4.32 ± 0.016
	•20910-01B	3	3.07816	0.00178	0.168569	0.2	-0.32131	0.0125	2.1	2.1	-0.7	-25.042	55.23145	
	•20910-01C	5	2.73709	0.003	0.093653	0.4	0.11419	0.0428	7.1	9.3	0.4	8.89958	16.41947	
	•20910-01D	7	3.18807	0.0078	0.071141	0.6	0.0031	0.0549	9.1	18.4	0	0.24149	10.83295	
	•20910-01E	10	3.35357	0.00893	0.057403	0.8	0.04355	0.0725	12	30.4	0.3	3.39378	8.28299	
	•20910-01F	15	2.52524	0.006	0.040334	0.8	0.15756	0.2266	37.7	68.1	1.3	12.27992	3.66793	
	•20910-01G	20	3.20378	0.00702	0.037912	1.1	0.11647	0.1498	24.9	93	1	9.07707	4.93455	
	•20910-01H	25	4.80904	0.00104	0.047491	1.4	0.35154	0.0423	7	100	2.5	27.3977	14.3246	
	Integ. Age											14	4	
	(•) Plat. Age								99.9			**10**	3	
TUR-08	20901-01A	1	0.18969	0.00926	0.229736	0	2.4737	0.0074	1.1	1.1	3.5	188.76402	74.24367	4.23 ± 0.091
	•20901-01B	3	0.91423	0.00605	0.108487	0.1	0.26036	0.0336	5	6.1	0.8	19.86843	21.61724	
	•20901-01C	5	0.59062	0.00045	0.036499	0.2	0.07316	0.0917	13.7	19.8	0.7	5.58281	9.25272	
	•20901-01D	7	0.66631	-0.00131	0.021081	0.4	0.0719	0.1269	18.9	38.7	1.1	5.487	4.92373	
	•20901-01E	10	0.86994	-0.00292	0.02738	0.4	0.00802	0.0993	14.8	53.5	0.1	0.61213	6.57773	
	•20901-01F	15	1.35758	0.00428	0.071115	0.3	-0.1566	0.0864	12.9	66.3	-0.8	-11.9508	12.07041	
	•20901-01G	20	1.28664	0.00435	0.081223	0.2	-0.09736	0.1009	15	81.4	-0.4	-7.42951	7.14094	
	•20901-01H	25	0.83732	0.0064	0.058341	0.2	0.10525	0.1252	18.6	100	0.6	8.03208	6.06878	
	Integ. Age											4	4	
	(•) Plat. Age								98.9			**3**	3	

Table 3. Major element data of the samples dated by $^{40}Ar/^{39}Ar$

Sample	TUR-38	TUR-30	TUR-19	TUR-32	TUR-33	TUR-12	TUR-36	TUR-08	T-68*
SiO_2	55.89	59.06	52.28	61.42	52.34	66.17	54.05	63.74	64.11
TiO_2	0.97	0.79	1.04	0.75	0.94	0.54	0.97	0.62	0.6
Al_2O_3	17.54	16.09	17.63	16.08	15.36	15.34	17.64	16.23	16.65
Fe_2O_3	6.71	6.12	8.1	5.41	8.06	3.76	7.56	4.54	4.81
MnO	0.11	0.1	0.13	0.09	0.13	0.07	0.12	0.08	0.09
MgO	3.45	4.18	5.25	3.28	8.32	1.67	4.68	2.13	1.93
CaO	7.06	6.48	8.96	5.37	8.48	3.5	8.48	4.5	4.51
Na_2O	3.37	3.61	3.33	3.8	3.07	3.96	3.54	3.96	3.88
K_2O	2.68	2.47	1.54	2.88	1.57	3.56	1.57	3.27	3.11
P_2O_5	0.31	0.27	0.38	0.27	0.39	0.19	0.38	0.25	0.33
Totals	98.09	99.17	98.64	99.35	98.66	98.76	98.99	99.32	100.44
LOI	1.68	0.6	1.13	0.43	1.1	1.01	0.79	0.44	1.06
Zr	237	212	116	255	146	297	136	290	280
Rb	70	59	28	73	32	95	31	82	82.5
Cr	49.6	133.56	87.36	140.49	392.57	44.17	71.56	66.19	12
Ni					162				12.4

*Taken from *Reagan et al* [2006]

Table 4. Summary of the petrography of the samples dated by $^{40}Ar/^{39}Ar$

Sample	$^{40}Ar/^{39}Ar$ age	Mineralogy	Petrographic notes
TUR-38	251 ± 4 ka	mt + pl + cpx + opx ± ol ± bt	Mildly vesicular, phenocryst-rich, hypocrystalline, large plag and cpx phenocrysts, common sieved-texture at plag rims, cpx rimming opx.
TUR-30	99 ± 3 ka	mt + pl + cpx + opx + ol	Not vesicular, fluidal texture, microcrystalline groundmass, occurrence of ultramafic enclaves. In one case: olivine rimmed by cpx.
TUR-19	90 ± 4 ka	mt + pl + cpx + ol ± opx	Weakly vesicular, phenocrysts-rich, occasional sieved-texture in plag, abundant Fe-Mg minerals.
TUR-32	62 ± 2 ka	mt + pl + cpx + opx ± ol ± bt	Not vesicular, hypocrystalline, common sieved-texture at plag rims, evident strong zoning in plag, contain ultramafic enclaves.
TUR-33	61 ± 6 ka	mt + pl + cpx + ol + opx	Mildly vesicular, fluidal texture, phenocryst-rich, hypocrystalline, abundant oxides in groundmass, common sieved-texture at plag rims.
TUR-12	25.6 ± 2 ka	mt + pl + cpx ± ol ± opx	Mildly to highly vesicular, plag-rich, few Fe-Mg minerals, contains ultramafic enclaves: holocrystalline & vesicular, with olivine + cpx.
TUR-36	10 ± 3 ka	mt + ap + pl + cpx ± ol ± opx	Mildly to highly vesicular, hypocrystalline, phenocryst-rich, very fresh with unpitted plag, common sieved-texture at plag rims.
TUR-08	3 ± 3 ka	mt + pl + cpx ± opx ± ol	Not vesicular, hypocrystalline, plag-rich, plag commonly zoned and/or displaying sieved-texture (either at cores or rims), with ultramafic enclaves.

Curriculum Vita

Pablo Ruiz Cubillo
Electronic mail:pruiz@rci.rutgers.edu and pruiz_cr@yahoo.com
Telephones: Office: 732-445-2044 (USA), Mobile 1-786-395-4479 (USA)
Address (USA): Rutgers University Wright-Rieman Labs 610 Taylor Road, Piscataway, NJ 08854.

EDUCATION

Rutgers University, Department of Earth and Planetary Sciences:
PhD. in Geology, 10/12 Advisor: PhD. Michael Carr.

University of Costa Rica, Central American School of Geology:

Licenciatura in Geology. 10/06. Advisor: PhD. S. Kussmaul

Bachelor in Geology, 12/04. Advisor: PhD Guillermo Alvarado

PROFESIONAL EXPERIENCE

Costa Rican Institute of Electricity (ICE), San Jose Costa Rica.
Internship Jun-Aug. 2009

- Mapping and sampling campaign on Poás Volcano near hydro-electrical projects Cariblanco & Toro III.
- Analyses and interpretation of LiDAR images from Poás Volcano and hydro-electrical projects Cariblanco & Toro III.
- Slope stability analysis of the transmission towers of Cariblanco hydro-electrical project.

CEMEX Costa Rica, Colorado Abangares, Guanacaste Costa Rica
Exploration Campaign of clays with high alkalis contents, Feb-Apr. 2005-Jan-Oct 2006

- Geochemical sampling campaign and chemical analysis (XRF) of clays.
- Geological mapping of the exploration area.
- Determination of zones with greater contents of alkalis and iron oxides in the clays.
- Elaboration of geologic and geochemical anomalies maps by GIS.

SICORSA of Costa Rica (VICESA) Coris, Cartago
Exploration of clays and silica sand, Apr. 2005-Dec 2005

- Exploration campaign of clays and silica sand.
- Sampling and chemical analysis of sandstones and clays from Cartago and Central Valley.
- Elaboration of iso-values maps of Fe_2O_3 contents from the areas of production and extraction.
- Attendance in workings of environmental regency (control of slopes and dams, reforestation).

Metales Procesados MRWS –Bellavista Gold Mine Miramar,Puntarenas Costa Rica
Internship, Jan-Mar 2003

- Construction of geologic profiles based on data and drill logs samples.

- Multidisciplinary collaboration with geologists, engineers, surveyors and technicians

ACADEMIC EXPERIENCE

Rutgers University, Department of Earth and Planetary Science, **Teaching Assistant**

- **Petrology and Igneous Rocks** Spring 2008 – 2009 & 2012. Curse Professor: C.T. Herzberg.
- **Lab Geology 101 TA.** Fall 2009-Present. Course Professor C.Swisher Jan 2008, 2010

University of Costa Rica, Central America School of Geology, **Invited Professor**

- General Geology & Introduction to Geology. Mar-Jul 2007

University of Wyoming- University of Costa Rica, Costa Rica.

- **Geology and logistic Assistant (TICO-CAVA Project).** Jul. 2004-2005

University of Costa Rica, Seismological National Network.

- **Seismology Assistant.** Jan. 2002-2005

University of Costa Rica, Seismic Engineer Laboratory

- **Geology Assistant** Jan. 2002-2005**PABLO RUIZ CUBILLO**

FIELD EXPERIENCE

- Geologic mapping of the Poás volcano (Costa Rica) 2007-2011
- Newark basin geology (United States) 2007-2012
- Sampling of intrusive rocks at Talamanca (Costa Rica) 2010
- Volcanology of Etna, Eolian Islands, Vesuvius and Roman Volcanic Province (Italy) 2008
- Sampling of back-arc rocks in Tortuguero (Costa Rica) and Pearl Lagoon (Nicaragua) 2006
- Field survey after the 6.5 M_w earthquake at Puerto Armuelles (Panama). Dec 2003

PUBLICATIONS

- Alvarado, G., Soto G., Salani F., **Ruiz P**., Hurtado L.,: 2011 The formation and evolution of the Hule and Río Cuarto maars, Costa Rica. Journal of volcanology and Geothermal Research 201. 342-356.
- **Ruiz, P.,** Gazel, E.,Alvarado, G., Carr, M.,and Soto, G.: 2010 Geochemical and petrographical characterization of the geological units of the Poás volcano massif, Costa Rica.- Rev Geol. 43. America Central.
- **Ruiz, P.,** 2006: Prospection analysis and technical feasibility use of clays as sulfur neutralizer in the fabrication of clinker in CEMEX Costa Rica, Colorado Abangares. Central America School of Geology. Univ of Costa Rica. 83 Pag. Licenciatura Geology Thesis. San José, C.R.
- Gazel, E. & **Ruiz, P**. 2006: The Sabana Redonda Cinder Cones; Enriched Magmatic Component of Poás Volcano, Costa Rica.- Rev. Geol. 33. America. Central.
- **Ruiz, P**., Murillo, S., 2004: Parametric data from the Arenal volcano lava flows between 1968 and 2002 Boletín del Observatorio sismológico y vulcanológico de Arenal y Miravalles OSIVAM, 15 (27): 25-34.
- **Ruiz, P.,** Rojas, E., 2004: Search of natural hazards that can affect the security and stability of the water pipes < 500 mm of the metropolitan aqueduct of the San Jose city, Costa Rica. University service.